

**UNIVERSITY OF GAZİANTEP
GRADUATE SCHOOL OF
NATURAL & APPLIED SCIENCES**

**GEOMETRICALLY NONLINEAR
ANALYSIS OF PLATES AND
SHELLS**

**PhD THESIS
IN
CIVIL ENGINEERING**

**BY
FİLİZ KOLCU
JULY 2010**

**Geometrically Nonlinear Analysis of Plates and
Shells**

**PhD Thesis
in
Civil Engineering
University of Gaziantep**

**Supervisor
Prof. Dr. Mustafa ÖZAKÇA**

**by
Filiz KOLCU
July 2010**

T.C.
GAZİANTEP UNIVERSITY
GRADUATE SCHOOL OF
NATURAL & APPLIED SCIENCES
CIVIL ENGINEERING

Name of the thesis: Geometrically Nonlinear Analysis of Plates and Shells

Name of the student: Filiz KOLCU

Exam date: 28 .07. 2010

Approval of the Graduate School of Natural and Applied Sciences

Prof. Dr. Ramazan KOÇ
Director

I certify that this thesis satisfies all the requirements as a thesis for the degree of Doctor of Philosophy.

Assoc. Prof. Dr. Mustafa GÜNAL
Head of Department

This is to certify that we have read this thesis and that in our opinion it is fully adequate, in scope and quality, as a thesis for the degree of Doctor of Philosophy.

Prof. Dr. Mustafa ÖZAKÇA
Supervisor

Examining Committee Members

Prof. Dr. Orhan AKSOĞAN (Chairman)

Prof. Dr. Mustafa ÖZAKÇA

Assoc. Prof. Dr. Mustafa GÜNAL

Assoc. Prof. Dr. Abdülkadir ÇEVİK

Assist. Prof. Dr. Nildem TAYŞI

ABSTRACT

GEOMETRICALLY NONLINEAR ANALYSIS OF PLATES AND SHELLS

KOLCU, Filiz

PhD in Civil Engineering

Supervisor: Prof. Dr. Mustafa ÖZAKÇA

July 2010, 125 pages

This thesis deals with the geometrically nonlinear analysis of prismatic plates and shells using the finite strip method. The analysis is based on the use of Mindlin plate theory and therefore includes the effects of transverse shear deformation. The nonlinearity is introduced via the strain-displacement equations and correspondingly the analysis pertains to problems involving moderate displacements but small rotations. The principle of minimum potential energy is used in the development of the element and the complete structure stiffness equations and latter equations are solved using Newton-Raphson method. The postbuckling performance of optimized panels with sub-stiffening is investigated. The panels have been optimized for minimum weight or maximum performance. The linear elastic eigenvalue finite strip code which has a built-in optimizer provided a practical way of doing so, at least for the initial (skin) buckling. Optimization is also used to obtain insight into the importance of different design variables, and derive a method for sizing. Linear finite strip analysis allowed the optimization of one of the sub-stiffened panels, revealing a potential for further improvement of the initial buckling load.

Keywords: Geometrically nonlinear, Stiffened plates, (Post) buckling analysis, Structural optimization, Finite strip

ÖZET

PLAK VE KABUK YAPILARIN GEOMETRİK NONLİNEER ANALİZİ

KOLCU, Filiz

Doktora Tezi, İnşaat Mühendisliği

Tez yöneticisi: Prof. Dr. Mustafa ÖZAKÇA

Temmuz 2010, 125 sayfa

Bu tezde, plak ve kabuk yapıların geometrik nonlinear analizi için sonlu şerit metodu sunulmuştur. Analizde, Mindlin plak teorisinin kullanımı temel alınır ve bu sebeple kayma deformasyonu etkilerini kapsar. Nonlineerlik birim uzama-yer değiştirme denklemleri aracılığıyla ifade edilmiş ve benzer şekilde analiz küçük dönmelerin olduğu yer değiştirme problemlerini içermektedir. Elemanın geliştirilmesinde ve plak rijitlik denklemlerinin tamamlanmasında potansiyel enerjinin minimize edilmesi ilkesi kullanılmakta ve bu denklemler Newton Raphson metodu ile çözülmektedir. Sayısal uygulamalarda farklı sınır koşulları, düzgün yüklü plaklar ile verilmektedir. Optimize edilmiş takviyeli panellerin burkulma sonrası (veya ötesi) performansları araştırılmıştır. Paneller, minimum ağırlık veya maksimum performans için optimize edilmiştir. Lineer elastik özdeğer sonlu şerit kodu, optimizasyon yapan kişiye, en azından ilk burkulma için pratik bir yol sağlamaktadır. Optimizasyon, farklı tasarım değişkenlerinin önemini kavrama ve boyutlandırma için bir metot geliştirmek için de kullanılmıştır. Lineer sonlu şerit analizi ile takviyeli panellerin birinin optimizasyonu potansiyelde ilk burkulma yükünün üzerinde iyileşme sağlamıştır.

Anahtar Kelime: Geometrik nonlinear, Takviyeli plakalar, Burkulma (sonrası) analiz, Yapısal optimizasyon, Sonlu şeritler

ACKNOWLEDGEMENTS

I would like to express my sincere deepest gratitude to my supervisor Prof. Dr. Mustafa ÖZAKÇA, for his guidance, advice, encouragement and sharing his extensive experience during the preparation of this thesis.

My thanks also go to my thesis observing committee members, Prof. Dr. Orhan AKSOĞAN and Assoc Prof. Dr. Mustafa GÜNAL for their helpful discussion.

I would also like to thank Prof. Dr. H. İbrahim GÜZELBEY for his encouragement, advice and great help.

Many thanks to Assist.Prof.Dr Nildem TAYŞI, for her friendship, help, useful technical discussions, support, encouragement and reading early versions of my thesis during the last stage of this research.

I would also like to thank Res. Asst. Talha EKMEKYAPAR and Dr. Mehmet Tolga GÖĞÜŞ for helping me with various aspects of conducting this research and their support and encouragement during the preparation of it.

Finally, I would like to express my special gratitude to my father Mustafa Kemal NAZLI, my mother Mediha NAZLI, my sisters Feray KARACA, Ebru UNCU, Ela NAZLI, my husband Yakup KOLCU, my sons Kutay and Kaan for their encouragement and patience.

CONTENTS

	Page
ABSTRACT	iii
ÖZET	iv
ACKNOWLEDGEMENTS	v
CONTENTS	vi
LIST OF FIGURES	ix
LIST OF TABLES	xii
LIST OF SYMBOLS	xiv

CHAPTER 1 INTRODUCTION

1.1 General Information	1
1.2 Principle Objectives	2
1.3 About Computer Program	3
1.4 Layout of Thesis	4

CHAPTER 2 LITERATURE SURVEY

2.1 General Information	5
2.2 Linear Buckling Analysis	6
2.3 Geometric Nonlinear Analysis	10
2.4. Structural Optimization	15
2.5. Summary of Literature Survey	17

CHAPTER 3 LINEAR BUCKLING FORMULATION OF PLATES

3.1 Introduction	18
3.2 Structural Theories	19
3.3 Strip Formulation	20
3.3.1 Strain energy	20
3.3.2 Potential energy of the applied inplane stresses	21
3.3.3 Finite strip idealization	23

3.4 Plate Examples.....	25
3.4.1 Square simply supported ($S_h/S_h/S_h/S_h$) isotropic plates under uniaxial stress.....	26
3.4.2 Rectangular isotropic plates under uniaxial stress.....	27
3.5 Stiffened Plate Examples.....	30
 CHAPTER 4 GEOMETRIC NONLINEAR ANALYSIS	
4.1 Introduction	37
4.2 General Theory and Solution Algorithms	39
4.2.1 Direct iteration method.....	39
4.2.2 Modified Newton-Raphson method.....	40
4.2.3 Tangential stiffness method.....	41
4.2.4 Initial stiffness method	42
4.2.5 Arc-length method (Riks-Wempner method)	43
4.3 Plane Formulation.....	43
4.4 Plane Example	48
4.5 Plate and Shell Formulation	49
4.5.1 Strains	49
4.5.2 Stresses	50
4.5.3 Total Lagrangian virtual work equation	51
4.5.4 Variation of strain.....	53
4.5.5 Finite strip formulation of equilibrium equations	54
4.5.6 Solution to nonlinear equilibrium equations.....	58
4.5.7 Tangent stiffness matrix	59
4.5.8 Equivalent nodal loads due to stresses	61
4.6 Examples	63
4.6.1 Isotropic square plates under uniform loading with various boundary conditions	63
4.6.2 Postbuckling of isotropic square plates with various boundary conditions	67
4.6.3 Postbuckling of straight stiffened plate	74
4.6.3 Comparison of postbuckling performance of optimized stiffened plate	78

CHAPTER 5 OPTIMIZATION OF BUCKLING PERFORMANCE

5.1 Introduction	88
5.2 Structural Optimization Algorithm	89
5.2.1 Mathematical definition of optimization problem	91
5.2.2 Shape definition	93
5.2.3 Mesh generation for finite strip analysis	94
5.2.4 Structural finite strip analysis	94
5.2.5 Sensitivity analysis	95
5.2.6 Derivative of buckling load	95
5.2.7 Derivative of volume	96
5.3 Mathematical Programming	96
5.4 Examples	97
5.4.1 Maximization of critical buckling load of square isotropic plates	97
5.4.2 Maximization of critical buckling load of straight stiffened plates	100
5.4.3 Maximization of critical buckling load of sub-stiffened plates	104
5.4.4 Maximization of critical buckling load of sculpted skin panels	105

CHAPTER 6 CONCLUSION

6.1 Introduction	108
6.2 Conclusion	108
6.3 Recommendation of future work	109

REFERENCES	111
-------------------------	-----

APPENDIX A: Strain terms, strain-displacement matrices, elemental volumes, membrane rigidity matrix, flexural rigidity matrix, and shear rigidity matrix.....	124
--	-----

APPENDIX B: Geometric stiffness matrices and inplane matrices	125
--	-----

CURRICULUM VITAE	126
-------------------------------	-----

LIST OF FIGURES

	Page
Figure 3.1	Classical buckling 18
Figure 3.2	Definition of Mindlin-Reissner finite strips 20
Figure 3.3	a) ($\mathbf{S}_h / \mathbf{F} / \mathbf{S}_h / \mathbf{F}$) plate under uniaxial stress σ_y^0 , b) ($\mathbf{S}_h / \mathbf{S}_h / \mathbf{S}_h / \mathbf{F}$) plate under uniaxial stress σ_y^0 and c) ($\mathbf{S}_h / \mathbf{C} / \mathbf{S}_h / \mathbf{C}$) plate under uniaxial stress σ_x^0 28
Figure 3.4	Isotropic baseline stiffened panels (Profile B) along with the three 'proof of concept' specimens, namely Profile 1, 2 and 3 (all dimensions in mm) 31
Figure 3.5	Profile B-buckling loads and corresponding buckling modes (mode shapes are plotted for mid span, i.e. at $x = a/2 = 300$) 33
Figure 3.6	Profile 1-buckling loads and corresponding buckling modes (mode shapes are plotted for mid span, i.e. at $x = a/2 = 300$) 34
Figure 3.7	Profile 2-buckling loads and corresponding buckling modes (mode shapes are plotted for mid span, i.e. at $x = a/2 = 300$) 35
Figure 3.8	Profile 3-buckling loads and corresponding buckling modes (mode shapes are plotted for mid span, i.e. at $x = a/2 = 300$) 36
Figure 4.1	Buckling and bifurcation point 38
Figure 4.2	Newton-Raphson flow chart 42
Figure 4.3	Eccentrically loaded column material and shape properties 48
Figure 4.4	Plate problem flowchart 62
Figure 4.5	Square isotropic plate ($\mathbf{S}_h / \mathbf{S}_h / \mathbf{S}_h / \mathbf{S}_h$) under uniformly distributed load 64
Figure 4.6	Square isotropic plate ($\mathbf{S}_h / \mathbf{F} / \mathbf{S}_h / \mathbf{F}$) under uniformly distributed load 65
Figure 4.7	Square isotropic plate ($\mathbf{S}_h / \mathbf{C} / \mathbf{S}_h / \mathbf{C}$) under uniformly distributed load 66
Figure 4.8	($\mathbf{S}_h / \mathbf{S}_h / \mathbf{S}_h / \mathbf{S}_h$) plate under uniaxial load 67

Figure 4.9	Variation of load versus the longitudinal displacement at the edge of the plate, U , for postbuckling of a square ($S_h / S_h / S_h / S_h$) isotropic plate.....	68
Figure 4.10	Variation of load versus center deflection, W , for the postbuckling of a square ($S_h / S_h / S_h / S_h$) isotropic plate.....	69
Figure 4.11	($S_h / F / S_h / F$) Plate under uniaxial load	70
Figure 4.12	Variation of load versus the longitudinal displacement at the edge of the plate, U , for the postbuckling of a square ($S_h / F / S_h / F$) isotropic plate.	71
Figure 4.13	Variation of load versus the deflection at the center of the plate, W , for the postbuckling of a square ($S_h / F / S_h / F$) isotropic plate.....	71
Figure 4.14	($S_h / C / S_h / C$) Plate under uniaxial load.....	72
Figure 4.15	Variation of load versus the longitudinal displacement at the edge of the plate, U , for the postbuckling of a square ($S_h / C / S_h / C$) isotropic plate	73
Figure 4.16	Variation of load versus the deflection at the center of the plate, W , for the postbuckling of a square ($S_h / C / S_h / C$) isotropic plate.....	73
Figure 4.17	Dimensions of typical stiffened panel	74
Figure 4.18	Loading and boundary conditions of stiffened plate	75
Figure 4.19	Variation of load versus the longitudinal shortening of the plate with 3 stiffeners.....	76
Figure 4.20	Variation of load versus the longitudinal shortening of the plate with 4 stiffeners.....	77
Figure 4.21	Variation of load versus the longitudinal shortening of the plate with 5 stiffeners.....	77
Figure 4.22	Comparison of postbuckling performance of straight stiffened plates	78
Figure 4.23	Examined stiffened plate types.....	79
Figure 4.24	Comparison of postbuckling loads according to the number of stiffeners ‘type a’	83
Figure 4.25	Comparison of postbuckling loads according to the number of stiffeners ‘type b’	84
Figure 4.26	Comparison of postbuckling loads according to the number of stiffeners ‘type c’	85

Figure 4.27	Comparison of postbuckling loads according to the number of stiffeners ‘type d’	86
Figure 4.28	Comparison of postbuckling loads according to the number of stiffeners ‘type e’	87
Figure 5.1	Structural optimization flowchart	89
Figure 5.2	Geometric representation of stiffened plate.....	93
Figure 5.3	Mesh representation of plates	94
Figure 5.4	Position of design variables of plate.	97
Figure 5.5	sample three-dimensional aspect of stiffened plate (with five straight stiffeners)	101
Figure 5.6	Loading and boundary conditions.....	101
Figure 5.7	Straight stiffened plate.....	102
Figure 5.8	Design variables of sub stiffened plate	104
Figure 5.9	Buckling modes corresponding to each of the optimum designs of Table 5.9 from 3 DV – case I on top left to 5 DV – case VI on bottom right	105
Figure 5.10	Sculpted skin panels	106
Figure 5.11	Design variables of Sculpted skin panels	106
Figure 5.12	Buckling modes for the sculpted skin design, from the initial design on top left to optimized case 5 (Table 5.10) on bottom right.	107

LIST OF TABLES

	Page
Table 3.1	Buckling factors for a set of square ($S_h / S_h / S_h / S_h$) simply supported isotropic plates under uniaxial stress27
Table 3.2	Buckling factors for a set of rectangular ($S_h / C / S_h / C$) isotropic plates under uniaxial stress29
Table 3.3	Buckling factors for a set of rectangular ($S_h / S_h / S_h / F$) isotropic plates under uniaxial stress29
Table 3.4	Buckling factors for a set of rectangular ($S_h / F / S_h / F$) isotropic plates under uniaxial stress30
Table 3.5	Buckling loads for profiles.....31
Table 4.1	Column end horizontal deflections49
Table 4.2	Central deflection, W , for ($S_h / S_h / S_h / S_h$) isotropic square plates64
Table 4.3	Central deflection, W , for ($S_h / F / S_h / F$) isotropic square plates.....65
Table 4.4	Central deflection, W , for ($S_h / C / S_h / C$) isotropic square plates66
Table 4.5	The longitudinal displacement at the edge of the plate, U , and central deflection, W , for postbuckling of a square ($S_h / S_h / S_h / S_h$) isotropic plate68
Table 4.6	The longitudinal displacement at the edge of the plate, U , and central deflection, W , for postbuckling of a square ($S_h / F / S_h / F$) isotropic plate70
Table 4.7	The longitudinal displacement at the edge of the plate, U , and central deflection, W , for postbuckling of a square ($S_h / C / S_h / C$) isotropic plate72
Table 4.8	Longitudinal shortening of the straight stiffened plate75
Table 4.9	Stiffened plate types and their baseline design rules80
Table 4.10	Initial, optimum design variables, critical buckling loads and postbuckling collapse loads of ‘type a’81

Table 4.11	Initial, optimum design variables, critical buckling loads and postbuckling collapse loads of ‘type b’	81
Table 4.12	Initial, optimum design variables, critical buckling loads and postbuckling collapse loads of ‘type c’	81
Table 4.13	Initial, optimum design variables, critical buckling loads and postbuckling collapse loads of ‘type d’	82
Table 4.14	Initial, optimum design variables, critical buckling loads and postbuckling collapse loads of ‘type e’	82
Table 5.1	Square plate with ($S_h / S_h / S_h / S_h$) boundary condition under uniaxial force: values of the optimal design variables and volume	98
Table 5.2	Square plate with ($S_h / S_h / S_h / S_h$) boundary condition under uniaxial force: values of the optimal design variables and buckling ratio.....	99
Table 5.3	Square plate with ($S_h / S_h / S_h / S_h$) boundary condition under uniaxial stress: values of the optimal design variables and volume ...	99
Table 5.4	Square plate with ($S_h / S_h / S_h / S_h$) boundary condition under uniaxial stress: values of the optimal design variables and buckling ratio	100
Table 5.5	Common constraints.....	100
Table 5.6	Design constraints of straight stiffened plate.....	102
Table 5.7	Size optimization of straight stiffened plate	103
Table 5.8	Shape optimization of straight stiffened plate	103
Table 5.9	The optimised critical buckling load for sub-stiffened plates	105
Table 5.10	The optimised critical buckling load for Sculpted skin panels	106

LIST OF SYMBOLS

Abbreviations

FE	Finite Element
FS	Finite Strip
DVs	Design Variables
Dof	Degrees of Freedom

Scalars

A	Area
b	Length of strip
C_p, S_p	Cosine and sine function
$C(0)$	Order of continuity
d	Displacement
E	Young's modulus
$F(\mathbf{s})$	Objective function to be minimized
$g_j(\mathbf{s})$	Inequality constraint function
$h_k(\mathbf{s})$	Equality constraint function
J	Jacobian
ℓ	The arc length parameter of the curve
δ	Displacement
(m,n)	Mode and half-sine wave
N_i	Shape function associated with node i
R	Radius of curvature
s	Design variables
t	Thickness
u_ℓ, v_ℓ, w_ℓ	Displacement components in ℓ , y and n -direction
u, v, w	Global displacement parameters
u^p, v^p, w^p	Displacement amplitudes of p^{th} harmonic
V	Volume of the structure

U	Total strain energy
V_g	Potential energy of volume
P_{cr}	Critical buckling load
P_0	Initial load

Vectors

\mathbf{d}	Vector of unknown displacements (eigenvector)
\mathbf{d}_i^p	Vector of nodal degrees of freedom
\mathbf{d}_i^e	Displacement (eigenvector) vector associated with element e and node i
$\bar{\mathbf{d}}_i^p$	Displacement (eigenvector) vector at node i and harmonic p
\mathbf{s}	Design variable vector
$\boldsymbol{\varepsilon}_0$	Linear strains
$\boldsymbol{\varepsilon}_m$	Inplane strains
$\boldsymbol{\varepsilon}_m$	Inplane strains
$\boldsymbol{\varepsilon}_b$	Bending strains
$\boldsymbol{\varepsilon}_s$	Transverse shear strains
$\boldsymbol{\varepsilon}^{ML}$	Nonlinear strains
$\boldsymbol{\varepsilon}_\ell^{nl}, \boldsymbol{\varepsilon}_y^{nl}, \boldsymbol{\gamma}_{\ell y}^{nl}$	Second order strains
\mathbf{f}	Force vector
\mathbf{f}^i	Force vector at node i
$\boldsymbol{\sigma}_m^p, \boldsymbol{\sigma}_b^p, \boldsymbol{\sigma}_s^p$	Membrane, bending and shear stress resultant vectors
$\boldsymbol{\sigma}_{m\ell}^p, \boldsymbol{\sigma}_{my}^p, \boldsymbol{\sigma}_{m\ell y}^p$	Membrane stress resultant vectors
$\boldsymbol{\sigma}_{b\ell}^p, \boldsymbol{\sigma}_{by}^p, \boldsymbol{\sigma}_{b\ell y}^p$	Bending stress resultant vectors
$\boldsymbol{\sigma}_\ell^0, \boldsymbol{\sigma}_y^0, \boldsymbol{\tau}_{\ell y}^0$	Applied inplane stresses
$\boldsymbol{\psi}$	Residual force vector
$\boldsymbol{\psi}^i$	Residual force vector at node i
$\boldsymbol{\delta}$	Vector of unknown displacements for large deformation

δ_i^p	Vector of nodal degrees of freedom for large deformation
δ_i^e	Displacement (eigenvector) vector associated with element e at node i for large deformation
θ	Vector of displacement gradient
θ_i^p	Vector of displacement gradient at node i and harmonic p
\mathbf{u}	Vector of displacements
\mathbf{P}	Load vector
\mathbf{R}	Equivalent nodal load vector due to body forces and inplane loads

Matrices

\mathbf{A}_θ	Matrices of w displacement derivatives
\mathbf{B}	Strain-displacement matrix
\mathbf{B}_{0i}^p	Linear strain-displacement matrix for node i and harmonic p
\mathbf{B}_{mi}^e	Membrane strain-displacement matrix for element e at node i
\mathbf{B}_{bi}^e	Bending strain-displacement matrix for element e at node i
\mathbf{B}_{si}^e	Shear strain-displacement matrix for element e at node i
\mathbf{B}_{mi}^p	Membrane strain-displacement matrix for node i and harmonic p
\mathbf{B}_{si}^p	Shear strain-displacement matrix for node i and harmonic p
\mathbf{B}_{si}	Shear strain displacement matrix
\mathbf{B}_L	Nonlinear strain displacement matrix
\mathbf{B}_{Li}^p	Nonlinear strain displacement matrix for node i and harmonic p
\mathbf{D}	Matrix of rigidities
$\mathbf{D}_m, \mathbf{D}_b, \mathbf{D}_s$	Matrices of membrane, bending and shear rigidities
\mathbf{G}_i	Cartesian shape function derivatives matrix for node i
\mathbf{G}_i^p	Cartesian shape function derivatives matrix for node i and harmonic p
\mathbf{J}	Jacobian matrix

\mathbf{K}_0	Linear stiffness matrix
\mathbf{K}_L	Initial displacement matrix
$[\mathbf{K}_{Lij}^e]^{pq}$	Initial displacement matrix linking nodes i and j and harmonics p and q
\mathbf{K}_σ	Initial stress matrix
$[\mathbf{K}_{\sigma ij}^e]^{pq}$	Initial stress matrix for element e linking nodes i and j and harmonics p and q
\mathbf{K}_T	Tangent stiffness matrix
\mathbf{K}_{ij}^e	Stiffness matrix associated with element e and node i and j
$[\mathbf{K}]^{pp}$	Global stiffness matrix associated with harmonic p
$[\mathbf{K}_{ij}^e]^{pq}$	Stiffness matrix for element e linking nodes i and j and harmonics p and q
\mathbf{K}_{mij}^e	Membrane stiffness matrix for element e linking nodes i and j
\mathbf{K}_{bij}^e	Bending stiffness matrix for element e linking nodes i and j
\mathbf{K}_{sij}^e	Shear stiffness matrix for element e linking nodes i and j
\mathbf{N}	Shape function matrix

Greek Symbols

α	Angle between local and global axes
Δs_k	Small perturbation of design variables s_k
$\varepsilon_\ell, \varepsilon_y$	Strain in ℓ direction and longitudinal strain
$\gamma_{\ell y}, \gamma_{yn}$	Shear strain
κ	Shear modification factor
κ_ℓ	Curvature in the ℓ -direction
κ_y	Longitudinal curvature
$\kappa_{\ell y}$	Twisting curvature
λ^p	Load factor (eigenvalues)
ν	Poisson's ratio
ϕ, ψ	Rotation of the midsurface normal in the ℓn and yn planes

ϕ^p, ψ^p	Rotation amplitude for the p^{th} harmonic term
ξ	Isoparametric element natural (curvilinear) coordinate
σ	Stress component
$\partial \ell$	Partial differential w.r.t. ℓ
γ	% convergence tolerance

CHAPTER 1

INTRODUCTION

1.1 General Information

Rectangular plate and stiffened plate structures are used frequently as structural components in a number of branches of engineering. In the civil engineering context nonlinear response has proved valuable in the analysis of cooling towers. In aircraft and ship design, plate structures are often subjected to lateral and inplane loading and in consequence there is considerable interest in predicting the buckling and postbuckling behavior of such structures. In many instances the efficient design of plate structures may be based on the assumption of nonlinear response to loading.

Nonlinear behaviors of structures are classified as geometric nonlinearity, material nonlinearity and combined geometric and material nonlinearity. In material nonlinearity stress is not linearly proportional to the strain. In geometric nonlinearity strain-displacement relation is nonlinear. If accurate determination of the displacements is needed, geometric nonlinearity may have to be considered in some structures. For instance, stresses due to membrane action, usually neglected in plate flexure, may cause a considerable decrease of displacements as compared with the linear solution, even though displacements are still quite small. Conversely, it may be found that a load is reached where deflections increase more rapidly than predicted by a linear solution and indeed a state may be attained where load carrying capacity decreases with continuing deformation.

The load at which the bifurcation occurs in the load deflection spaces is called the critical buckling load or simply critical load. The deflection path that exists prior to bifurcation is known as the primary path, and the deflection path after bifurcation is called the secondary or postbuckling path. A nonlinear analysis capability provides

the engineer with a means of determining post-buckling behavior. This is important because often the ultimate load occurring in the postbuckled region exceeds the critical load rendering the structure adequate within this range. Frequently, though, postbuckling deflections increase rapidly and may become irreversible, consequently a nonlinear analysis becomes essential if these reserve of strength are to be safely utilized.

Many engineering structures have constant geometrical properties along a particular direction. Such prismatic structures are very common in plate and shell problems where the transverse cross-section of the structure often remains constant in the longitudinal direction. If the material properties of the structures are also constant in the same direction, the nonlinear analysis can be simplified by the combined use of finite elements FE and Fourier expansions to model the transverse and longitudinal behavior. The Finite Strip (FS) method is one of a number of procedures which can be used to solve nonlinear plate structure problems.

In this thesis the main concern is to develop a program based on FS method for geometric nonlinear analysis of plates and shells by extending the earlier studies [1].

1.2 Principle Objectives

The crucial motivation of the thesis is geometrically nonlinear analysis of plates and shells using a powerful computer code.

The specific objectives may be expressed as follows:

- Finding the critical buckling load of the considered plates.
- Maximizing the critical buckling load of unstiffened and stiffened plates.
- Investigating the performance of each structural element on the critical buckling loads of plates.
- Evaluating the strains using a deformation Jacobian matrix for the geometric nonlinear effects in plane problems.
- Using Newton-Raphson iteration method for the solution.
- Giving a formulation based on the FS method for the geometric nonlinear analysis of plates.

- Considering the displacements for nonlinear performance and investigating the load-deflection curve.
- Observing the change in the element shape during the nonlinear analysis to evaluate the efficiency of each structural element.
- Comparing the results with the literature and FE solution.
- Analyzing the postbuckling behavior of optimized panels.
- Compared the postbuckling performance of initial and optimum plates.

1.3 About Computer Program

A free vibration analysis using FS method and shape optimization with Sequential Quadratic Programming programs for straight folded plates and shells were developed by Özakça [2]. In the present thesis buckling analysis subroutines of folded plates, shells and stiffened plates called EBUCK included into program. Then program GNPLATE is developed for geometrically nonlinear analysis of plates and shells. For postbuckling performance of initial and optimized plates FS method is used. In plane stress-plane strain program GNPLANE Finite Element (FE) method is used. All programs are written in FORTRAN 90 using double precision and run on LINUX main frame and personal computer.

1.4 Layout of Thesis

The contents of each chapter can be expressed as:

- Chapter 2 contains literature survey about linear buckling analysis, geometric nonlinear analysis and optimization methods.
- In Chapter 3, FS formulation for plates is presented in condensed form. Accuracy and efficiency of the method is illustrated using several examples. Results obtained are compared with previous published results.
- Chapter 4 is composed of two parts. In the first part nonlinear formulation based on FE for plane stress-plane strain are given with column example. Then FS formulation for nonlinear analysis of plates and flowchart are presented. Plate examples are given for different loading and boundary conditions.
- Optimization process, definition of elements and design variables, and structural optimization flowchart are presented in Chapter 5. Several

examples of prismatic and stiffened plates are presented to illustrate structural shape optimization.

- In Chapter 6, conclusions based on the present thesis are underlined and recommendations for future work are expressed.

CHAPTER 2

LITERATURE SURVEY

2.1 General Information

The first buckling studies are carried out in the eighteenth century by Leonhard Euler [3]. He proved that there was a critical load for the buckling of a slender column which bends sideways with very large displacements before reaching the ultimate stress capacity of the used material. At that time principal structural materials were wood and stone. The relatively low strength of these materials necessitated stout structural members for which the question of elastic stability was not of primary importance. Thus, Euler's theoretical solution, developed for slender bars, remained for a long time without practical application. Only with the beginning of the extensive construction of steel railway bridges during the middle of the past century did the question of buckling of compression members gained practical importance. The use of steel led naturally to types of structures including slender compression members, thin plates, and thin shells. Experience showed that such structures may fail in some cases not on account of high stress, surpassing the strength of material, but owing to insufficient elastic stability of slender or thin-walled members [4].

In the use of thin sheet material, as in plate girders and airplane structures, we have to keep in mind that thin plates may prove unstable under the action of forces in their own planes, and fail by buckling sideways. Thin cylindrical shells, such as vacuum vessels, which have to withstand uniform external pressure, may exhibit instability and collapse at a relatively low stress if the thickness of the shell is too small in comparison with the diameter. A thin cylindrical shell may buckle also under axial compression, bending, torsion, or combinations of these. Because of the two dimensional action, the buckling behavior of plates and shells are different and complex when compared with columns [4].

Thin steel plates loaded in their mid-plane may buckle under very small loads, and if the plate is adequately supported along its boundaries, it will be able to carry much higher loads than the theoretical buckling load. Such plates are referred to have postbuckling strength. Failure of such structures is usually due to large out-of-plane deflections, yielding and rupture.

The stiffened plates with longitudinal stiffeners their response against axial loads must be designed to function under buckling and postbuckling conditions to complete on weight-efficiency basis. Analytical solutions for those types of structures may become insufficient and tedious. In this regard, numerical solutions are inevitable.

The linear buckling problem is an eigenvalue problem, making possible to obtain critical load factors and buckling modes with a simple procedure. However, postbuckling results from an equilibrium problem solved using incremental solution strategy where loads and displacements change by small but finite increments.

In this chapter, the history of linear buckling and geometric nonlinear (postbuckling) analysis of plates and shells are reviewed. Also the existing literature is grouped based on solution methods such as analytical methods, FE method and FS method. Then, literature survey of optimization is briefly given.

2.2 Linear Buckling Analysis

a) *Analytical method:* The limitations imposed by analytical techniques are well known. Only in special cases of loading, plate geometry and edge conditions is closed form solution possible [4, 5]. Classical analytical techniques are not suitable for plates and shells with an abrupt change of thickness, complex geometry and mixed boundary conditions. Approximate methods are therefore not only permissible but, in many cases, are the only means of solution to this problem.

b) *Finite element method:* Because of severe economic constraints and stringent deadlines coupled with the enormous growth in computer speed and power, engineers are resorting to numerical methods for the analysis of plates and shells.

Among the various numerical methods, FE method becomes firmly established as an engineering tool for the stability analysis of shells.

Ley et al. [6] developed the analysis to predict buckling loads of ring-stiffened anisotropic cylinders subject to axial compression, torsion and internal pressure. Buckling displacements are represented by a Fourier series in the circumferential coordinate and the FE method applied in the axial coordinate.

FE analysis applications to plate buckling problem have been carried out by the following researchers; Allman [7], Przemieniecki [8] and Fafard et al. [9]. For complex boundaries, Anderson et al. [10] approximated curved boundaries with a large number of straight-edged triangular elements.

Sheikh et al. [11] investigated the stability of a tee-shaped steel stiffened plate under uniaxial compression using FE. They investigated the effect of five dimensionless parameters (the transverse slenderness of the plate, the slenderness of the web and flange of the stiffener, the ratio of torsional slenderness of the stiffener to the transverse slenderness of the plate, and the stiffener-to-plate area ratio) on the stability of stiffened plates.

Sridharan and Zeggane [12] studied the interaction of local and overall buckling in plate structures and stiffened shells by FE using a specially formulated shell element. Grondin et al. [13] investigated the stability of stiffened plates with tee-shaped stiffeners using FE. They validated the model using results of tests on full size stiffened plate specimens. Some of the investigated parameters are the plate aspect ratio, the plate to stiffener cross-sectional area ratio and the plate slenderness ratio.

Some other studies are available for different mechanical properties of stiffened plates. For example Jiang [14] carried out an investigation of bending and buckling of unstiffened, sandwich and hat-stiffened orthotropic, rectangular plates using first order shell elements and first and second order three dimensional solid elements by FE.

Mukhopadhyay and Mukherjee [15] presented an isoparametric stiffened plate bending element for the buckling analysis of stiffened plates. Wang and coworkers [16, 17] considered the elastic buckling of rectangular Mindlin plates with internal line support. Rayleigh-Ritz method based on the energy functional derived from the incremental total potential energy approach was applied for the solution of plates under normal in-plane forces and uniform shear. Wang et al. [18] extended their earlier work [16, 17] and studied the axisymmetric buckling of radially loaded circular Mindlin plates with internal concentric ring support.

Teng and Rotter [19] studied the problem of elastic unstiffened thin cylinders with axisymmetric imperfections. Rao and Ramanjaneyulu [20] presented the stability analysis of a natural draught cooling tower shell subjected to non axisymmetric wind pressure carried out using finite ring elements. The FE method was based on the development of a geometric stiffness matrix consistent with the elastic stiffness matrix of the element. The most suitable element for the plates of arbitrary configuration was the triangular one. The minimum number of degrees of freedom at each node being three, this method led to the solution of a large eigenvalue problem for the total structure which was time consuming and uneconomical.

Sato [21] designed a set of partial differential equations to enable elastic buckling analysis of incomplete composite plates with regard to the thickness of a steel plate. The relationship of the critical buckling loads of complete composite plates, incomplete composite plates and individual plates was analyzed.

Singh and Dey [22] studied the total potential energy during the buckling of a plate with variable stiffness which has been discretized by the method of finite difference. In this approach the type of element selected can greatly affect the efficiency and quality of the approximate solution obtained.

c) *Finite strip method*: The FS method is a semi-analytical method which combines the use of Fourier expansions and one-dimensional FE to model the longitudinal and transverse structural behavior, respectively.

The FS method, published first in 1968 by Cheung [23], was a special form of the FE procedure. There are two main types of strips successfully developed: the semi analytical or classical FS [24-38] and the spline FS [39]. In the above mentioned types of FS, reducing partial differential equations to ordinary or partial differential equations of lower order was achieved by a separation of variables approach. The last development formulates a so-called precise FS method. Closely related to the FS for two-dimensional problems are the finite prisms and the finite layers for the three-dimensional domain. The main subjects include static, dynamic (vibrations, earthquake) and stability (buckling) analyses of Kirchhoff and Mindlin-Reissner plates with various shapes, folded plates, walls and shells for different load-bearing structures such as ceilings, roofs, tall buildings and box-girder bridges.

Benson and Hinton [32] presented a comprehensive study including static, free vibration and stability analyses of thick and thin rectangular and curved plates using quadratic strips. Hinton and coworkers [33-36] used linear, quadratic and cubic FS based on Mindlin-Reissner assumptions for the free vibration and static analysis of curved and variable thickness, prismatic structures straight or curved planform. Later Hinton et al. [37] have dealt with linear buckling analysis of prismatic folded plate structures supported on diaphragms along two opposite edges.

Kwon and Hancock [39] have described the analysis of the general buckling behavior of thin walled sections using the spline FS method (i.e. polynomial spline functions, rather than analytical functions, used in the longitudinal representation of displacement), but only one application to plate structures was presented.

Takahasni and Nakazawa [40] studied the vibration and buckling of plate girders by FS using small deflection theory. They obtained natural frequencies and the buckling stresses of the simply supported plate girder. In this study the effect of the flange plate on the natural frequencies of the web plate was also investigated.

Hinton [41] studied the buckling of initially stressed Mindlin plates using the thick FS method. He obtained some further results for initially stressed rectangular plates with two opposite edges simply supported and various support conditions on the remaining sides. Hinton et al. [42] investigated the buckling analysis of prismatic

folded plate structures supported on diaphragms along two opposite edges. They carried out the analysis using variable thickness FS based on Mindlin-Reissner assumptions which allow for transverse shear deformation effects.

It seems that FS method is an accurate and inexpensive analysis procedure and presents the best prospect of dealing successfully with the full range of buckling problems of prismatic plates and shells with diaphragm ends.

2.3 Geometric Nonlinear Analysis

a) *Analytical method*: The solution of plate buckling problems by analytical methods is applicable when plate geometry, loading conditions and boundary conditions are simple. Otherwise, it is nearly impossible and tedious to solve this type of problems. The analytical solutions of various types of plates are extensively studied by Timoshenko [4]. Navazi et al. [43] studied the nonlinear cylindrical bending of a functionally graded plate. The material properties of the plate were assumed to be graded continuously in the direction of thickness. The variation of the material properties followed a simple power-law distribution in terms of the volume fractions of constituents. The von Karman strains are used to construct the nonlinear equilibrium equations of the plates subjected to in-plane and transverse loadings. The governing equations are reduced to a linear differential equation with nonlinear boundary conditions yielding a simple solution procedure.

Bisagni and Vescovini [44] presented an analytical formulation for the study of linearized local skin buckling load and nonlinear post-buckling behavior of isotropic and composite stiffened panels subjected to axial compression. The skin was modeled as a thin plate introducing Donnell-Von Karman and Kirchhoff hypothesis and applying classical lamination theory, while the stiffeners were considered as torsion bars.

b) *Finite element method*: The first work on the extension of the FE procedure to geometrically nonlinear structures was reported by Turner et al. [45]. Gallagher and Padlog [46] introduced the geometric nonlinearity as the displacement based FE

method. Their formulation was restricted to a stability analysis in which the response prior to buckling (bifurcation) was linear.

In the FE approach to solving geometrically nonlinear problems [47-49] the load was applied as a sequence of sufficiently small increments so that the structure can be assumed to respond linearly during each increment. For each increment of load, increments of displacements and corresponding increments of stress and strain were computed.

The iterative approach for solving the governing nonlinear algebraic equations has been used by many investigators [50-52]. This approach was relatively simple to apply. Starting with an initial estimate to the displacement solution, the nonlinear effects were estimated and a set of linearized equations was solved to obtain an improved solution. This solution was back substituted into the equations and the iteration continued until the convergence of successive iterations was obtained. The success of the method depends to a large extent upon the accuracy of the initial estimate of the displacements. The load may be applied in increments and various extrapolation procedures may be utilized to obtain accurate estimates. Relaxation schemes [51, 53, and 54] may be used to accelerate convergence.

While the iterative method was extremely fast from a computational standpoint, it has a serious disadvantage in that it will converge only for moderately nonlinear problems [55]. In order to obtain convergence for problems exhibiting high nonlinearity, many investigators have utilized the Newton-Raphson iterative approach. This procedure was extremely accurate and usually converges quite rapidly for realistic initial estimates of the solution. Its primary drawback is the excessive computational effort required to form the stiffness matrix and invert it at each iterative cycle.

Most investigators [55-57] now use a modified Newton-Raphson procedure wherein the stiffness matrix is held constant for a number of iterations and then updated after the convergence rate begins to deteriorate. Moreover, various extrapolation and relaxation procedures can be incorporated into the iterative cycle to insure and accelerate convergence [55].

Murray and Wilson [58] determine the unbalance in nodal forces at the end of a load increment and then use an iterative approach to reduce the unbalance to zero. Their procedure was essentially a modified Newton-Raphson approach. References [55] and [59] formulate the incremental equations so that the out-of-balance in the equilibrium forces was explicitly taken into account. The resulting self-correcting incremental procedure had the advantage in that it was as easy to apply as the standard incremental procedure but was much more accurate.

Wood and Zienkiewicz [60] developed a geometrically nonlinear analysis in either a total Lagrangian or an Eulerian coordinate system, the former in terms of the initial position; the latter in terms of the final deformed state. By adopting a continuum approach, employing a parilinear isoparametric element, the formulation was applicable to structures consisting of straight or curved members. Displacements and rotations were unrestricted in magnitude. The nonlinear equilibrium equations were solved using the Newton-Raphson method.

Sabir and Djoudi [61, 62] used the foregoing method for the analysis of shallow shells and plates. A p-version FE model was developed by Woo et al. [63] based on degenerate shell element for the analysis of orthotropic laminated plates. In the nonlinear formulation of the model, the total Lagrangian formulation was adopted with moderately large deflections and small rotations being accounted for in the sense of von Karman hypothesis. Then, the hierarchical FE method, an eight-node hexahedral isoparametric FE, 3 nodes, 18-degree of freedom flat triangular plate FE, was used for the analysis of rectangular plates [52-64].

Cho et al. [65] applied a solid shell element model with six degrees of freedom per node for the buckling and postbuckling analysis of geometrically nonlinear shell structures. This model allows changes in the thickness direction and does not require rotational angles or parameters for the description of the kinematics of deformation. The FE model was constructed based on the assumed strain formulation in which an assumed strain field was chosen to prevent locking while maintaining kinematic stability.

Kumar et al. [66] developed a mixed beam FE for three-dimensional nonlinear analysis of steel frames. The kinematics of deformation of the element includes finite rotation and warping of the cross-section due to torsion. The material inelasticity was based on a two-space model that included the effect of shear stresses due to uniform torsion in addition to normal stresses due to axial force, biaxial bending and bimoment. The formulation was based on a two-field (displacement and generalized stress) Hellinger-Reissner (HR) variational principle. The interpolation of the generalized stresses along the element length was based on the geometrically-exact nonlinear governing differential equations of equilibrium.

Levy and Spillers [67] used the FE method for the geometrically nonlinear analysis of structures. Using the deformed configuration implied nonlinear analysis in the work which would typically involve applying Newton's method to compute the effect of a load perturbation upon some given initial state.

The FE method has become firmly established as an engineering tool for the linear and nonlinear analysis of plate and shell structures. The predominant advantage of the FE method lies in its applicability to analyze complex structures with varying thickness, difficult boundary conditions and arbitrary loading. However, from the engineering point of view, the use of the FE method for structural analysis has drastically increased the computation time which may not be affordable.

c) *Finite strip method*: The FS method for a plate undergoing large deflection has been formulated on the basis of the non-linear relationship of strain and displacement which took into account the interaction between out of plane and in plane deformations [77-80]. The selection of the non-linear terms in the strain-displacement relation can be somewhat different depending on the primary components of displacements chosen for a strip to simulate a plate or a web member in a box girder.

Plank [64] reported on the analyses of the inelastic stability of stiffened panels carried out by the FS method. Then, the report on FS analysis of geometrically non-linear structures was made by Delcourt [76] in her thesis.

Gierlinski et al. [79] discussed a particular difficulty with the FS method when analyzing structures whose non-linear load deflection curves contain maxima. The commonly used method to solve this problem was to replace load incrementation with displacement incrementation. However, such a strategy did not appear to work with classical FS, because the continuous series representation of displacements does not allow localized displacements to be imposed on structures. They proposed to overcome this difficulty by using an improved iteration strategy of selecting variable load increments on both the loading and the unloading curves.

The large deflection elastic-plastic analysis of plate structures and cylindrical shells under uniform loads were carried out by Abayakoon et al. [81] and Kumar et al. [82]. The work has been later extended by Khalil et al. [83] to investigate the large deflection, elastic-plastic dynamic response of air-blast loaded stiffened plates. The loads have been modeled as uniformly distributed time dependent pressures.

Dawe and coworkers [84-86] have applied the geometrically non-linear FS method to the large deflection problems of Mindlin plates and laminated plates. Then Wang and Dawe [87] developed a semi-analytical FS method for the analysis of the overall, geometrically non-linear, elastic behavior of diaphragm-supported prismatic plate structures which could be made of composite laminated material and could have initial geometric imperfections. The development was made in the contexts of both first-order shear deformation and classical plate theories. Further work was carried out by Dawe et al. [88-90]. Sekulovic and Milasinović [91] presented a FS analysis of plates and folded plates taking into account the geometrical non-linearities and the effects of creep.

Cheung et al. [92] applied the FS to model the non-linear behavior of cable-stayed bridges. Then Cheung and Wenchang [93] developed a modified FS method for the geometrically nonlinear analysis of plates. The initial linear elastic stiffness matrix of the plate was kept unchanged during the iteration to make the best use of the orthogonal property between different eigenfunctions and enhance the efficiency of the analysis. However, the bending stiffness matrix of the plate had to be multiplied by an amplification factor to ensure the convergence of the iteration. Then, Cheung

and Tham [94] used spline FS method for the geometrically nonlinear analysis of plates and shells.

Kwon et al. [95, 96] further developed the spline FS method to handle local, distortional and overall buckling modes in the post-buckling range, and the interaction between the various modes. The method also allowed for geometric imperfections, arbitrary loading and complicated support conditions. Advanced theories based on the convective curvilinear coordinate system were used to carry out a non-linear analysis for plates and shells by Zhu and Cheung [97, 98].

Akhras et al. [99] studied the geometrically nonlinear FS analysis of laminated composite plates. The higher order shear deformation theory was used for different plate thicknesses, fiber orientations and boundary conditions. The modified Newton-Raphson method was employed for the solution process.

2.4 Structural Optimization

Since the inception of engineering it is the most significant aim of structural engineers to construct structures which are lightest and strongest. Hence, some changes in structure dimensions and shape should be made. For example very low in-plane load carrying capacity of straight plates can be increased to very high values by adding stiffener elements to plate surface. Including only stiffener elements is not adequate to use plate volume very efficiently. In this regard, size and shape optimization procedures should be carried out to increase in-plane load carrying capacity of such structures, efficiently.

In engineering science, mathematical programming methods are the early and powerful methods that engineers have used since the inception of computer applications. Structural optimization using two dimensional representations was first investigated by Zienkiewicz and Campbell [100]. Since then much work has been reported.

Levy and Ganz [101] analyzed plates using variational calculus to obtain the optimality condition stating that the thickness was proportional to the strain energy density. They used truncated Fourier series solution to obtain an optimal shape.

Hojjat and Kok [102] developed a prototype knowledge based expert system for the optimum design of steel plate girders used in highway bridges. They developed a mathematical optimization algorithm for the minimum weight design of plate girders using a generalized geometric programming technique.

Jarmai et al. [103] investigated optimal design of cylindrical orthogonally stiffened shell member of an offshore fixed platform truss, loaded by axial compression and external pressure using various mathematical programming the methods. In their optimization and design they used ring stiffeners of welded box sections and stringers of halved rolled I-type sections.

Bedair [104] developed approaches for the minimum weight design of stiffened plates. He described an alternative energy based approach for the stability analysis of multi-stiffened plates under uniform compression and idealized the structure as being assembled plate and beam elements rigidly connected at their junctions. Then, he derived the strain energy components for the plate and the stiffener elements in terms of out-of and in-plane displacement functions and used sequential quadratic programming to find the buckling load of the structure for given plate/stiffener geometric proportions.

Two main fundamental aims of computer applications are creating algorithms that have short run time and capability of finding optimal solutions. With the magnificent improvement of computers some other alternative algorithms are developed for optimization problems which are called heuristic methods and improved in the last three decades. The most significant characteristic of heuristic methods is the fast running times of their algorithms.

Bisagni and Lanzi [105] investigated the post buckling optimization procedure for the design of composite stiffened panels subjected to compression loads using neural networks. To overcome too expensive analyses from a computational point of view,

he developed an optimization procedure. It was based on a global approximation strategy, where the structure response was given by a system of neural networks trained by means of FE analyses, and on genetic algorithms that proves particularly profitable due to the presence of integer variables.

Kang and Kim [106] studied the minimum weight design of compressively loaded composite plates and composite stiffened panels under constrained post buckling strength. As an optimization technique, they used a modified Genetic Algorithm to find the optimum points.

2.5 Summary of Literature Survey

In this chapter, a summary of 106 previous researches on the geometric nonlinear analysis of plates and shells are given. In early studies, linear buckling analysis has been investigated which consider small deformation theory. Analytical and numerical methods have been used to solve this problem. Then geometric nonlinear analysis which considers large deformation theory has been employed. Some researchers studied nonlinear problems using different methods and different linear incremental solutions. In these methods it is found that FS is a useful method for the linear and geometric nonlinear analysis of prismatic and stiffened plates.

CHAPTER 3

LINEAR BUCKLING FORMULATION OF PLATES

3.1 Introduction

A structure that is initially stable may lose stability as it moves to another equilibrium position when the control parameter(s) change. Under certain conditions, that transition is associated with the occurrence of a critical point (see Figure 3.1).

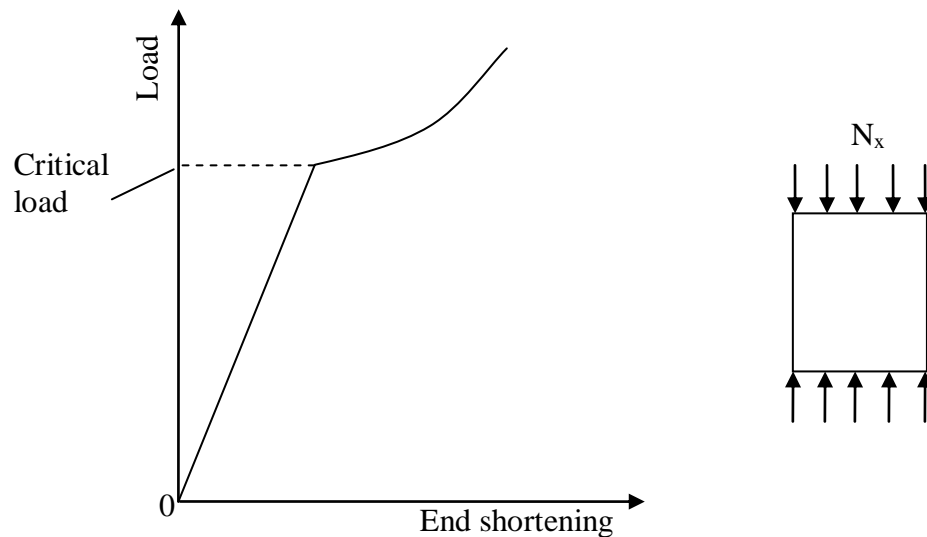


Figure 3.1 Classical buckling

For structures that occur in aerospace, civil and mechanical engineering, bifurcation points are practically more important than limit points. Consequently, attention will be initially directed to the phenomena of bifurcation or branching of equilibrium states, a set of phenomena also informally known as linear buckling.

For the linear buckling analysis of structures, which have constant geometrical properties along a particular direction, FS method is used. Such prismatic structures are very common in plate and shell problems where the transverse cross-section of the structure often remains constant in the direction of compression. If the material properties of the structures are also constant in the same direction, the buckling analysis can be simplified by the combined use of FEs and Fourier expansions to model the transverse and longitudinal behaviors, respectively.

3.2. Structural Theories

Thin shell theories neglect transverse shear and rotary inertia effects and consequently may yield incorrect results, especially for higher values of the ratio of the thickness-to-minimum span, particularly for higher modes. In addition, many structures may not be considered as a ‘thin plate’. In this regard transverse shear strains in plates cannot be ignored. Therefore, the plate theory is more suitable in general, and the elements developed based on the Mindlin-Reissner plate theory are more practical and useful for practical engineering problems. For example, in plate analysis, the buckling loads are overestimated for all buckling modes in shear-weak situations and for the higher buckling modes in shear-stiff cases. In such circumstances, the effects of shear deformation and rotatory inertia should be taken into account.

The Mindlin-Reissner shell theory allows for transverse shear deformation effects and thus offers a more attractive analysis than the classical Kirchhoff-Love thin shell theory. The main assumptions are that:

- Displacements are small compared to the shell thickness,
- Stress component normal to the mid-surface is negligible,
- Normals to the mid-surface before deformation remain straight but not necessarily normal to the mid-surface after deformation [107].

It is well known that displacement-based Mindlin-Reissner FSs require only $C(0)$ continuity of the displacements and independent normal rotations between adjacent elements. This provides an important advantage over FS based on classical

The displacement components u_ℓ and w_ℓ may be written in terms of global displacements u and w in the x and z directions as

$$\begin{aligned} u_\ell &= u \cos \alpha + w \sin \alpha \\ w_\ell &= -u \sin \alpha + w \cos \alpha \end{aligned} \quad (3.1)$$

where α is the angle between the x and ℓ axes (see Figure 3.2). The radius of curvature R may be obtained from the expression

$$\frac{d\alpha}{d\ell} = -\frac{1}{R} \quad (3.2)$$

Note that the displacement components v_ℓ and v coincide.

The strain energy for a typical curved Mindlin-Reissner strip e of length b shown in Figure 3.2 is given in terms of the global displacements u, v, w and the rotations ϕ and ψ of the mid-surface normal in the ℓn and yn planes respectively by the expressions (3.1)

$$U^e = \frac{1}{2} \int_0^b \int_{\ell^e} (\boldsymbol{\varepsilon}_m^T \mathbf{D}_m \boldsymbol{\varepsilon}_m + \boldsymbol{\varepsilon}_b^T \mathbf{D}_b \boldsymbol{\varepsilon}_b + \boldsymbol{\varepsilon}_s^T \mathbf{D}_s \boldsymbol{\varepsilon}_s) d\ell dy \quad (3.3)$$

where $\boldsymbol{\varepsilon}_m$, $\boldsymbol{\varepsilon}_b$ and $\boldsymbol{\varepsilon}_s$ are the membrane, bending or curvatures and transverse shear strains respectively and given in Appendix A for plate and shell in straight and curved planforms.

For an isotropic material of elastic modulus E , Poisson's ratio ν and thickness t , membrane, flexural, and shear rigidity matrices have been given in Appendix A. where κ^2 is the shear modification factor and is usually taken as $5/6$ for an isotropic material.

3.3.2 Potential energy of the applied inplane stresses

Buckling occurs when a structure converts inplane strain energy into strain energy of bending with no change in externally applied load. A critical condition, at which

buckling impends, exist when it is possible that the deformation state may change slightly in a way that makes the loss in inplane strain energy numerically equal to the gain in bending strain energy. In a thin-walled structure such as a shell, inplane stiffness is typically orders of magnitude greater than bending stiffness. Accordingly, small inplane deformations can store a large amount of strain energy, but comparatively large lateral deflections and cross-section rotations are needed to absorb this energy in bending deformations.

The potential energy of the applied inplane stresses σ_ℓ^0 , σ_y^0 and $\tau_{\ell y}^0$ arises from the action of the applied stresses on the corresponding second order strains ε_ℓ^{nl} , ε_y^{nl} , $\gamma_{\ell y}^{nl}$ are taken from Dawe and Peshkam [19]. The potential energy of the shell of volume V is

$$V_g = \int_V (\sigma_\ell^0 \varepsilon_\ell^{nl} + \sigma_y^0 \varepsilon_y^{nl} + \tau_{\ell y}^0 \gamma_{\ell y}^{nl}) dV \quad (3.4)$$

integrating through the thickness, this becomes

$$\begin{aligned} V_g = & \frac{1}{2} t \iint_A \left[\sigma_\ell^0 \left[\left(\frac{\partial u}{\partial \ell} \right)^2 + \left(\frac{\partial v}{\partial \ell} \right)^2 + \left(\frac{\partial w}{\partial \ell} \right)^2 \right] + \sigma_y^0 \left[\left(\frac{\partial u}{\partial y} \right)^2 + \left(\frac{\partial v}{\partial y} \right)^2 + \left(\frac{\partial w}{\partial y} \right)^2 \right] \right. \\ & + 2\tau_{\ell y}^0 \left[\frac{\partial u}{\partial \ell} \frac{\partial u}{\partial y} + \frac{\partial v}{\partial \ell} \frac{\partial v}{\partial y} + \frac{\partial w}{\partial \ell} \frac{\partial w}{\partial y} \right] \\ & + \frac{t^2}{12} \left\{ \sigma_\ell^0 \left[\left(\frac{\partial \phi}{\partial \ell} \right)^2 + \left(\frac{\partial \psi}{\partial \ell} \right)^2 \right] + \sigma_y^0 \left[\left(\frac{\partial \phi}{\partial y} \right)^2 + \left(\frac{\partial \psi}{\partial y} \right)^2 \right] \right. \\ & \left. \left. + 2\tau_{\ell y}^0 \left[\frac{\partial \phi}{\partial \ell} \frac{\partial \phi}{\partial y} + \frac{\partial \psi}{\partial \ell} \frac{\partial \psi}{\partial y} \right] \right\} d\ell dy \quad (3.5) \end{aligned}$$

In equation (3.5), the terms involving the first derivative of w , ϕ and ψ represent the out of plane destabilizing influence of the prescribed stresses. The remaining terms which are dependent upon first derivatives of u and v , are in plane destabilizing influences. The prescribed inplane shear stress $\tau_{\ell y}$ are rarely applied to the present type of structures, and is not considered in the present study.

$$\begin{aligned}
V_g^e = \frac{1}{2} \int_0^b \int_{\ell^e} \left(t \left\{ \sigma_\ell^0 \left[\left(\frac{\partial u}{\partial \ell} \right)^2 + \left(\frac{\partial v}{\partial \ell} \right)^2 + \left(\frac{\partial w}{\partial \ell} \right)^2 \right] + \sigma_y^0 \left[\left(\frac{\partial u}{\partial y} \right)^2 + \left(\frac{\partial v}{\partial y} \right)^2 + \left(\frac{\partial w}{\partial y} \right)^2 \right] \right\} \right. \\
\left. + \frac{t^3}{12} \left\{ \sigma_\ell^0 \left[\left(\frac{\partial \phi}{\partial \ell} \right)^2 + \left(\frac{\partial \psi}{\partial \ell} \right)^2 \right] + \sigma_y^0 \left[\left(\frac{\partial \phi}{\partial y} \right)^2 + \left(\frac{\partial \psi}{\partial y} \right)^2 \right] \right\} \right) d\ell dy \quad (3.6)
\end{aligned}$$

3.3.3 Finite strip idealization

Using n -noded, $C(0)$ strips, the global displacements and rotations may be interpolated within each strip in terms of truncated Fourier series along direction y , in which both the material and geometrical properties of the plate are taken to be constant,

$$\begin{aligned}
u(\ell, y) &= \sum_{p=p_1}^{p_2} u^p(\ell) S_p; & v(\ell, y) &= \sum_{p=p_1}^{p_2} v^p(\ell) C_p \\
w(\ell, y) &= \sum_{p=p_1}^{p_2} w^p(\ell) S_p; & \phi(\ell, y) &= \sum_{p=p_1}^{p_2} \phi^p(\ell) S_p \\
\psi(\ell, y) &= \sum_{p=p_1}^{p_2} \psi^p(\ell) C_p \quad (3.7)
\end{aligned}$$

where $C_p = \cos(p\pi y/b)$ and $S_p = \sin(p\pi y/b)$, u^p, v^p, w^p, ϕ^p and ψ^p are displacement and rotation amplitudes for the p^{th} harmonic term. This corresponds to a single diaphragm support at the ends of the structure at $y=0$ and $y=b$, so that $v = w = \phi = 0$. As shown later, this will lead to an uncoupling of each harmonic term which in turn leads to an economic solution. Note that the strip displacement and rotation fields are generally expressed as a summation of a set of contributions from a lower limit p_1 to an upper limit p_2 . In the present work, as there is no coupling between the harmonics, p_1 and p_2 coincide. For many cases taking $p_1 = p_2 = 1$ provides the lowest buckling mode; however, in some cases p_1 and p_2 may be associated with a higher mode.

The next step is to discretize the displacement and rotation amplitudes (which are functions of the ℓ -coordinate only) using an n -noded FE representation so that within a strip e the amplitudes can be written as

$$\begin{aligned} u^p(\ell) &= \sum_{i=1}^n N_i u_i^p; & v^p(\ell) &= \sum_{i=1}^n N_i v_i^p; & w^p(\ell) &= \sum_{i=1}^n N_i w_i^p \\ \phi^p(\ell) &= \sum_{i=1}^n N_i \phi_i^p; & \psi^p(\ell) &= \sum_{i=1}^n N_i \psi_i^p \end{aligned} \quad (3.8)$$

where u^p, v^p, w^p, ϕ^p and ψ^p are typical nodal degrees of freedom associated with node i and harmonic p .

Thus, the process is equivalent to dividing the structure into longitudinal elements (or strips) so that each strip has a certain number of nodes (one more accurately, nodal lines) associated with its transverse direction. The displacement field is defined longitudinally by the Fourier expansion of (3.7) and transversely by the FE discretization of (3.8). Substituting (3.8) into (3.7) it is possible to write

$$\mathbf{u} = \sum_{p=p_1}^{p_2} \sum_{i=1}^n \mathbf{N}_i^p \mathbf{d}_i^p \quad (3.9)$$

where

$$\mathbf{u} = [u, v, w, \phi, \psi]^T$$

$$\mathbf{d}_i^p = [u_i^p, v_i^p, w_i^p, \phi_i^p, \psi_i^p]^T$$

and

$$\mathbf{N}_i^p = \begin{bmatrix} N_i S_p & 0 & 0 & 0 & 0 \\ 0 & N_i C_p & 0 & 0 & 0 \\ 0 & 0 & N_i S_p & 0 & 0 \\ 0 & 0 & 0 & N_i S_p & 0 \\ 0 & 0 & 0 & 0 & N_i C_p \end{bmatrix} \quad (3.10)$$

$N_i(\xi)$ is the shape function associated with node i [2]. These elements are essentially isoparametric so that

$$x = \sum_{i=1}^n N_i x_i; \quad y = \sum_{i=1}^n N_i y_i; \quad t = \sum_{i=1}^n N_i t_i \quad (3.11)$$

where x_i and y_i are typical coordinates of node i and t_i is the thickness at node i .

If $p \neq q$ because of the orthogonality conditions on assembly of the contributions to the total potential energy $U + V$ from all of the strips and subsequent minimization with respect to the nodal values the following eigenvalue expression is obtained for each harmonic p

$$[\mathbf{K}^{pp} + \lambda^p \mathbf{K}_\sigma^{pp}] \bar{\mathbf{d}}^p = 0 \quad (3.12)$$

where λ^p is the load factor by which the inplane stress components σ_x^0 and σ_y^0 are multiplied to produce instability and $\bar{\mathbf{d}}^p$ is the associated buckling mode. These submatrices have the forms

$$[\mathbf{K}_{ij}^e]^{pq} = \int_0^b \int_{-1}^{+1} \left([\mathbf{B}_{mj}^p]^T \mathbf{D}_m \mathbf{B}_{mj}^q + [\mathbf{B}_{bj}^p]^T \mathbf{D}_b \mathbf{B}_{bj}^q + [\mathbf{B}_{sj}^p]^T \mathbf{D}_s \mathbf{B}_{sj}^q \right) J d\xi dy \quad (3.13)$$

$$\begin{aligned} [\mathbf{K}_{\sigma ij}^e]^{pq} = & \int_0^b \int_{-1}^{+1} \left(t [\mathbf{S}_{ui}^p]^T \mathbf{H} \mathbf{S}_{uj}^q + t [\mathbf{S}_{vi}^p]^T \mathbf{H} \mathbf{S}_{vj}^q + t [\mathbf{S}_{wi}^p]^T \mathbf{H} \mathbf{S}_{wj}^q \right) \\ & + \left(\frac{t^3}{12} [\mathbf{Q}_i^p]^T \mathbf{H} \mathbf{Q}_j^q + \frac{t^3}{12} [\mathbf{R}_i^p]^T \mathbf{H} \mathbf{R}_j^q \right) J d\xi dy \end{aligned} \quad (3.14)$$

and $\mathbf{B}_{mi}^p, \mathbf{B}_{bi}^p$ and \mathbf{B}_{si}^p are the membrane, bending and shear strain displacement matrices associated with harmonic p , node i and Jacobian J , geometric stiffness matrices $\mathbf{S}_{ui}^p, \mathbf{S}_{vi}^p, \mathbf{S}_{wi}^p, \mathbf{Q}_i^p, \mathbf{R}_i^p$ and the inplane stress matrix \mathbf{H} are given in Appendix B.

3.4 Plate Example

The first set of examples is concerned with the buckling of plates with various combinations of boundary conditions. For the sake of convenience we adopt the following notations to describe the boundary conditions for the plates analyzed in this section: **A/B/C/D** which implies (boundary condition on side $y = 0$) / (boundary condition on side $x = a$) / (boundary condition on side $y = b$) / (boundary condition on side $x = 0$). A hard simply supported edge (i.e. with the lateral displacements and tangential edge rotations constrained to zero) is represented by **S_h**, a clamped edge by **C** and a free edge **F**. Because of the nature of the FS Fourier series representations of

the displacements and rotations, hard simple supports always occur at the ends $y = 0$ and $y = b$ but the other two edges can be arbitrarily restrained.

3.4.1 Square simply supported ($S_h / S_h / S_h / S_h$) isotropic plates under uniaxial stress

A set of square simple supported isotropic plates under uniaxial stress σ_y^0 is now considered to illustrate the convergence characteristics of various FSs. The plates have thickness to span ratios t/b varying from 0.001 to 0.2. The results are represented in non-dimensional form using the buckling factor K which has the following form

$$K = \frac{(\sigma_y^0)_{cr} b^2 t}{\pi^2 D} \quad (3.15)$$

where $(\sigma_y^0)_{cr}$ is the critical value of the longitudinal axial stress and the flexural rigidity is written as

$$D = \frac{Et^3}{12(1-\nu^2)} \quad (3.16)$$

in which ν is the Poisson's ratio, E is the elastic modulus. Poisson's ratio ν is taken as 0.3.

The results generated by the present approach are given in Table 3.1 in the form of a convergence study with respect to both type of strip and numbers of degrees of freedom. Linear, quadratic and cubic strips are used with identical sets of numbers of degrees of freedom.

It can be seen from Table 3.1 that results obtained using 3-noded quadratic strips are almost identical to those obtained using 4-noded cubic strips and very close to the values obtained by Dawe and Roufaeil [17]. Linear, quadratic and cubic strips are used with identical sets of numbers of degrees of freedom. For the thicker plates the

thin plate solutions overestimate the buckling load. The lowest buckling load for each plate occurs with a single longitudinal half-wave so that $p_1 = p_2 = 1$.

Table 3.1 Buckling factors for a set of square ($S_h / S_h / S_h / S_h$) simply supported isotropic plates under uniaxial stress

		Buckling factors, K				
Strip type	dof	$t/b = 0.001$	$t/b = 0.005$	$t/b = 0.1$	$t/b = 0.15$	$t/b = 0.2$
Linear	17	4.00212	3.92916	3.72754	3.43954	3.11149
	71	3.99997	3.92861	3.73106	3.44804	3.12449
	143	3.99997	3.92867	3.73132	3.44853	3.12520
Quadratic	17	3.99998	3.92860	3.73103	3.44797	3.12440
	71	3.99997	3.92870	3.73141	3.44869	3.12543
	143	3.99997	3.92870	3.73141	3.44869	3.12543
Cubic	17	3.99997	3.92869	3.73138	3.44863	3.12534
	71	3.99997	3.92870	3.73141	3.44869	3.12543
	143	3.99997	3.92870	3.73141	3.44869	3.12543
Thin plate [17]		4.00000	4.00000	4.00000	4.00000	4.00000
MR [17]		4.000	3.929	3.731	3.449	3.125

3.4.2 Rectangular isotropic plates under uniaxial stress

The second set of examples is concerned with the buckling of rectangular plates with various boundary conditions, aspect ratios and thickness to span ratios. The geometry and boundary conditions of the rectangular plates subject to uniform axial stress are shown in Figure 3.3.

Two thickness to span ratios are considered; for a moderately thick plate, a thickness-to-span ratio $t/a = 0.1$ is adopted whereas for a thin plate a value of $t/a = 0.01$ is used. The results are presented in terms of non-dimensional buckling factors K , defined in (3.15). The following boundary conditions are examined:

a-) ($S_h / C / S_h / C$) with aspect ratios $a/b = 0.6$, 1.0 and 1.4

b-) ($S_h / S_h / S_h / F$) with aspect ratios $a/b = 0.5, 1.0$ and 1.5

c-) ($S_h / F / S_h / F$) with aspect ratios $a/b = 1.0, 2.0$ and 4.0

It is generally assumed that Poisson's ratio $\nu = 0.3$. However, in the case of the plate with ($S_h / C / S_h / C$) $\nu = 0.25$.

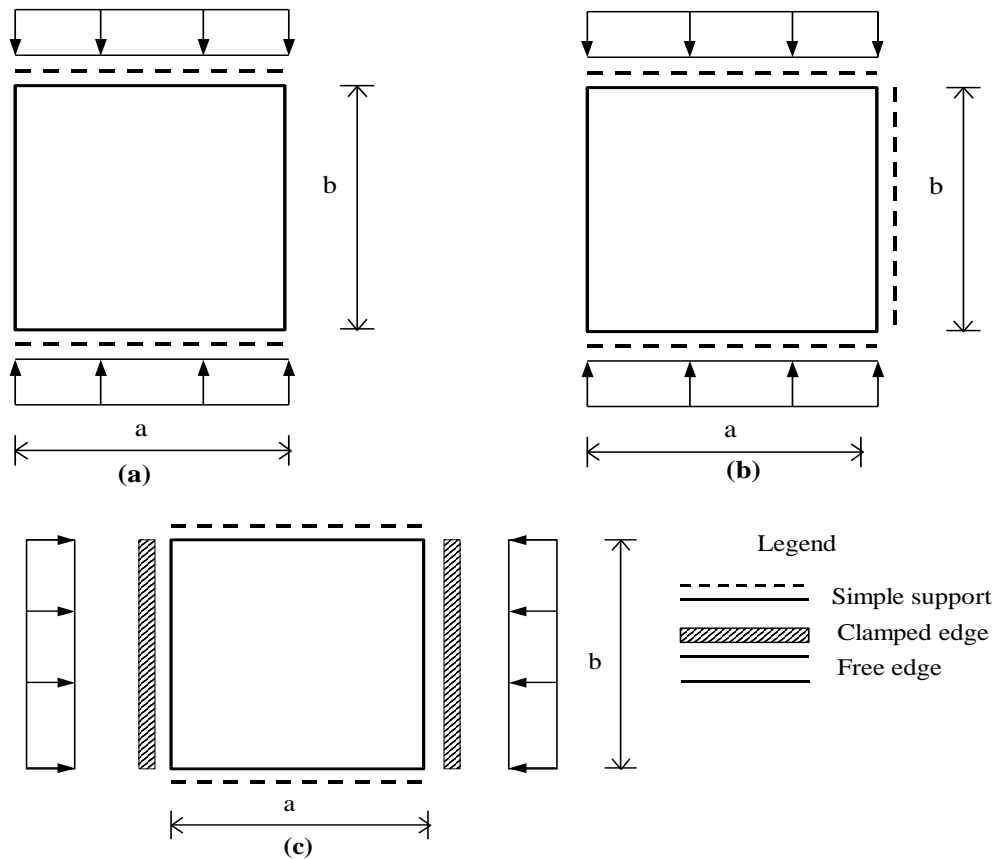


Figure 3.3 (a) ($S_h / F / S_h / F$) plate under uniaxial stress σ_y^0 , (b) ($S_h / S_h / S_h / F$) plate under uniaxial stress σ_y^0 and (c) ($S_h / C / S_h / C$) plate under uniaxial stress σ_x^0

Table 3.2 to 3.4 list the buckling factor K for the different boundary conditions and each table contains results from solutions obtained using cubic strips for both thin and moderately thick plates. The plates are analyzed using ten 4-noded FSs.

When transverse shear deformation is taken into account in the buckling analysis of thick plates slightly lower values of buckling load are usually obtained compared with the values predicted using formulations ignoring transverse shear deformation.

It can be seen from Tables 3.2 and 3.3 that the results are identical to those obtained by Dawe and Roufaeil [17] and are very close to the closed form plate solution.

Table 3.2 Buckling factors for a set of rectangular ($S_h / C / S_h / C$) isotropic plates under uniaxial stress

		Buckling factors, K		
b/a	t/a	Present FS	MR FS[17]	Thin plate[17]
0.6	0.01	14.778	13.361	13.38
	0.1	11.135	11.611	13.38
1.0	0.01	6.731	6.732	6.74
	0.1	5.773	5.773	6.74
1.4	0.01	5.207	5.443	5.45
	0.1	4.511	4.516	5.45

Results for ($S_h / F / S_h / F$) boundary condition are given in Table 3.4. It can be seen that convergence of buckling factor calculated using present approach is again satisfactory with respect to Euler value's for thin and thick plates. The percentage differences between the computed buckling and corresponding Euler formula values range from 0.4% to 5%. The present results and Euler formula values are getting closer at higher aspect ratios. In all cases, plates buckle with one longitudinal half-wave and so that $p_1 = p_2 = 1$.

Table 3.3 Buckling factors for a set of rectangular ($S_h / S_h / S_h / F$) isotropic plates under uniaxial stress

		Buckling factors, K		
b/a	t/a	Present FS	MR FS[17]	Thin plate[17]
0.5	0.01	4.394	4.398	4.4
	0.1	3.835	3.839	4.4
1.0	0.01	1.432	1.433	1.44
	0.1	1.364	1.366	1.44
2.0	0.01	0.696	0.698	0.698
	0.1	0.675	0.677	0.698

Table 3.4 Buckling factors for a set of rectangular ($S_h / F / S_h / F$) isotropic plates under uniaxial stress

		Buckling factors, K	
b/a	t/a	Present FS	Euler formula
0.5	0.01	3.922	3.735
	0.1	3.451	3.750
1.0	0.01	0.967	0.934
	0.1	0.933	0.938
2.0	0.01	0.237	0.233
	0.1	0.235	0,234

3.5 Stiffened Plate Example

To check that the present formulation is applicable to prismatic structures, the critical buckling load of the stiffened panel given by Murphy et al. [3] are investigated. The buckling performance of panels with three sub-stiffening subjected to longitudinal compression was analyzed and experimentally tested by Murphy et al. [3]. The experiments were also simulated using non-linear FE analyses. The FE model employed 8-node quadrilateral thick shell elements (MARC type 22). Changes in thickness (pad-ups, sub-stiffeners) were modelled as changes in element thickness; the corresponding offset of the neutral axis was simply neglected.

Figure 3.4 shows the geometry and dimensions of the panel which is simply supported at two opposite ends with the other edges free. The plate is loaded in uniform compression in the stiffeners direction.

The results given by Murphy et al. [108] are used to check the performance of the present formulation. The baseline stiffened panels (Profile B) along with the three ‘proof of concept’ specimens (namely Profile 1, 2 and 3) are analyzed using 84 cubic strips with a total of 1620 degrees of freedom. The results of the analysis, the corresponding experimental values and FE results [108] are shown in Table 3.5. Using FS method, the initial buckling modes of all profiles were successfully reproduced (see Figure 3.4). Given the uncertainty on the skin buckling loads (large differences between experiment and FE, plus the slight difference in boundary

conditions between FS on the one hand and FE and experiment on the other), the reproduction of the skin buckling loads were also considered sufficiently accurate.

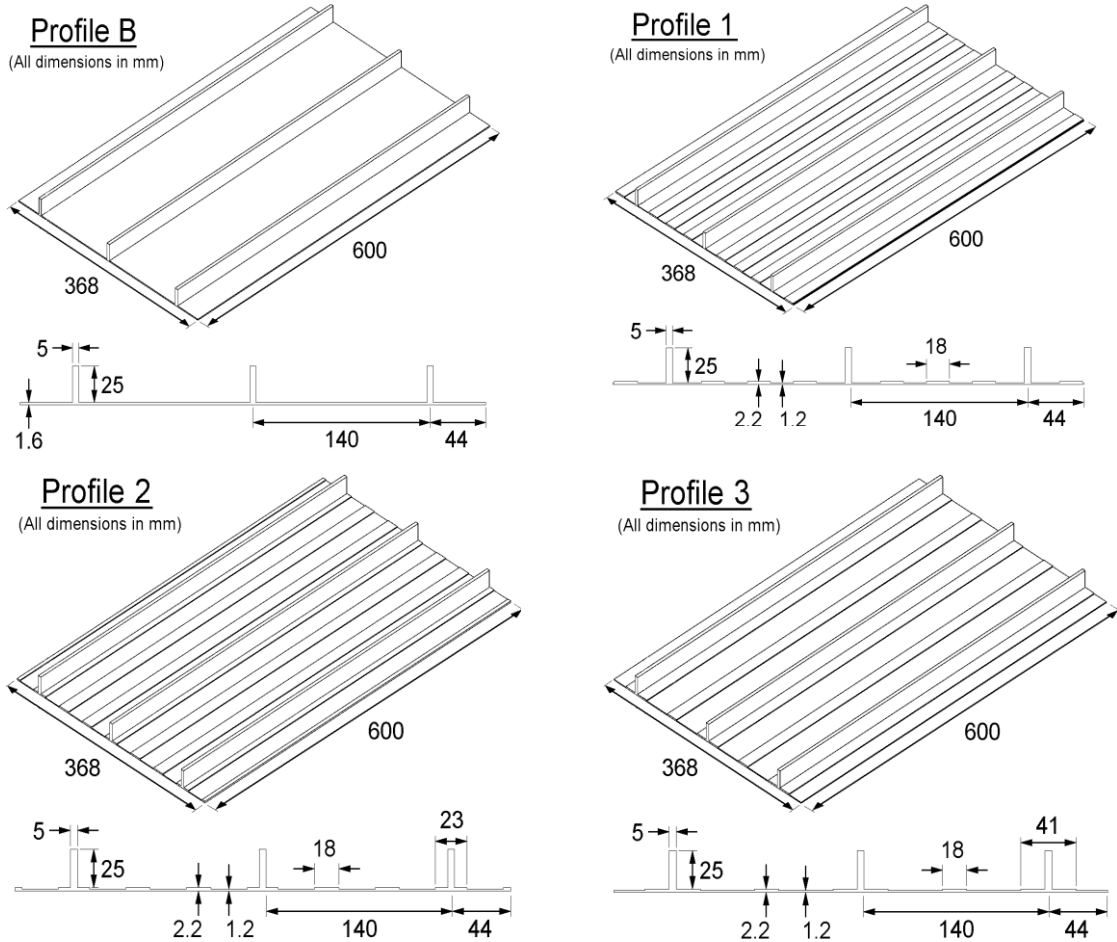


Figure 3.4 Isotropic baseline stiffened panels (Profile B) along with the three ‘proof of concept’ specimens (namely Profile 1, 2 and 3) (all dimensions in mm).

Table 3.5 Buckling loads for profiles

	Buckling load kN			
	Profile B	Profile 1	Profile 2	Profile 3
FE solution [108]]	57.4	57.3	57.7	58.2
Experimental sol.[108]	69.3	62.7	82.5	77.7
FS solution	54.8	54.8	61.5	58.5

The material used in Profile B stiffened plate has 71000 MPa modulus of elasticity and 0.33 Poisson's ratio. The Profile B has three stiffeners subjected to buckling load 54.8 kN at sixth harmonic number. The FE and experimental results [108] are 57.4 kN and 69.3 kN, respectively, which are in agreement with one another for the lowest buckling mode shown in Figure 3.5.

In Profile 1 the resulting buckling load of 54.8 kN compares well with the values of 57.3 kN and 62.7 kN obtained using the FE and experimentally, respectively. The lowest buckling load is obtained within $p_1 = p_2 = 5$ in Figure 3.6. The material used in Profile 1 and Profile 2 stiffened plate has 75000 MPa modulus of elasticity and 0.33 Poisson's ratio.

The Profile 2 has three stiffeners with four pads and two half pads yielding a buckling load 61.5 kN. The FE and experimental results [108] as shown in Table 3.5 are 57.7 kN and 82.5 kN, respectively. A good agreement is found among the FE, experimental and FS solutions. The lowest buckling mode is shown in Figure 3.7.

The resulting buckling load of 58.5 kN in Profile 3 which has modulus of elasticity $E=71000$ MPa and Poisson's ratio $\nu=0.33$, compares well with the values of 58.2 kN and 77.7 kN as shown in Table 3.5 obtained using the FE and experimental method, respectively. This agrees with the shape of the buckling modes obtained using the FE and FS solutions as seen in Figure 3.8.

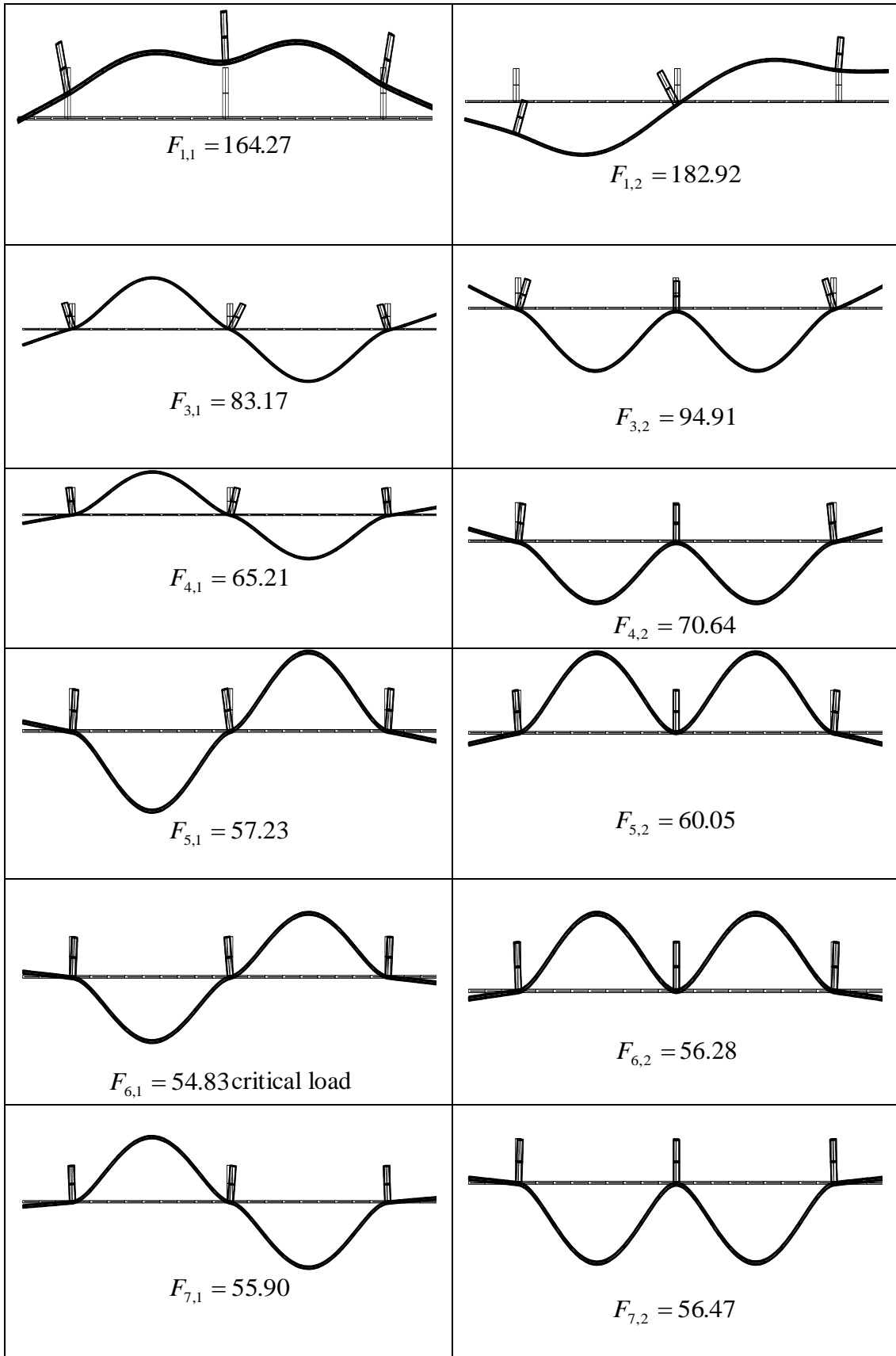


Figure 3.5 Profile B-Buckling loads and corresponding buckling modes (mode shapes are plotted for mid span, i.e at $x = a/2 = 300$)

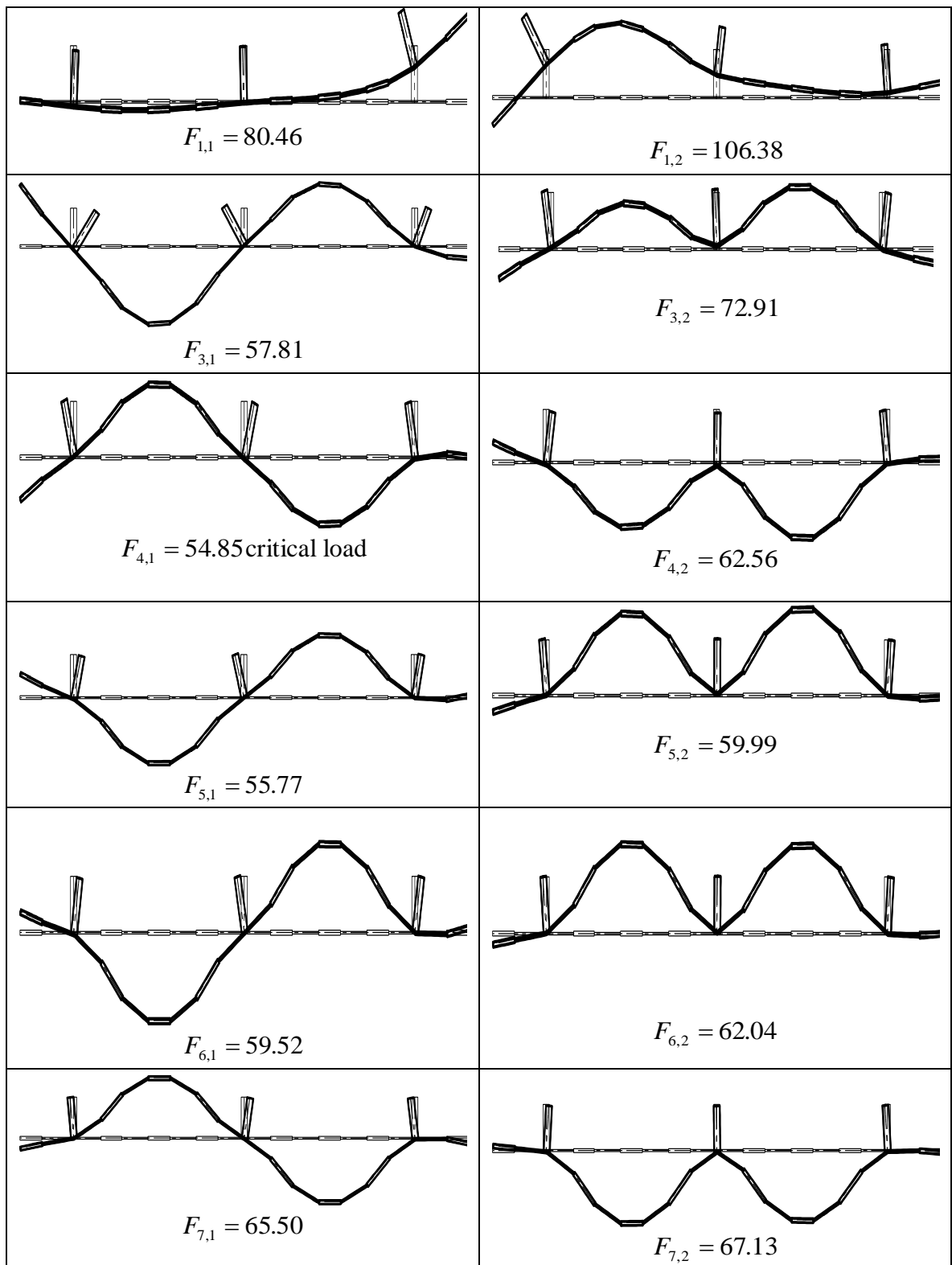


Figure 3.6 Profile 1-Buckling loads and corresponding buckling modes (mode shapes are plotted for mid span, i.e at $x = a/2 = 300$)

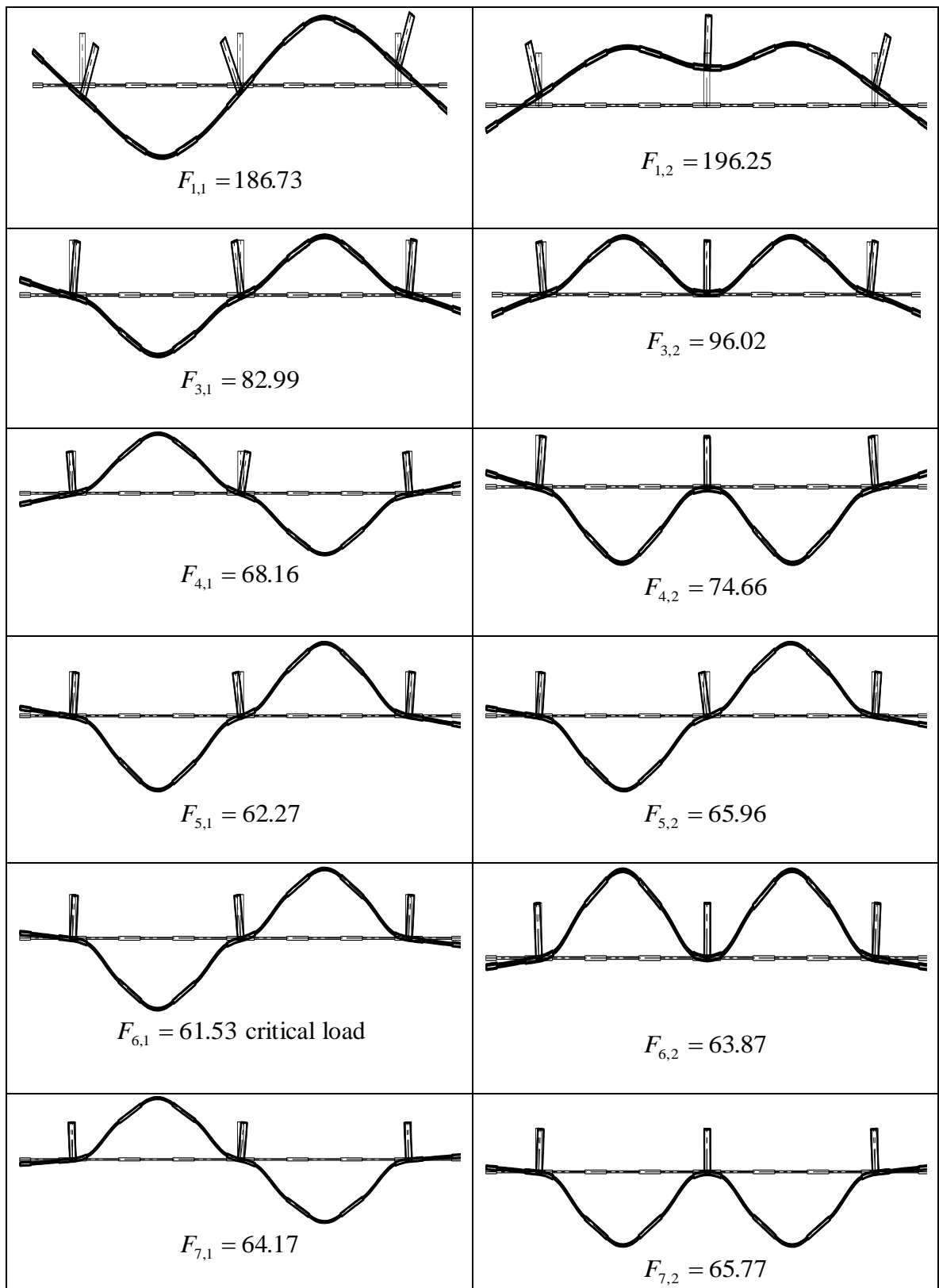


Figure 3.7 Profile 2-Buckling loads and corresponding buckling modes (mode shapes are plotted for mid span, i.e at $x = a/2 = 300$)

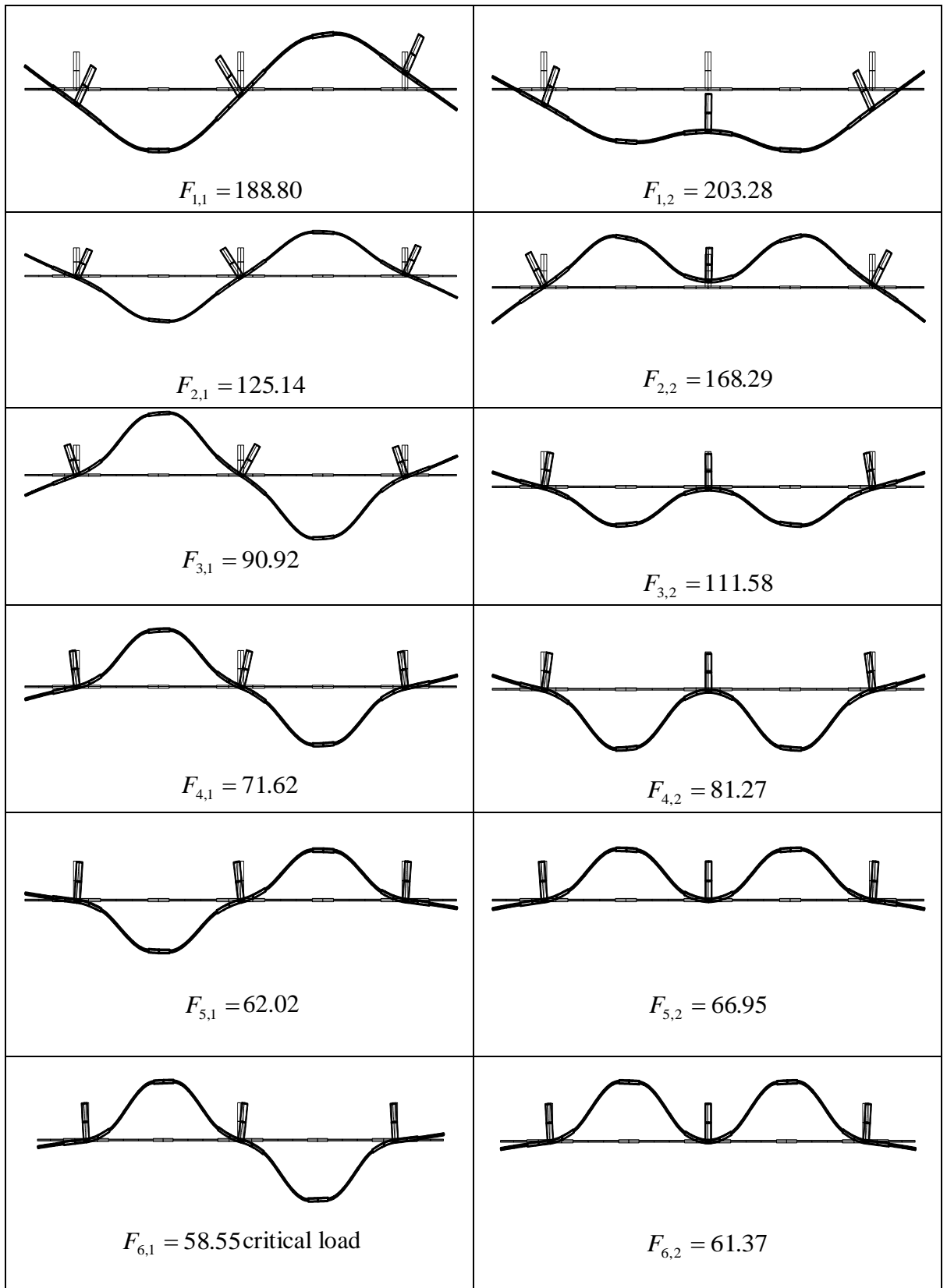


Figure 3.8 Profile 3-Buckling loads and corresponding buckling modes (mode shapes are plotted for mid span, i.e at $x = a/2 = 300$)

CHAPTER 4

GEOMETRIC NONLINEAR ANALYSIS

4.1 Introduction

Many problems faced by designers and engineers are nonlinear in nature. The response of a structure cannot be simply assessed using linear assumptions. Nonlinear behavior can take many forms and can be bewildering to the newcomer. All physical systems in the real world are inherently nonlinear in nature. One of the most difficult tasks facing an engineer is to decide whether a nonlinear analysis is really needed and if so what degree of nonlinearity should be applied.

The ability to predict accurately the response of a structure to a given loading allows engineers to improve their knowledge of the structure and to increase their confidence in their understanding of the structure's behavior. Ultimately, more accurate analysis enables engineers to improve their products.

Geometric nonlinear buckling analysis is more accurate than eigenvalue analysis for stability analysis because it employs non-linear, large deflection, static analysis to predict buckling loads. Its mode of operation is very simple: it gradually increases the applied load until a load level is found whereby the structure becomes unstable (i.e. suddenly a very small increase in the load will cause very large deflections). The true non-linear nature of this analysis thus permits the modeling of geometric imperfections, load perturbations, material nonlinearities and gaps. For this type of analysis, note that small off-axis loads are necessary to initiate the desired buckling mode.

The linear buckling analysis assumes the existence of a bifurcation point where the primary and secondary loading paths intersect (point A in the Figure 4.1). At this point, more than one equilibrium position is possible. The primary path is not usually

followed after loading exceeds this point and the structure is in the post-buckling state. The slope of the secondary path at the bifurcation point determines the nature of the post-buckling. A positive slope indicates that the structure will have post buckling strength whilst a negative slope means that the structure will snap through or simply collapse. Real structures have geometric and loading imperfections, often causing the primary path curve and the bifurcation point to disappear.

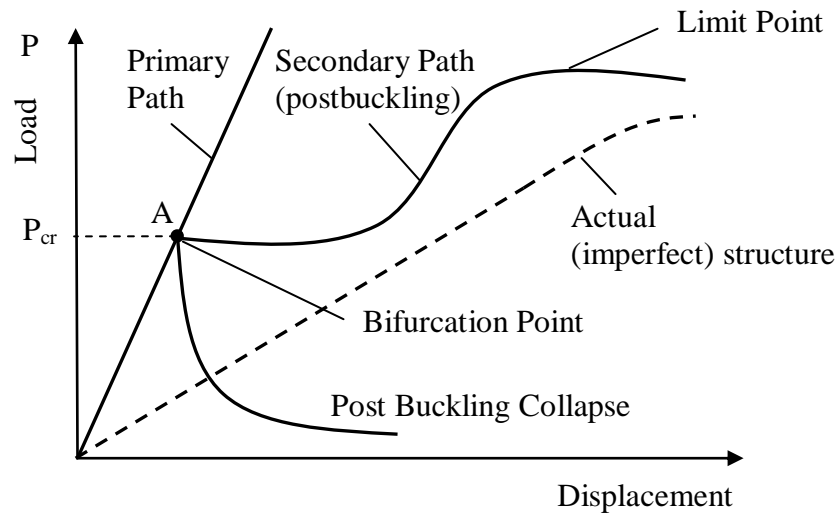


Figure 4.1 Buckling and bifurcation point

For real structures linear buckling analysis is best used method for preliminary design and studying the effects of various parameters. If a more accurate estimate of the buckling load is required, it is recommended that a nonlinear analysis is carried out so that the effect of pre-buckling deformation can be included and the post buckling capacity predicted.

For nonlinear situations, in which the stiffness depends on the degree of displacement in some manner, \mathbf{K} is equal to the local gradient of the force/displacement relationship of the structure at any point and is termed the tangential stiffness. The analysis of such problems must proceed in an incremental manner since the solution at any stage may not only depend on the current displacements of the structure, but also on the previous loading history.

4.2 General Theory and Solution Algorithms

The use of FE or FS discretization in a large class of nonlinear problems results in a system of simultaneous equations of the form

$$\mathbf{K}\boldsymbol{\delta} - \mathbf{f} = 0 \quad (4.1)$$

in which $\boldsymbol{\delta}$ is the vector of the basic unknowns, \mathbf{f} is the vector of applied loads and \mathbf{K} is the assembled stiffness matrix. For structural applications, the terms load and stiffness are directly applicable, but for other situations the interpretation of these quantities varies according to the physical problem under consideration. If the coefficients of the matrix \mathbf{K} depend on the unknowns $\boldsymbol{\delta}$ or their derivatives, the problem clearly becomes nonlinear. In this case, direct solution of equation system (4.1) is generally impossible and an iterative scheme must be adopted. Many options remain open for the iterative sequence to be employed. Some of the most generally applicable methods are given as

1. Direct iteration method
2. Modified Newton-Raphson method.
3. Tangential stiffness method (Generalized Newton-Raphson Method)
4. Initial stiffness method
5. Arc-length method

4.2.1 Direct iteration method

In direct iteration method [109] successive solutions are performed, in each of which the previous solution for the unknowns $\boldsymbol{\delta}$ is used to predict the current values of the coefficient matrix $\mathbf{K}(\boldsymbol{\delta})$. Rewriting (4.1) as

$$\boldsymbol{\delta} = [\mathbf{K}(\boldsymbol{\delta})]^{-1} \mathbf{f} \quad (4.2)$$

Then the iterative process yields the $(i + 1)^{th}$ approximation to be

$$\boldsymbol{\delta}^{i+1} = [\mathbf{K}(\boldsymbol{\delta}^i)]^{-1} \mathbf{f} \quad (4.3)$$

If the process is convergent then in the limit as i tends to infinity δ^i tends to the true solution. It is seen from (4.3) that it is necessary to recalculate the stiffness matrix \mathbf{K} for each iteration. To commence the process, an initial guess for the unknown δ is required in order to calculate \mathbf{K} . Generally a value of δ^0 based on the solution for an average material property throughout the region is found to be satisfactory. If the nonlinearity of the material properties is very marked at certain values of δ , an approximate prescription of the field variable at all nodes may be necessary. For practical purposes, the iterative process is deemed to have converged when some measure (usually a norm of the nodal unknowns) of the change in the unknown δ between successive iterations has become tolerably small.

4.2.2 Modified Newton-Raphson method

In the Newton-Raphson method during any step of an iterative process of solution, (4.1) will not be satisfied unless convergence has occurred. A system of residual forces can be assumed to exist, so that

$$\boldsymbol{\psi} = \mathbf{K}\boldsymbol{\delta} - \mathbf{f} \neq 0 \quad (4.4)$$

These residual forces $\boldsymbol{\psi}$ can be interpreted as a measure of the departure of equilibrium. Since \mathbf{K} is a function of $\boldsymbol{\delta}$ and possibly its derivatives, then at any stage of the process, $\boldsymbol{\psi} = \boldsymbol{\psi}(\boldsymbol{\delta})$. These equations may have multiple solutions. Thus, if a solution is achieved it may not necessarily be the solution sought. Physical insight into the nature of the problem and, usually, small-step incremental approaches from known solutions are essential to obtain realistic answers. Such increments are indeed always required if the constitutive law relating stress and strain changes is path dependent or if the load-displacement path has bifurcations or multiple branches at certain load levels. The general problem should always be formulated as the solution of

$$\boldsymbol{\psi}^{i+1} = \boldsymbol{\psi}(\boldsymbol{\delta}^{i+1}) = \mathbf{K}(\boldsymbol{\delta}^{i+1}) \boldsymbol{\delta}^{i+1} - \mathbf{f}^{i+1} = 0 \quad (4.5)$$

which starts from a nearby solution at

$$\delta = \delta^i, \quad \psi^i = 0, \quad \mathbf{f} = \mathbf{f}^i \quad (4.6)$$

Correction is computed as

$$\Delta\delta^i = (\mathbf{K}^i)^{-1}\psi^i \quad (4.7)$$

and often arises from the changes in the forcing function \mathbf{f} to

$$\mathbf{f}^{i+1} = \mathbf{f}^i + \Delta\mathbf{f} \quad (4.8)$$

The determination of the change $\Delta\delta$ such that

$$\delta^{i+1} = \delta^i + \Delta\delta^i \quad (4.9)$$

will be the objective and generally the increments of $\Delta\mathbf{f}$ will be kept reasonably small so that path dependence can be followed. Further, such incremental procedures will be useful in avoiding excessive numbers of iterations and in following the physically correct path. A typical non-uniqueness which may occur if the function ψ decreases and subsequently increases as the parameter δ uniformly increase is shown in Figure 4.2. It is clear that to follow the path $\Delta\delta^i$ will have both positive and negative signs during a complete computation process.

4.2.3 Tangential stiffness method (Generalized Newton-Raphson method)

For nonlinear situations, in which the stiffness depends on the degree of displacement in some manner, \mathbf{K} is equal to the local gradient of the force/displacement relationship of the structure at any point and is termed the tangential stiffness. The analysis of such problems must proceed in an incremental manner since the solution at any stage may not only depend on the current displacements of the structure, but also on the previous loading history. Consequently the problem can be linearized over any increment of load and therefore the matrix, which contains the nonlinear terms, can be discarded from (4.7) and (4.8) with this modification, the solution process is identical the modified Newton-Raphson Method and for this reason, the method is sometimes termed a generalized Newton-Raphson Method.

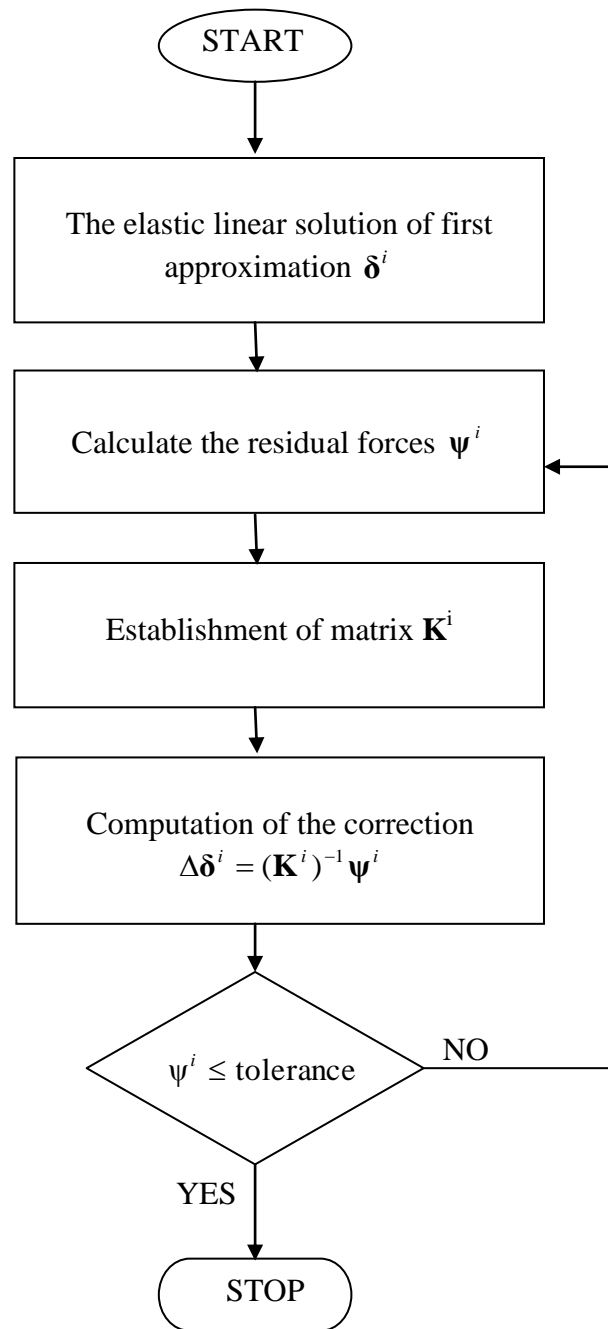


Figure 4.2 Newton-Raphson flow chart

4.2.4 Initial stiffness method

In this method, the tangential stiffness matrix is replaced, at all steps of the computation, by the stiffness corresponding to the initial trial value of δ a complete factorization, or reduction, of the assembled equations can be avoided. In this case a complete equation solution needs only be performed for the first iteration and subsequent approximations to the nonlinear solution performed, via the expression

$$\Delta\delta^i = [\mathbf{K}(\delta^0)]^{-1} \psi(\delta^i) \quad (4.10)$$

Since the same stiffness matrix $\mathbf{K}(\delta^0)$ is employed at each stage, the reduced equations can be stored in their reduced or factored form and a second or subsequent solution merely necessitates the reduction of right hand side ($\psi(\delta^i)$) terms, together with a back substitution. This has the immediate advantage of significantly reducing computing cost per iteration but reduces the convergence rate.

4.2.5 Arc-length method (Riks-Wempner method)

Passing through critical points during the geometrically nonlinear response is challenging. Two critical points encountered during this type of behavior are: load limit points that are reached whenever the response path has a local snap through; and control limit points that define a local snap-back. At a control limit point the loading may reverse as the deflections change directions and a local maximum is passed. An important family of nonlinear equations solvers called the arc-length method as developed by Riks-Wempner [110] can overcome the difficulties of passing critical points. The technique resembles the Newton-Raphson method described in Riks-Wempner except the applied load increment becomes an additional unknown. The Riks-Wempner method computes load magnitudes as part of the solution. The length of a vector tangent to the equilibrium path is used to find a new point that is the intersection of the plane normal to the tangent. A user-supplied load will estimate magnitudes of the initial load increment for a step. The termination of the method is accomplished by the user specifying a maximum load proportionality factor or a maximum nodal displacement.

4.3 Plane Formulation

If a body is subjected to a set of body forces \mathbf{b} then by the virtual work principle we can write

$$\int_{\Omega} [\partial\epsilon]^T \boldsymbol{\sigma} d\Omega - \int_{\Omega} [\partial\mathbf{u}]^T \mathbf{b} d\Omega - \int_{\Gamma} [\partial\mathbf{u}]^T \mathbf{P} d\Gamma = 0 \quad (4.11)$$

where $\boldsymbol{\sigma}$ is the vector of stress, \mathbf{P} is the vector of boundary tractions, $\partial\mathbf{u}$ is the vector of virtual displacements, $\partial\boldsymbol{\varepsilon}$ is the vector of associated virtual strains, Ω is the domain of interest, Γ is that part of the boundary on which boundary tractions are prescribed.

If we wish to cater for geometrically nonlinear elastic behavior we can choose either a total or updated Lagrange coordinate system. Here we choose a total Lagrange coordinate system which coincides with the initial undeformed position of the body.

It transpires that, with the central difference scheme, the only changes required to account for geometrically nonlinear effects are:

- (i) The modification of the strain-displacement matrix $\mathbf{B}(d_n)$,
- (ii) The evaluation of the strains using a deformation Jacobian matrix $\mathbf{J}_D(d_n)$.

All vectors and matrices are given explicitly for the plane stress and plane strain. The coordinates of a particle in an undeformed initial configuration are given as

$$[x_0, y_0]^T \quad (4.12)$$

Displacements are given as

$$[u_n, v_n]^T \quad (4.13)$$

The coordinates of particle in deformed configuration are given as

$$[x_n, y_n]^T = [x_0 + u_n, y_0 + v_n]^T \quad (4.14)$$

The vector of Green's strains is given as

$$\begin{bmatrix} \boldsymbol{\varepsilon}_x \\ \boldsymbol{\varepsilon}_x \\ \boldsymbol{\gamma}_{xy} \end{bmatrix}_n = \begin{bmatrix} \frac{\partial u_n}{\partial x} + \frac{1}{2} \left(\frac{\partial u_n}{\partial x} \right)^2 + \frac{1}{2} \left(\frac{\partial v_n}{\partial x} \right)^2 \\ \frac{\partial v_n}{\partial y} + \frac{1}{2} \left(\frac{\partial u_n}{\partial y} \right)^2 + \frac{1}{2} \left(\frac{\partial v_n}{\partial y} \right)^2 \\ \frac{\partial u_n}{\partial y} + \frac{\partial v_n}{\partial x} + \frac{\partial u_n}{\partial x} \frac{\partial u_n}{\partial y} + \frac{\partial v_n}{\partial x} \frac{\partial v_n}{\partial y} \end{bmatrix} \quad (4.15)$$

The deformation Jacobian matrix is given as

$$\mathbf{J}_D(u_n) = [J_D]_n \quad (4.16)$$

$$[J_D]_n = \begin{bmatrix} \frac{\partial x_n}{\partial x} & \frac{\partial x_n}{\partial y} \\ \frac{\partial y_n}{\partial x} & \frac{\partial y_n}{\partial y} \end{bmatrix} \quad (4.17)$$

The linear strain $\boldsymbol{\varepsilon}_0$ is given as

$$\boldsymbol{\varepsilon}_0 = \left[\frac{\partial u_n}{\partial x}, \frac{\partial v_n}{\partial y}, \left(\frac{\partial u_n}{\partial y} + \frac{\partial v_n}{\partial x} \right) \right]^T \quad (4.18)$$

Nonlinear strain $\boldsymbol{\varepsilon}_{NL}$ is given as

$$\boldsymbol{\varepsilon}_{NL} = \frac{1}{2} \mathbf{A}_\theta \boldsymbol{\theta}_n \quad (4.19)$$

where

$$\mathbf{A}_\theta = \begin{bmatrix} \frac{\partial u_n}{\partial x} & \frac{\partial v_n}{\partial x} & 0 & 0 \\ 0 & 0 & \frac{\partial u_n}{\partial y} & \frac{\partial v_n}{\partial y} \\ \frac{\partial u_n}{\partial y} & \frac{\partial v_n}{\partial y} & \frac{\partial u_n}{\partial x} & \frac{\partial v_n}{\partial x} \end{bmatrix} \quad (4.20)$$

and displacement gradients

$$\boldsymbol{\theta}_n = \begin{bmatrix} \frac{\partial u_n}{\partial x} & 0 & \frac{\partial u_n}{\partial x} \\ \frac{\partial v_n}{\partial x} & 0 & \frac{\partial v_n}{\partial x} \\ 0 & \frac{\partial u_n}{\partial y} & \frac{\partial u_n}{\partial y} \\ 0 & \frac{\partial v_n}{\partial y} & \frac{\partial v_n}{\partial y} \end{bmatrix} \quad (4.21)$$

For a set of virtual displacements, the corresponding virtual Green's strain are given as

$$\partial \boldsymbol{\varepsilon} = \boldsymbol{\varepsilon}_0 + \mathbf{A}_\theta \partial \boldsymbol{\theta}_n \quad (4.22)$$

Thus, the virtual work statement can be rewritten as

$$\int_V [\partial \boldsymbol{\varepsilon}_n]^T \boldsymbol{\sigma}_n dv = \int_a [\partial \mathbf{u}_n]^T \mathbf{P} da \quad (4.23)$$

Elastic Piola-Kirchoff stresses are given as

$$\boldsymbol{\sigma}_n = \mathbf{D}_n \boldsymbol{\varepsilon}_n \quad (4.24)$$

$$[\sigma_x, \sigma_y, \tau_{xy}]_n^T \quad (4.25)$$

If we adopt the FE discretization scheme described earlier, then the displacement gradients $\boldsymbol{\theta}_n$ are given in terms of the nodal displacements \mathbf{d}_i by the linear relation

$$\boldsymbol{\theta}_n = \sum_{i=1}^m \mathbf{G}_i \mathbf{d}_i \quad (4.26)$$

where \mathbf{G}_i contains Cartesian shape function derivatives as

$$\mathbf{G}_i = \begin{bmatrix} \frac{\partial N_i}{\partial x} & 0 & \frac{\partial N_i}{\partial y} & 0 \\ 0 & \frac{\partial N_i}{\partial x} & 0 & \frac{\partial N_i}{\partial y} \end{bmatrix} \quad (4.27)$$

The components of the vector of Green's strains $\boldsymbol{\varepsilon}_n$ can be written as

$$\boldsymbol{\varepsilon}_n = \sum_{i=1}^m \left[\mathbf{B}_{Li} + \frac{1}{2} \mathbf{B}_{NLi} \right] \mathbf{d}_i \quad (4.28)$$

Furthermore, it can be shown that the virtual strains can be expressed as

$$\partial \boldsymbol{\varepsilon}_n = \sum_{i=1}^m \mathbf{B}_i [\partial \mathbf{d}_i]_n \quad (4.29)$$

where strain displacement matrix associated with node i is

$$\mathbf{B}_i = \mathbf{B}_{Li} + \mathbf{A}_\theta \mathbf{G}_i = \begin{bmatrix} \frac{\partial x_n}{\partial x} \frac{\partial N_i}{\partial x} & \frac{\partial y_n}{\partial x} \frac{\partial N_i}{\partial x} \\ \frac{\partial x_n}{\partial y} \frac{\partial N_i}{\partial y} & \frac{\partial y_n}{\partial y} \frac{\partial N_i}{\partial y} \\ \frac{\partial x_n}{\partial x} \frac{\partial N_i}{\partial y} + \frac{\partial x_n}{\partial y} \frac{\partial N_i}{\partial x} & \frac{\partial y_n}{\partial x} \frac{\partial N_i}{\partial y} + \frac{\partial y_n}{\partial y} \frac{\partial N_i}{\partial x} \end{bmatrix} \quad (4.30)$$

Since the nodal virtual displacements $d\boldsymbol{\delta}$ are arbitrary the element nonlinear equilibrium equation takes the following form:

$$\boldsymbol{\psi}(\boldsymbol{\delta}) = \int_A \mathbf{B}^T \boldsymbol{\sigma} da - \mathbf{P} = 0 \quad (4.31)$$

The load vector \mathbf{P} may also contain nodal point loads.

Equation (4.31) can have the dual role of representing either the element, or in an assembled form, the total equilibrium equation. It is a nonlinear equation in $\boldsymbol{\delta}$ since \mathbf{B} and $\boldsymbol{\sigma}$ is linear and quadratic functions of $\boldsymbol{\delta}$, respectively. The solution algorithms for the assembled nonlinear equilibrium equations are based on the Newton-Raphson method which consists of a series of linear solutions.

To evaluate the residual nodal force vector $\boldsymbol{\psi}(\boldsymbol{\delta})$ of equation (4.31) the equivalent nodal forces due to the stress resultants $\boldsymbol{\sigma}$ may be written for a typical node i as

$$\mathbf{P}_i = \int_A \{(\mathbf{B}_i)\boldsymbol{\sigma}\} da \quad (4.32)$$

For all the Mindlin elements stresses are extrapolated from Gauss point values in a manner consistent with the integration rule used for the tangent stiffness matrix calculation. Newton-Raphson iteration technique is used for iteration. Convergence is checked using total residual norm criteria as

$$\frac{\sqrt{\sum_{i=1}^N \Psi^2}}{\sqrt{\sum_{i=1}^N \mathbf{P}^2}} \times 100 \leq \text{toler} \quad (4.33)$$

where N is the total number of nodal points in the problem and *toler* is the value at which convergence occurs if the norm of the residual forces becomes less than the norm of the total applied forces.

4.4 Plane Example

Here, the problem is to determine the shape of a column under vertical end loads higher than the elastic buckling load. The column is divided into eight node elements and to initiate sway deformation it is loaded eccentrically (see Figure 4.3).

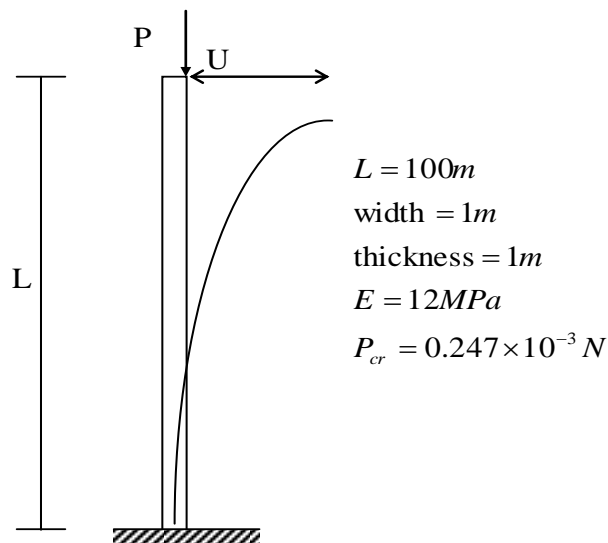


Figure 4.3 Eccentrically loaded column (material and geometric properties)

Table 4.1 Column end horizontal deflections,

P/P _{cr}	Present U (m)	ANSYS U (m)
0.20	0.155	0.155
0.40	0.416	416
0.60	0.944	0.944
0.80	2.528	2.525
0.90	5.589	5.918
1.00	19.859	20.469
1.015	22.635	26.713
1.017	29.188	27.685
1.063	42.212	38.919
1.152	59.301	52.182
1.293	71.921	72.484
1.518	79.231	78.699
1.884	80.304	82.385

Column end horizontal deflections compared with ANSYS results which shows negligible difference up to the critical load. After that point the deflection increases rapidly and there is a fair agreement between the results given in Table 4.1.

4.5 Plate and Shell Formulation

A typical FS given in Chapter 3 is illustrated in Figure 3.2 which is subjected to a lateral loading or inplane loading. At any general point in the plate the displacement components in the x, y, and z directions namely u_ℓ, v_ℓ, w_ℓ and rotations about the x and y axes ϕ, ψ are given in Chapter 3.

4.5.1 Strains

If a structure undergoes large deformations, the second order terms of the strains cannot be ignored. Consequently, the membrane and bending actions are coupled. For a Mindlin plate the relevant Green's strain vector is given as

$$\boldsymbol{\varepsilon} = \begin{Bmatrix} \varepsilon_x \\ \varepsilon_y \\ \gamma_{xy} \\ \gamma_{xz} \\ \gamma_{yz} \end{Bmatrix} = \begin{Bmatrix} \frac{\partial u}{\partial x} + \frac{1}{2} \left(\frac{\partial u}{\partial x} \right)^2 + \frac{1}{2} \left(\frac{\partial v}{\partial x} \right)^2 + \frac{1}{2} \left(\frac{\partial w}{\partial x} \right)^2 \\ \frac{\partial v}{\partial y} + \frac{1}{2} \left(\frac{\partial u}{\partial y} \right)^2 + \frac{1}{2} \left(\frac{\partial v}{\partial y} \right)^2 + \frac{1}{2} \left(\frac{\partial w}{\partial y} \right)^2 \\ \frac{\partial u}{\partial x} + \frac{\partial v}{\partial x} + \frac{\partial u}{\partial x} \frac{\partial u}{\partial y} + \frac{\partial v}{\partial x} \frac{\partial v}{\partial y} + \frac{\partial w}{\partial x} \frac{\partial w}{\partial y} \\ \frac{\partial u}{\partial z} + \frac{\partial w}{\partial x} + \frac{\partial u}{\partial x} \frac{\partial u}{\partial z} + \frac{\partial v}{\partial x} \frac{\partial v}{\partial z} + \frac{\partial w}{\partial x} \frac{\partial w}{\partial z} \\ \frac{\partial v}{\partial z} + \frac{\partial w}{\partial y} + \frac{\partial u}{\partial y} \frac{\partial u}{\partial z} + \frac{\partial v}{\partial y} \frac{\partial v}{\partial z} + \frac{\partial w}{\partial y} \frac{\partial w}{\partial z} \end{Bmatrix} \quad (4.34)$$

Introducing the Von Karman assumptions [111] which imply that derivatives of u and v with respect to x , y and z are small and nothing that w is independent of z allows Green's strain to be rewritten in terms of the midplane deformations of equation (4.26) as

$$\boldsymbol{\varepsilon} = \begin{Bmatrix} \varepsilon_x \\ \varepsilon_y \\ \gamma_{xy} \\ \gamma_{xz} \\ \gamma_{yz} \end{Bmatrix} = \begin{Bmatrix} \boldsymbol{\varepsilon}_m \\ \mathbf{0} \end{Bmatrix} + \begin{Bmatrix} z\boldsymbol{\varepsilon}_b \\ \boldsymbol{\varepsilon}_s \end{Bmatrix} + \begin{Bmatrix} \boldsymbol{\varepsilon}^{NL} \\ \mathbf{0} \end{Bmatrix} \quad (4.35)$$

where strain components $\boldsymbol{\varepsilon}_m, \boldsymbol{\varepsilon}_b, \boldsymbol{\varepsilon}_s$ are given in Appendix A and the nonlinear component of inplane strain is

$$\boldsymbol{\varepsilon}^{NL} = \begin{Bmatrix} \frac{1}{2} \left(\frac{\partial w}{\partial x} \right)^2 \\ \frac{1}{2} \left(\frac{\partial w}{\partial y} \right)^2 \\ \frac{\partial w}{\partial x} \frac{\partial w}{\partial y} \end{Bmatrix} \quad (4.36)$$

4.5.2 Stresses

The Piola-Kirchhoff stress vector $\boldsymbol{\sigma}$ associated with the Green's strain vector $\boldsymbol{\varepsilon}$ of equation (4.34) is

$$\boldsymbol{\sigma} = [\sigma_x, \sigma_y, \tau_{xy}, \tau_{xz}, \tau_{yz}]^T \quad (4.37)$$

4.5.3 Total Lagrangian virtual work equation

The basis of the formulation is the virtual work equation for a continuous medium written in a total Lagrangian coordinate system under the assumption of small strains and conservative loading as [112]

$$\int_{\Omega} [\partial \boldsymbol{\varepsilon}]^T \boldsymbol{\sigma} d\Omega - \int_{\Omega} \rho [\partial \mathbf{u}]^T \mathbf{q} d\Omega - \int_{\Gamma} [\partial \mathbf{u}]^T \mathbf{P} d\Gamma = 0 \quad (4.38)$$

where Ω is the undeformed volume, $\boldsymbol{\sigma}$ the Piola-Kirchhoff stress vector, $\partial \boldsymbol{\varepsilon}$ the virtual Green's strain vector due to the virtual displacement vector $\partial \mathbf{u}$, ρ the mass density, \mathbf{q} the body force vector per unit mass and \mathbf{P} surface tractions acting over an undeformed area A . For the plate formulation this virtual work equation is to be rewritten in terms of area integrals over the mid-surface. The internal virtual work dW_i can be written as

$$dW^i = \frac{1}{2} t \int_0^b \int_{\ell^e} d\boldsymbol{\varepsilon}^T \boldsymbol{\sigma} d\ell dy \quad (4.39a)$$

or

$$dW^i = t \int_0^b \int_{\ell^e} (d\varepsilon_{\ell} \sigma_{\ell} + d\varepsilon_y \sigma_y + d\gamma_{\ell y} \tau_{\ell y} + d\gamma_{\ell z} \tau_{\ell z} + d\gamma_{yz} \tau_{yz}) d\ell dy \quad (4.39b)$$

Substituting the strain expression from equation (4.35) into equation (4.39)

$$dW^i = \int_A d\boldsymbol{\varepsilon}^T \boldsymbol{\sigma} da \quad (4.40)$$

in which the stress resultant vector $\boldsymbol{\sigma}$ is,

$$\boldsymbol{\sigma} = \begin{Bmatrix} \boldsymbol{\sigma}_m \\ \boldsymbol{\sigma}_b \\ \boldsymbol{\sigma}_s \end{Bmatrix} \quad (4.41)$$

which contains the following components, inplane

$$\boldsymbol{\sigma}_m = [\sigma_{m\ell}, \sigma_{my}, \tau_{m\ell y}]^T \quad (4.42)$$

bending

$$\boldsymbol{\sigma}_b = [\sigma_{b\ell}, \sigma_{by}, \tau_{b\ell y}]^T \quad (4.43)$$

shear

$$\boldsymbol{\sigma}_s = [\tau_{\ell z}, \tau_{yz}]^T \quad (4.44)$$

The generalized strain vector $\boldsymbol{\varepsilon}$ corresponding to the stresses $\boldsymbol{\sigma}$ of equation (4.41) is,

$$\boldsymbol{\varepsilon} = \begin{Bmatrix} \boldsymbol{\varepsilon}_m \\ \boldsymbol{\varepsilon}_b \\ \boldsymbol{\varepsilon}_s \end{Bmatrix} = \boldsymbol{\varepsilon}^0 + \boldsymbol{\varepsilon}^{NL} \quad (4.45)$$

where the linear component $\boldsymbol{\varepsilon}^0$ is,

$$\boldsymbol{\varepsilon}^0 = \begin{Bmatrix} \boldsymbol{\varepsilon}_m^0 \\ \boldsymbol{\varepsilon}_b^0 \\ \boldsymbol{\varepsilon}_s^0 \end{Bmatrix} \quad (4.46)$$

and the nonlinear component $\boldsymbol{\varepsilon}^{NL}$ is,

$$\boldsymbol{\varepsilon}^{NL} = \begin{Bmatrix} \boldsymbol{\varepsilon}_m^{NL} \\ 0 \\ 0 \end{Bmatrix} \quad (4.47)$$

The second integral in equation (4.38) which represents the external virtual work due to body forces may be rewritten as

$$dW_{ex}^b = t \int_0^b \int_{\ell^e} \rho \mathbf{q} d\ell dy \quad (4.48)$$

Finally, the third integral of equation (4.38) which represents the external virtual work due to inplane loads may be expressed as

$$dW_{ex}^b = t \int_0^b \mathbf{P}_\ell dy \quad (4.49)$$

The virtual work equation (4.38) may now be written entirely in terms of mid-plane quantities as

$$\int_0^b \int_{\ell^e} d\boldsymbol{\varepsilon} \boldsymbol{\sigma} da = t \int_0^b \int_{\ell^e} \rho \mathbf{q} d\ell dy + t \int_0^b \mathbf{P}_\ell dy \quad (4.50)$$

4.5.4 Variation of strain

Before proceeding with the discretization of virtual work equation (4.50), it is necessary to consider further the variation of strain $d\boldsymbol{\varepsilon}$ due to the virtual displacements $d\mathbf{u}$ where \mathbf{u} is given as

$$\mathbf{u} = [u, v, w, \phi, \psi]^T \quad (4.51)$$

Generally $d\boldsymbol{\varepsilon}$ is given as the sum of the variations of the linear and nonlinear generalized strains as

$$d\boldsymbol{\varepsilon} = d\boldsymbol{\varepsilon}^0 + d\boldsymbol{\varepsilon}^{NL} \quad (4.52)$$

where

$$d\boldsymbol{\varepsilon}^0 = d\boldsymbol{\varepsilon}_m + d\boldsymbol{\varepsilon}_b + d\boldsymbol{\varepsilon}_s \quad (4.53)$$

in which $\boldsymbol{\varepsilon}_m$, $\boldsymbol{\varepsilon}_b$ and $\boldsymbol{\varepsilon}_s$ are the membrane, bending or curvature and transverse shear strain components, respectively, and given in Appendix A for plates and shells in straight and curved planforms. If the displacement gradients of the lateral displacement w are given as

$$\boldsymbol{\theta} = \left[\frac{\partial w}{\partial \ell}, \frac{\partial w}{\partial y} \right] \quad (4.54)$$

then the variation of the nonlinear component of the inplane strain is obtained from equation (4.28) in terms of the virtual gradients $d\boldsymbol{\theta}$ as

$$d\boldsymbol{\varepsilon}^{NL} = \mathbf{A}_\theta d\boldsymbol{\theta} \quad (4.55)$$

where

$$\mathbf{A}_\theta = \begin{bmatrix} \frac{\partial w}{\partial \ell} & 0 \\ 0 & \frac{\partial w}{\partial y} \\ \frac{\partial w}{\partial y} & \frac{\partial w}{\partial \ell} \end{bmatrix} \quad (4.56)$$

and

$$d\boldsymbol{\theta} = d \left[\frac{\partial w}{\partial \ell}, \frac{\partial w}{\partial y} \right]^T \quad (4.57)$$

4.5.5 Finite strip formulation of equilibrium equations

Using n -noded, $C(0)$ strips, the global displacements and rotations may be interpolated within each strip in terms of truncated Fourier series along direction y , in which both the material and geometrical properties of the plate are taken to be constant, i.e.

$$\begin{aligned} u(\ell, y) &= \sum_{p=p_1}^{p_2} u^p(\ell) S_p; & v(\ell, y) &= \sum_{p=p_1}^{p_2} v^p(\ell) C_p \\ w(\ell, y) &= \sum_{p=p_1}^{p_2} w^p(\ell) S_p; & \phi(\ell, y) &= \sum_{p=p_1}^{p_2} \phi^p(\ell) S_p \\ \psi(\ell, y) &= \sum_{p=p_1}^{p_2} \psi^p(\ell) C_p \end{aligned} \quad (4.58)$$

where $C_p = \cos(p\pi y/b)$ and $S_p = \sin(p\pi y/b)$, u^p, v^p, w^p, ϕ^p and ψ^p are displacement and rotation amplitudes for the p^{th} harmonic term. This corresponds to a single diaphragm support at the ends of the structure at $y=0$ and $y=b$, so

that $v = w = \phi = 0$. As shown later, this will lead to an uncoupling of each harmonic term which in turn leads to an economic solution. Note that the strip displacement and rotation fields are generally expressed as a summation of a set of contributions from a lower limit p_1 to an upper limit p_2 . In the present work as there is no coupling between the harmonics p_1 and p_2 coincide. For many cases taking $p_1 = p_2 = 1$ provides the lowest buckling mode; however, in some cases p_1 and p_2 may be associated with a higher mode.

The next step is to discretize the displacement and rotation amplitudes (which are functions of the ℓ -coordinate only) using an n -noded FE representation so that within a strip e the amplitudes can be written as

$$\begin{aligned} u^p(\ell) &= \sum_{i=1}^n N_i u_i^p; & v^p(\ell) &= \sum_{i=1}^n N_i v_i^p; & w^p(\ell) &= \sum_{i=1}^n N_i w_i^p \\ \phi^p(\ell) &= \sum_{i=1}^n N_i \phi_i^p; & \psi^p(\ell) &= \sum_{i=1}^n N_i \psi_i^p \end{aligned} \quad (4.59)$$

where u^p, v^p, w^p, ϕ^p and ψ^p are typical nodal degrees of freedom associated with node i and harmonic p .

Thus, the process is equivalent to dividing the structure into longitudinal elements (or strips) so that each strip has a certain number of nodes (more accurately, nodal lines) associated with its transverse direction. The displacement field is defined longitudinally by the Fourier expansion of (4.58) and transversely by the FE discretization of (4.59). Substituting (4.59) into (4.58) it is possible to write

$$\mathbf{u} = \sum_{p=p_1}^{p_2} \sum_{i=1}^n \mathbf{N}_i^p \boldsymbol{\delta}_i^p \quad (4.60)$$

where

$$\mathbf{u} = [u, v, w, \phi, \psi]^T$$

$$\boldsymbol{\delta}_i^p = [u_i^p, v_i^p, w_i^p, \phi_i^p, \psi_i^p]^T$$

and

$$\mathbf{N}_i^p = \begin{bmatrix} N_i S_p & 0 & 0 & 0 & 0 \\ 0 & N_i C_p & 0 & 0 & 0 \\ 0 & 0 & N_i S_p & 0 & 0 \\ 0 & 0 & 0 & N_i S_p & 0 \\ 0 & 0 & 0 & 0 & N_i C_p \end{bmatrix} \quad (4.61)$$

$N_i(\xi)$ is the shape function associated with node i [2]. These elements are essentially isoparametric so that

$$x = \sum_{i=1}^n N_i x_i; \quad y = \sum_{i=1}^n N_i y_i; \quad t = \sum_{i=1}^n N_i t_i \quad (4.62)$$

where x_i and y_i are typical coordinates of node i and t_i is the thickness at node i .

The virtual displacements $d\mathbf{u}$ are written in terms of the nodal displacements $d\boldsymbol{\delta}$ from equation (4.60)

$$d\mathbf{u} = \sum_{p=p_1}^{p_2} \sum_{i=1}^n \mathbf{N}_i^p d\boldsymbol{\delta}_i^p \quad (4.63)$$

where

$$d\boldsymbol{\delta}_i^p = d \left\{ \begin{array}{c} \delta_1 \\ \delta_2 \\ \vdots \\ \delta_n \end{array} \right\} \quad (4.64)$$

The displacement gradients $\boldsymbol{\theta}_i^p$ of equation (4.54) may now be written in terms of the nodal displacements $\boldsymbol{\delta}_i^p$ and Cartesian derivatives of the shape functions as

$$\boldsymbol{\theta}_i^p = \mathbf{G}_i^p \boldsymbol{\delta}_i^p \quad (4.65)$$

where

$$\mathbf{G} = [\mathbf{G}_1, \mathbf{G}_2, \dots, \mathbf{G}_n] \quad (4.66)$$

and

$$\mathbf{G}_i^p = \begin{bmatrix} 0 & 0 & \frac{\partial N_i}{\partial \ell} S_p & 0 & 0 \\ 0 & 0 & \bar{p} N_i C_p & 0 & 0 \end{bmatrix} \quad (4.67)$$

The virtual gradients of equation (4.57) are now written in terms of virtual nodal displacements as

$$d\boldsymbol{\theta}_i^p = \mathbf{G}_i^p d\boldsymbol{\delta}_i^p \quad (4.68)$$

The generalized Green's strain vector $\boldsymbol{\varepsilon}$ of equation (4.45) is given in terms of nodal displacements $\boldsymbol{\delta}$, displacement gradients \mathbf{A}_θ and Cartesian derivatives of \mathbf{N} as

$$\boldsymbol{\varepsilon} = \left[\mathbf{B}_0 + \frac{1}{2} \mathbf{B}_L(\boldsymbol{\delta}) \right] \boldsymbol{\delta} \quad (4.69)$$

where \mathbf{B}_0 is the strain matrix giving the linear strains $\boldsymbol{\varepsilon}_m, \boldsymbol{\varepsilon}_b, \boldsymbol{\varepsilon}_s$ and \mathbf{B}_L , which is linearly dependent upon $\boldsymbol{\delta}$, gives the non-linear strains $\boldsymbol{\varepsilon}^{NL}$. Consequently, the nonlinear strains are quadratically dependent upon the nodal displacements $\boldsymbol{\delta}$. The constant matrix \mathbf{B}_0 is written in terms of nodal submatrices as

$$\mathbf{B}_0 = [B_{01}, B_{02}, \dots, B_{0n}] \quad (4.70)$$

where

$$\mathbf{B}_{0i}^p = \begin{bmatrix} \mathbf{B}_{mi}^p & 0 \\ 0 & \mathbf{B}_{bi}^p \\ 0 & \mathbf{B}_{si}^p \end{bmatrix} \quad (4.71)$$

in which $\mathbf{B}_{mi}^p, \mathbf{B}_{bi}^p$ and \mathbf{B}_{si}^p are the membrane, bending and shear strain displacement matrices associated with harmonic p and node i and are given in Appendix A. The strain matrix \mathbf{B}_{Li}^p consists of the nodal submatrices as follows:

$$\mathbf{B}_{Li}^p = [B_{L1}, B_{L2}, \dots, B_{Ln}] \quad (4.72)$$

where

$$\mathbf{B}_{Li}^p = \begin{bmatrix} \mathbf{A}_{\epsilon}^p \\ 0 \\ 0 \end{bmatrix} \mathbf{G}_{Li}^p \quad (4.73)$$

Substituting equations (4.63) and (4.68) into (4.53) and (4.55), respectively, yields the strain variation in terms of the virtual nodal displacements $d\delta_i^p$ as

$$d\epsilon_i^p = \mathbf{B}_i^p d\delta_i^p \quad (4.74)$$

in which

$$\mathbf{B}_i^p = \mathbf{B}_{mi}^p + \mathbf{B}_{bi}^p + \mathbf{B}_{si}^p + \mathbf{B}_{Li}^p(\delta) \quad (4.75)$$

The virtual work equation (4.50) is discretized, for a strip, by substituting equations (4.63) and (4.74) for $d\mathbf{u}$ and $d\epsilon$, respectively, giving

$$d\delta \left[\int_0^b \int_{\ell^e} \mathbf{B}^T \boldsymbol{\sigma} d\ell dy - \mathbf{R} \right] = 0 \quad (4.76)$$

where the equivalent nodal load vector \mathbf{R} is due to body forces and inplane loads. Since the nodal virtual displacements $d\delta_i^p$ are arbitrary the strip nonlinear equilibrium equations become

$$\boldsymbol{\Psi}(\delta) = \int_0^b \int_{\ell^e} \mathbf{B}^T \boldsymbol{\sigma} d\ell dy - \mathbf{R} = 0 \quad (4.77)$$

This is a nonlinear equation in δ since \mathbf{B} and $\boldsymbol{\sigma}$ is linear and quadratic functions of δ , respectively.

4.5.6 Solution to nonlinear equilibrium equations

The solution algorithms for the assembled nonlinear equilibrium equations (4.77) are based on the Newton-Raphson method which consists of a series of linear solutions. If an initial estimate δ_i for the total displacements gives residual (unbalanced) forces $\boldsymbol{\Psi}(\delta_i) \neq 0$ then an improved value δ_{i+1} is obtained by equating to zero the linearized Taylor's series expansion of $\boldsymbol{\Psi}(\delta_{i+1})$ in the neighborhood of δ_i as

$$\boldsymbol{\psi}(\boldsymbol{\delta}_{i+1}) \approx \boldsymbol{\psi}(\boldsymbol{\delta}_i) + \mathbf{K}_T \Delta \boldsymbol{\delta}_i = 0 \quad (4.78)$$

where \mathbf{K}_T is known as the assembled tangent stiffness matrix evaluated at $\boldsymbol{\delta}_i$ and given by

$$\mathbf{K}_T = \left[\frac{\partial \boldsymbol{\psi}(\boldsymbol{\delta}_i)}{\partial \boldsymbol{\delta}} \right] \quad (4.79)$$

Equation (4.78) is the linear incremental equilibrium equation which gives the linearized approximation to the relation between the residual forces and incremental displacements, $\Delta \boldsymbol{\delta}_i$, at a point $\boldsymbol{\delta}_i$ on the equilibrium path. The improved solution is then found as,

$$\boldsymbol{\delta}_{i+1} = \boldsymbol{\delta}_i + \Delta \boldsymbol{\delta}_i \quad (4.80)$$

Equations (4.78) and (4.79) represent the Newton-Raphson solution to the nonlinear equation (4.78). The terms $\boldsymbol{\psi}(\boldsymbol{\delta}_i)$ and $\Delta \boldsymbol{\delta}_i$ give measures of the convergence of the solution. To improve numerical stability and to give intermediate results, the load \mathbf{R} is usually applied in increments. Since the Newton-Raphson method requires repeated calculation and inversion of \mathbf{K}_T , a modified Newton-Raphson method is also employed whereby \mathbf{K}_T is calculated only once on the second iteration of each load increment.

4.5.7 Tangent stiffness matrix

The tangent stiffness matrix given in equation (4.79) may be written as

$$\mathbf{K}_T = \begin{bmatrix} \frac{\partial \psi_1}{\partial \delta_1} & \frac{\partial \psi_1}{\partial \delta_2} & \dots & \frac{\partial \psi_1}{\partial \delta_m} \\ \frac{\partial \psi_2}{\partial \delta_1} & \frac{\partial \psi_2}{\partial \delta_2} & \dots & \frac{\partial \psi_2}{\partial \delta_m} \\ \vdots & \vdots & \dots & \vdots \\ \frac{\partial \psi_m}{\partial \delta_1} & \frac{\partial \psi_m}{\partial \delta_2} & \dots & \frac{\partial \psi_m}{\partial \delta_m} \end{bmatrix} \quad (4.81)$$

where m is the number of degrees of freedom per strip.

For convenience the eight stress resultants of equations (4.42-4.44) are written as

$$\boldsymbol{\sigma} = [\sigma_1, \sigma_2, \dots, \sigma_8]^T \quad (4.82)$$

This enables the equilibrium equation (4.78) to be expanded as

$$\boldsymbol{\psi}_i(\boldsymbol{\delta}) = \int_0^b \int_{\ell^e} \begin{pmatrix} \sum_{k=1}^8 \mathbf{B}_{k1} \sigma_k \\ \sum_{k=1}^8 \mathbf{B}_{k2} \sigma_k \\ \vdots \\ \sum_{k=1}^8 \mathbf{B}_{km} \sigma_k \end{pmatrix} d\ell dy - \mathbf{R} = 0 \quad (4.83)$$

Differentiating $\boldsymbol{\psi}_i$ with respect to $\boldsymbol{\delta}_j$ yields a typical term in \mathbf{K}_T as

$$\mathbf{K}_{Tij} = \frac{\partial \boldsymbol{\psi}_i}{\partial \boldsymbol{\delta}_j} = \int_0^b \int_{\ell^e} \left[\sum_{k=1}^8 \mathbf{B}_{ki} \frac{\partial \sigma_k}{\partial \boldsymbol{\delta}_j} + \sum_{k=1}^8 \sigma_k \frac{\partial \mathbf{B}_{ki}}{\partial \boldsymbol{\delta}_j} \right] d\ell dy \quad (4.84)$$

where $(\partial \mathbf{R}_i / \partial \boldsymbol{\delta}_j) = 0$ for conservative loading.

The tangent stiffness matrix can be written as

$$\mathbf{K}_T = \int_0^b \int_{\ell^e} \mathbf{B}^T \mathbf{D} \mathbf{B} d\ell dy + \int_0^b \int_{\ell^e} \mathbf{G}^T \begin{bmatrix} \sigma_{m\ell} & \sigma_{m\ell y} \\ \sigma_{m\ell y} & \sigma_{my} \end{bmatrix} \mathbf{G} da \quad (4.85)$$

Substituting for \mathbf{B} and \mathbf{G} , gives

$$\mathbf{K}_T = \mathbf{K}_0 + \mathbf{K}_L + \mathbf{K}_\sigma \quad (4.86)$$

where the constant linear elastic stiffness matrix \mathbf{K}_0 is given in Chapter 3 as

$$[\mathbf{K}_{ij}^e]^{pq} = \int_0^b \int_{-1}^{+1} \left([\mathbf{B}_{mj}^p]^T \mathbf{D}_m \mathbf{B}_{mj}^q + [\mathbf{B}_{bj}^p]^T \mathbf{D}_b \mathbf{B}_{bj}^q + [\mathbf{B}_{sj}^p]^T \mathbf{D}_s \mathbf{B}_{sj}^q \right) J d\xi dy \quad (4.87)$$

the initial displacement matrix \mathbf{K}_L , which is quadratically dependent displacement

$\boldsymbol{\delta}$ is

$$[\mathbf{K}_{Lij}^e]^{pq} = \int_0^b \int_{-1}^{+1} \left([\mathbf{B}_{mj}^p]^T \mathbf{D}_m \mathbf{B}_{Lj}^q + [\mathbf{B}_{Lj}^p]^T \mathbf{D}_m \mathbf{B}_{Lj}^q + [\mathbf{B}_{Lj}^p]^T \mathbf{D}_m \mathbf{B}_{Lj}^q \right) J d\xi dy \quad (4.88)$$

and the initial stress matrix \mathbf{K}_σ is

$$[\mathbf{K}_{\sigma ij}^e]^{pq} = \int_0^b \int_{-1}^{+1} \mathbf{G}^T \begin{bmatrix} \sigma_{m\ell} & \sigma_{m\ell y} \\ \sigma_{m\ell y} & \sigma_{my} \end{bmatrix} \mathbf{G} J d\xi dy \quad (4.89)$$

The matrices $\mathbf{D}_m, \mathbf{D}_b, \mathbf{D}_s$ of constitutive coefficients and $\mathbf{B}_{mi}^p, \mathbf{B}_{bi}^p, \mathbf{B}_{si}^p$ the membrane, bending and shear strain displacement matrices associated with harmonic p , node i and Jacobian J are given in Appendix A.

4.5.8 Equivalent nodal loads due to stresses

To evaluate the residual nodal force vector $\boldsymbol{\psi}(\boldsymbol{\delta})$ of equation (4.78) the equivalent nodal forces due to the stress resultants $\boldsymbol{\sigma}$ may be written for a typical node i as

$$\mathbf{P}_i = \int_0^b \int_{\ell^e} \left\{ (\mathbf{B}_{mi}^p)^T \boldsymbol{\sigma}_m + (\mathbf{B}_{Li}^p)^T \boldsymbol{\sigma}_m + (\mathbf{B}_{bi}^p)^T \boldsymbol{\sigma}_b + (\mathbf{B}_{si}^p)^T \boldsymbol{\sigma}_s \right\} d\ell dy \quad (4.90)$$

For all the Mindlin elements stresses are extrapolated from Gauss point values in a manner consistent with the integration rule used for the tangent stiffness matrix calculation. Newton-Raphson iteration technique is used for iteration. Convergence is checked using total residual norm criteria as

$$\frac{\sqrt{\sum_{i=1}^N \psi^2}}{\sqrt{\sum_{i=1}^N \mathbf{R}^2}} \times 100 \leq \gamma$$

where γ is convergence tolerance (%). The basic algorithm for the geometrically nonlinear analysis is given in Figure 4.4.

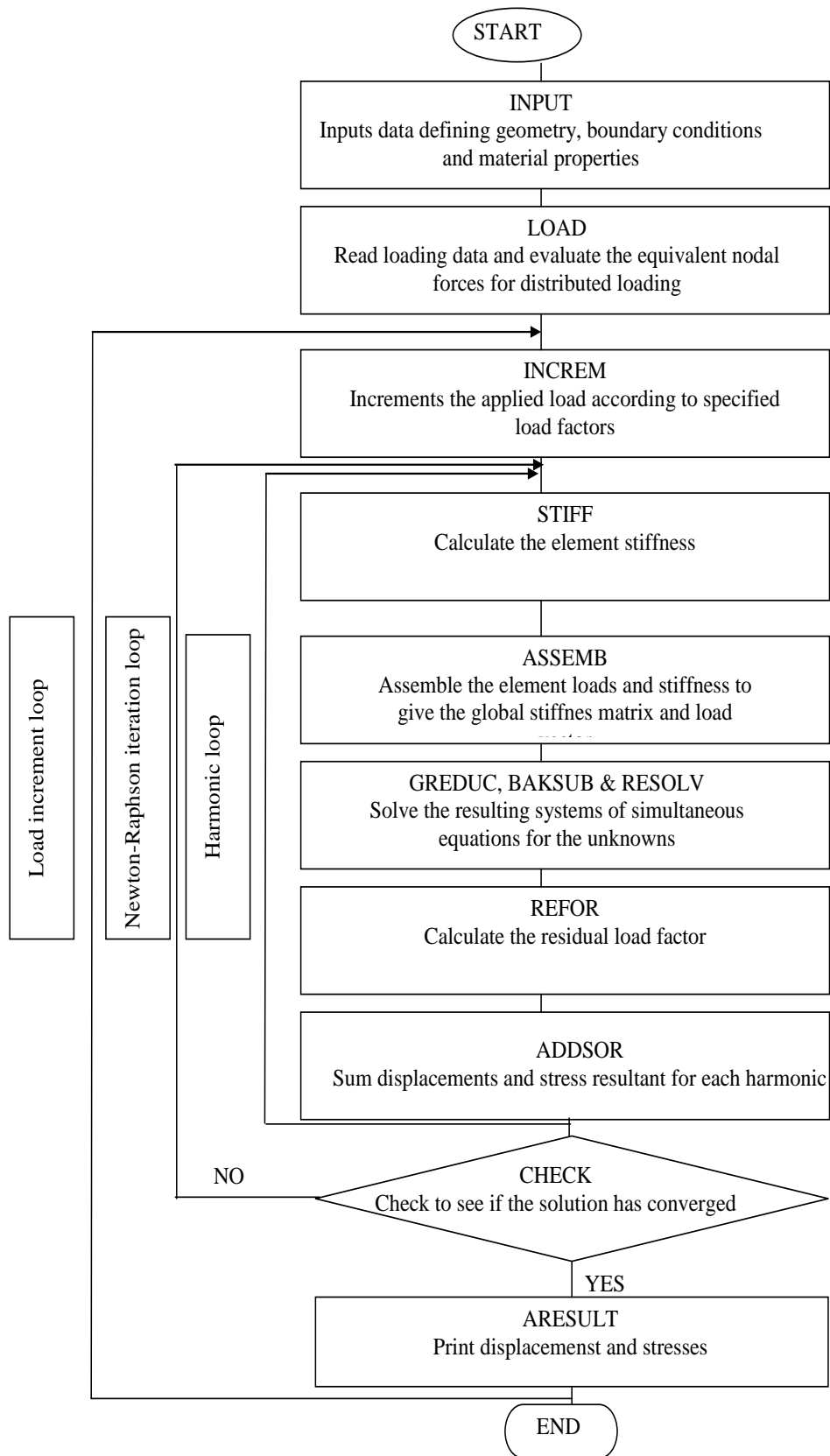


Figure 4.4 Plate problem flowchart

4.6 Examples

To verify that the present formulation can be used successfully for the geometric nonlinear analysis of plates, several examples for which solutions are available have been considered. In all cases, the boundary conditions at the ends of the structure, i.e. at $y = 0$ and $y = b$, correspond to ‘hard’ simple diaphragm supports-in other words $v = \omega = \phi = 0$.

4.6.1 Isotropic square plates under uniform transverse loading with various boundary conditions

The first set of examples is concerned with the geometric nonlinear analysis of plates with various combinations of boundary conditions. For the sake of convenience we adopt the following notations to describe the boundary conditions for the plates analyzed in this section: **A/B/C/D** which implies (boundary condition on side $y = 0$) / (boundary condition on side $x = A$) / (boundary condition on side $y = A$) / (boundary condition on side $x = 0$). A hard simply supported edge (i.e. with the lateral displacements and tangential edge rotations constrained to zero) is represented by **S_h**, a clamped edge by **C** and a free edge **F**. Because of the nature of the FS Fourier series representations of the displacements and rotations, hard simple supports always occurs at the ends $y = 0$ and $y = A$ but other two edges can be arbitrarily restrained. In this example central deflections and loads are given in non-dimensional form as follows:

$$\text{Central deflection} \quad W = w(A/2, A/2)/t$$

$$\text{Uniformly distributed load} \quad Q = (qA^4)/Et^4$$

Where A is characteristic plate dimension, q is uniformly distributed load. All examples use the modified Newton-Raphson approach and convergence is checked using a total residual norm criterion as;

$$\frac{(\Psi^T \Psi)^{1/2}}{(\mathbf{R}^T \mathbf{R})^{1/2}} \times 100 \leq \gamma$$

where γ is convergence tolerance (%). For the integration in equation (4.77) Gauss quadrature is used.

Square simply supported ($S_h / S_h / S_h / S_h$) isotropic plates: The first set of examples is concerned with uniformly loaded isotropic square plate with all edges simply supported (see Figure 4.5). The results generated by the present approach are given in Table 4.2 in the form of a convergence study with respect to both type of strip. Linear, quadratic and cubic strips are used with increased loading.

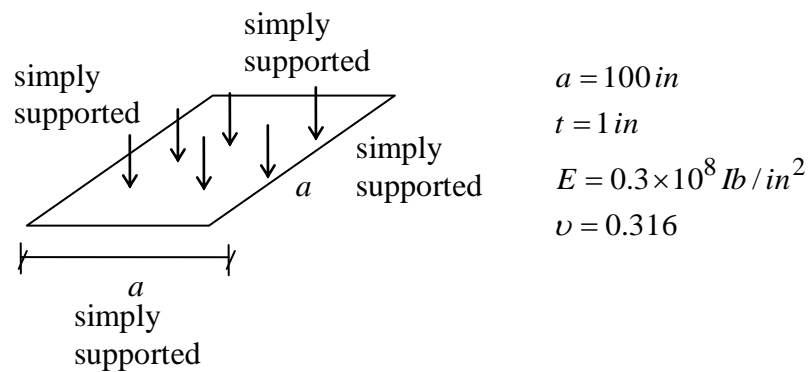


Figure 4.5 Square isotropic plate ($S_h / S_h / S_h / S_h$) under uniformly distributed load

Table 4.2 Central deflection, W , for ($S_h / S_h / S_h / S_h$) isotropic square plates

Load $Q(Ibs)$	$W (in)$				
	Linear	Quadratic	Cubic	Ref[113]	ANSYS
9.16	0.353	0.3477	0.3479	0.335	0.3543
36.6	0.83	0.8181	0.8182	0.818	0.8353
146.5	1.4932	1.4656	1.4658	1.47	1.5003
586	2.4382	2.3929	2.3934	2.4	2.453
2344	3.8988	3.8127	3.8137	3.83	3.9163
9377	6.1573	6.0524	6.0542	6.07	6.2543

It can be seen from Table 4.2 that results obtained using 3-noded quadratic strips are almost identical to those obtained using 4-noded cubic strips and very close to the values obtained by Rushton [113] who used a finite difference approach and ANSYS program results while the 2-noded linear strips gives less accurate, but acceptable, values. The convergence tolerance for the results is $\gamma = 1\%$.

Square simply supported and free supported ($S_h / F / S_h / F$) isotropic plates: The second example is concerned with uniformly loaded isotropic square plate having two free edges. The geometry and material properties are given in Figure 4.6. The plates are analyzed using 2-noded linear, 3-noded and 4-noded cubic strips.

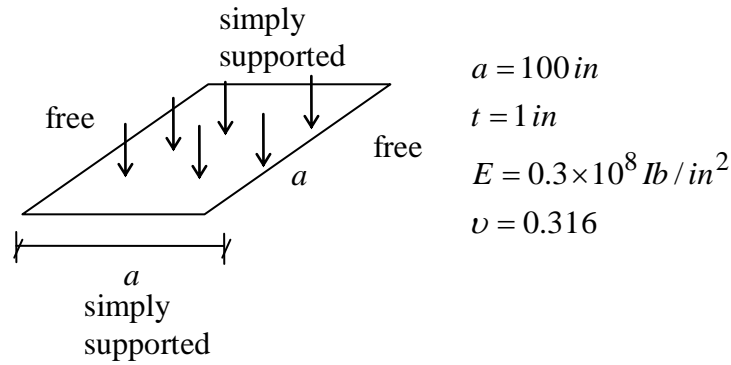


Figure 4.6 Square isotropic plate ($S_h / F / S_h / F$) under uniformly distributed load

In Table 4.3 results are given obtained using a 1% convergence tolerance for ($S_h / F / S_h / F$) boundary condition. The load is increased from 1.11 lbs to 38.3 lbs with doubling at each step. Again 3-noded quadratic strips and 4-noded cubic strips perform well in comparison with ANSYS program results.

Table 4.3 Central deflection, W , for ($S_h / F / S_h / F$) isotropic square plates

Load Q(lbs)	W (in)			
	Linear	Quadratic	Cubic	ANSYS
1.11	0.1549	0.1551	0.1568	0.1578
2.22	0.3253	0.3173	0.3199	0.3157
4.44	0.6446	0.6387	0.6396	0.6316
8.89	1.2736	1.2603	1.2629	1.2646
17.79	2.5405	2.5341	2.5363	2.5303
38.3	5.4503	5.449	5.5409	5.4476

Square simply supported and clamped ($S_h / C / S_h / C$) isotropic plates: The second example is concerned with uniformly loaded isotropic square plate having two clamped edges (see Figure 4.7). The analytical thin plate solution is given by Levy [114] who used Von Karman's equations employing double Fourier series.

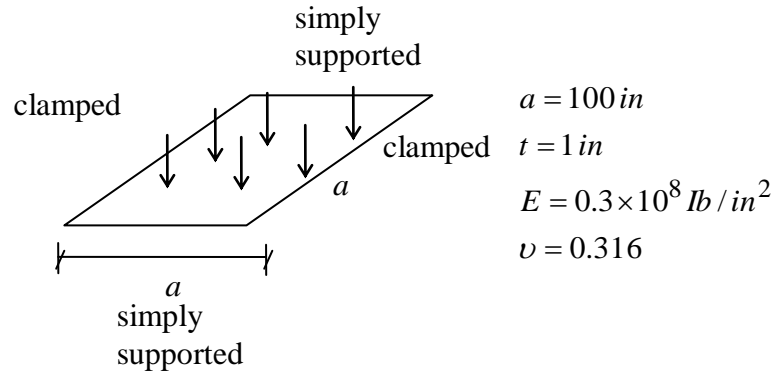


Figure 4.7 Square isotropic plate ($S_h / C / S_h / C$) under uniformly distributed load

Table 4.4 Central deflection, W , for ($S_h / C / S_h / C$) isotropic square plates

Load $Q(\text{lbs})$	$W \text{ (in)}$				
	Linear	Quadratic	Cubic	Ref[114]	ANSYS
17.79	0.2346	0.2349	0.2365	0.237	0.2402
38.3	0.4703	0.4671	0.4677	0.471	0.4833
63.4	0.5989	0.6886	0.6914	0.695	0.7393
95.0	0.9192	0.9004	0.903	0.912	0.9346
134.9	1.132	1.1043	1.1065	1.121	1.1503
184.0	1.3353	1.2993	1.3012	1.322	1.3566
245.0	1.5346	1.4912	1.4927	1.521	1.5676
318.0	1.7436	1.6772	1.6784	1.714	1.761
402.0	1.9105	1.8678	1.8541	1.902	1.795

Results for ($S_h / C / S_h / C$) boundary conditions are given in Table 4.4. The load is increased from 17.79 lbs to 402 lbs doubling at each step. It can be seen that 3-noded quadratic strips and 4-noded cubic strips give sufficiently good results for deflections in comparison to those found in reference [114] and by ANSYS program. A different result is the accuracy of the 2-noded linear strips for displacements. These results are obtained using a convergence tolerance $\gamma = 1\%$.

4.6.2 Postbuckling of isotropic square plates under in-plane uniaxial uniform loading with various boundary conditions

Square, isotropic plates of side length a which is subjected to linear buckling analysis using FS method by Özakça et al. [1], subjected to postbuckling are considered here. The behavior of three types of plates is examined, these being a plate with all edges simply supported ($S_h / S_h / S_h / S_h$) a plate with one pair of opposite edges simply supported, the other pair free ($S_h / F / S_h / F$) and the same plate with the other pair of edges clamped ($S_h / C / S_h / C$). In each case, the plates are loaded via the longitudinal displacement at the edge of the plate at the ends which are simply supported in the out of plane direction and are assumed to behave orthotropically in bending. In all examples thickness is taken as $t = 0.1a$.

Square simply supported ($S_h / S_h / S_h / S_h$) isotropic plates: In this example postbuckling analysis of plates which are subjected to linear buckling analysis by Kolcu [1] is considered. It is generally assumed that Poisson's ratio $\nu = 0.3$. The elastic modulus E is taken as 1106.43 MPa. The geometric properties are given in Figure 4.8.

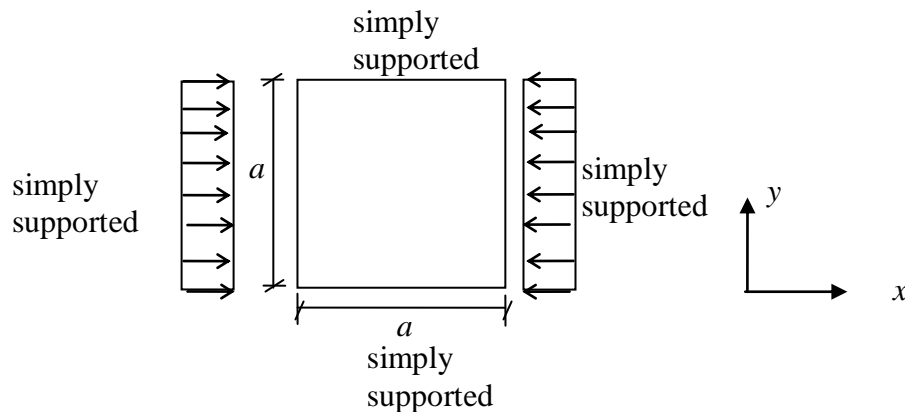


Figure 4.8 ($S_h / S_h / S_h / S_h$) plate under uniaxial load

Linear buckling load for ten 4-noded cubic strips is obtained using FS method [1] as 3.731 N. The plate is subjected to loads varying with small increments and subjected to postbuckling. Load level, the longitudinal displacement at the edge of the plate, U , in the x direction and central deflection, W , are given in Table 4.5.

Table 4.5 The longitudinal displacement at the edge of the plate, U , and central deflection, W , for postbuckling of a square ($S_h / S_h / S_h / S_h$) isotropic plate

Load (kN)	U (mm)		W (mm)	
	Present	ANSYS	Present	ANSYS
0.7312	0.00793	0.00832	0.00075	0.00079
1.7312	0.01613	0.01693	0.00274	0.00287
2.7312	0.02437	0.02559	0.00837	0.00878
3.7312	0.03666	0.03851	0.04193	0.04403
4.7312	0.05562	0.05888	0.09470	0.09944
5.7312	0.07718	0.08104	0.13100	0.13755
6.7312	0.09889	0.10432	0.15929	0.16725
7.7312	0.12269	0.12874	0.18299	0.19214
8.7312	0.14728	0.15465	0.2038	0.21399
9.7312	0.16744	0.17583	0.22293	0.23407
10.000	0.15363	0.18436	0.23933	0.22794

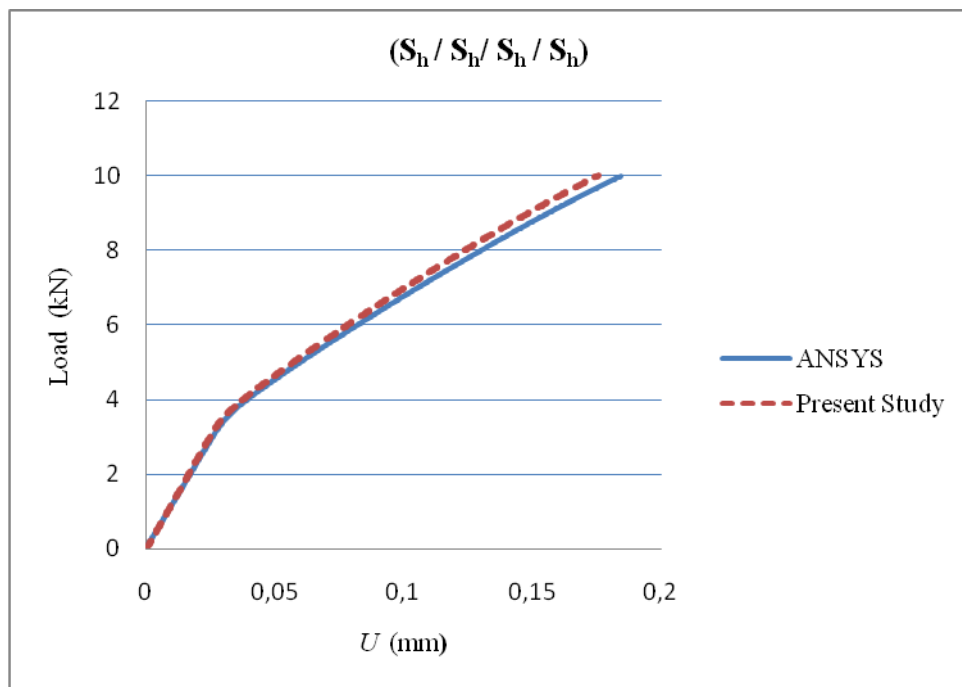


Figure 4.9 Variation of load versus the longitudinal displacement at the edge of the plate, U , for the postbuckling of a square ($S_h / S_h / S_h / S_h$) isotropic plate

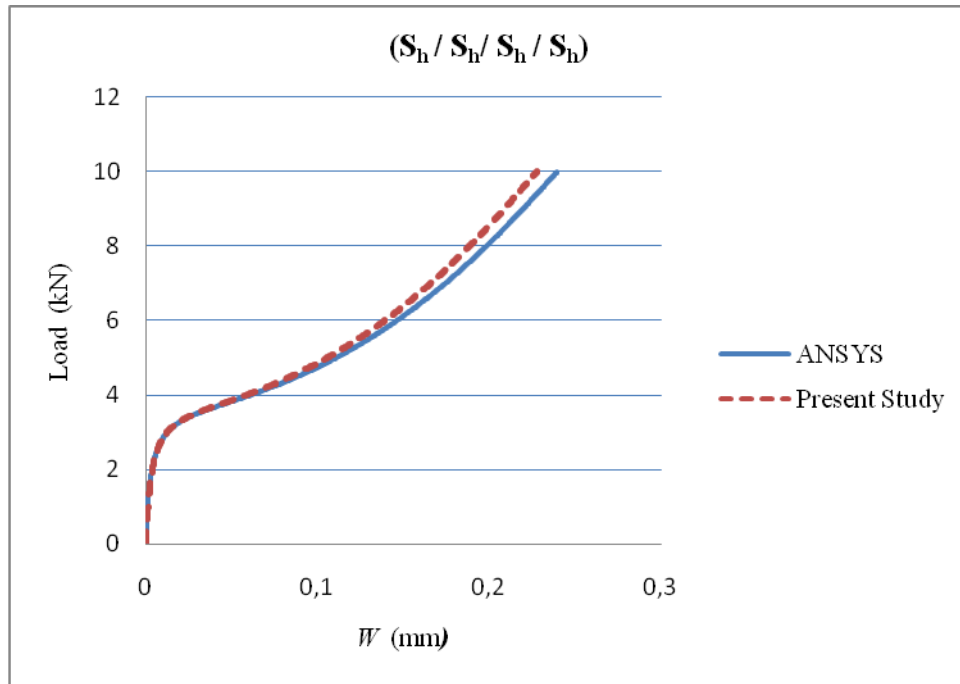


Figure 4.10 Variation of load versus center deflection, W , for the postbuckling of a square $(S_h / S_h / S_h / S_h)$ isotropic plate

Load increment and x displacement varies nearly linearly to bifurcation point. After that point, displacement increases more rapidly compared to the load increment. The results generated by the present approach are given in Figure 4.9 and Figure 4.10. A good agreement is found between the FS results and the FE results obtained by ANSYS program.

Square simply supported and free supported $(S_h / F / S_h / F)$ isotropic plates: The second example is concerned with uniformly loaded isotropic square plate having two free edges and two simply supported edges which is subjected to linear buckling analysis by Kolcu [1]. The geometric properties are given in Figure 4.11. The elastic modulus E is taken as 1139.86 MPa and Poisson's ratio as $\nu = 0.25$.

Numerical results are given in Table 4.6 for the longitudinal displacement at the edge of the plate, U , and central deflection, W . The load is increased from 0.03321 kN to 1 kN with 0.1 kN increments. The lowest buckling load for ten 4-noded cubic strips is obtained using FS method [1] in the previous study as 0.933 kN.

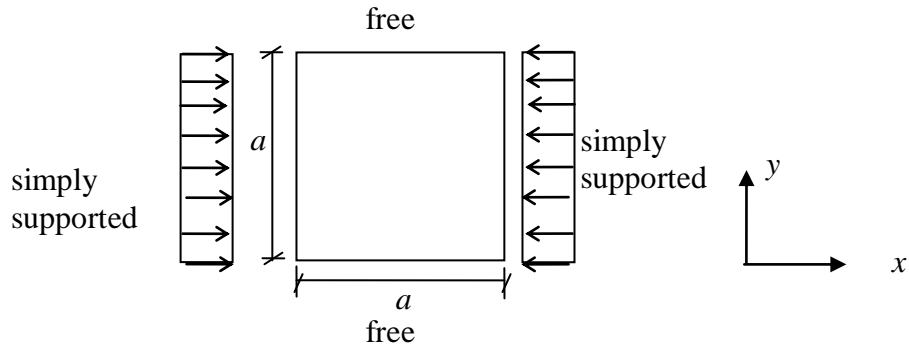


Figure 4.11 ($S_h / F / S_h / F$) plate under uniaxial load

Table 4.6 The longitudinal displacement at the edge of the plate, U , and central deflection, W , for postbuckling of a square ($S_h / F / S_h / F$) isotropic plate

Load (kN)	U (mm)		W (mm)	
	Present	ANSYS	Present	ANSYS
0.03321	0.00026	0.00029	0.00009	0.0001
0.13321	0.00105	0.00115	0.00043	0.00047
0.23321	0.00184	0.00202	0.00085	0.00093
0.33321	0.00266	0.00293	0.0014	0.00154
0.43321	0.00343	0.00377	0.00215	0.00236
0.53321	0.00426	0.00468	0.00324	0.00356
0.63321	0.00507	0.00557	0.00495	0.00544
0.73321	0.00602	0.00662	0.00795	0.00874
0.83321	0.00739	0.00812	0.01519	0.01671
0.93321	0.01386	0.01525	0.04534	0.04987
1.00000	0.05578	0.06136	0.12684	0.13952

It can be seen from Figure 4.12 and 4.13 that the present result and FE method values are getting closer at the lower loads. After linear buckling load, displacements increase rapidly. U is obtained as 0.03879 mm and W is 0.102746 mm for buckling load. The, plates buckle with one longitudinal half-wave and so the analysis of the single-term type $p_1 = p_2 = 1$. The postbuckling curve for FS method values is very close to the FE method values of ANSYS program.

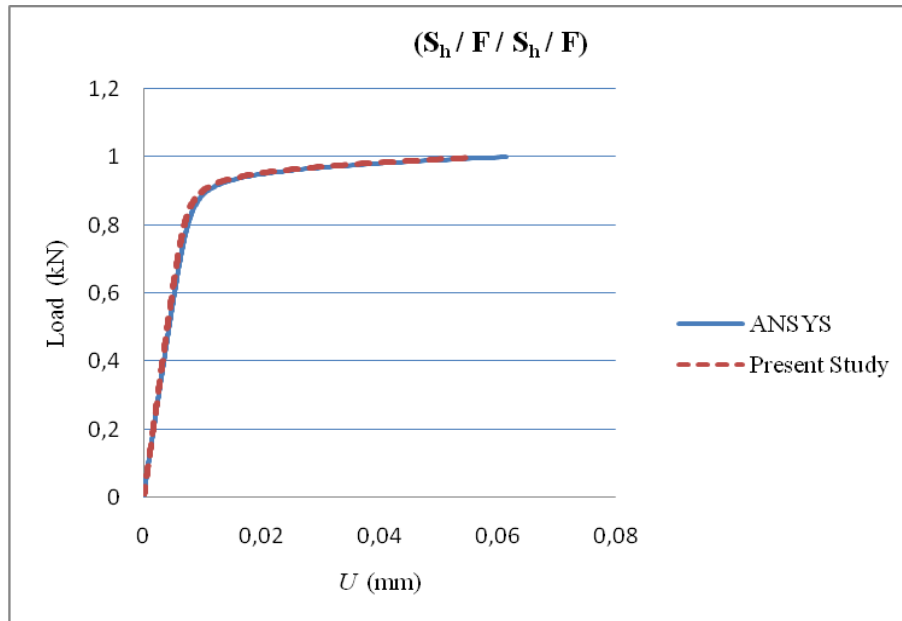


Figure 4.12 Variation of load versus the longitudinal displacement at the edge of the plate, U , for the postbuckling of a square $(S_h / F / S_h / F)$ isotropic plate

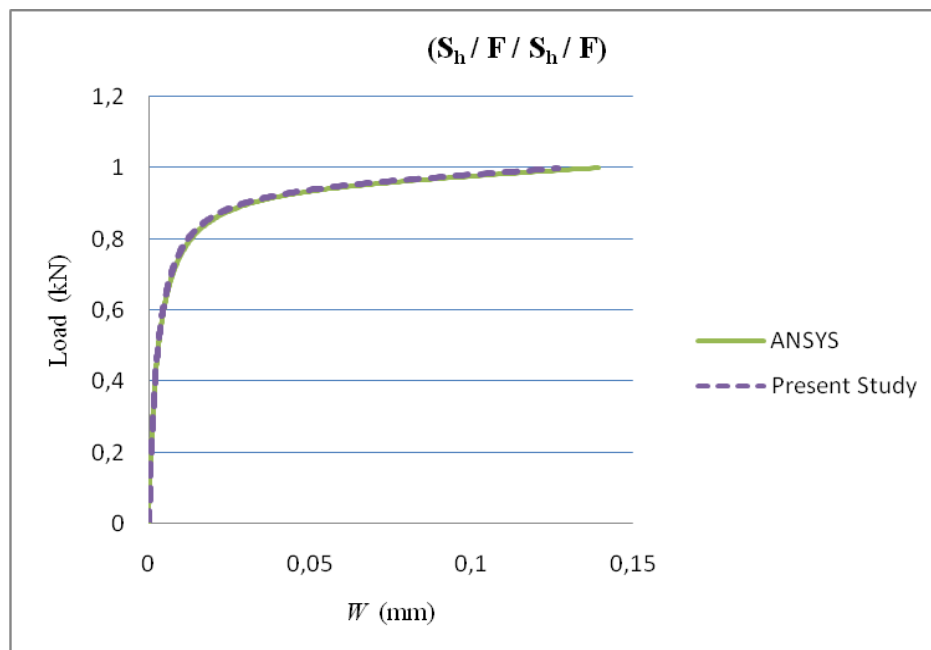


Figure 4.13 Variation of load versus the deflection at the center of the plate, W , for the postbuckling of a square $(S_h / F / S_h / F)$ isotropic plate

Square simply supported and clamped (S_h / C / S_h / C) isotropic plate: The third example is concerned with uniformly loaded isotropic square plate which has two edges clamped. It is generally assumed that Poisson's ratio is $\nu = 0.3$. The elastic modulus E is taken as 1106.43 MPa. The geometric properties are given in Figure 4.14

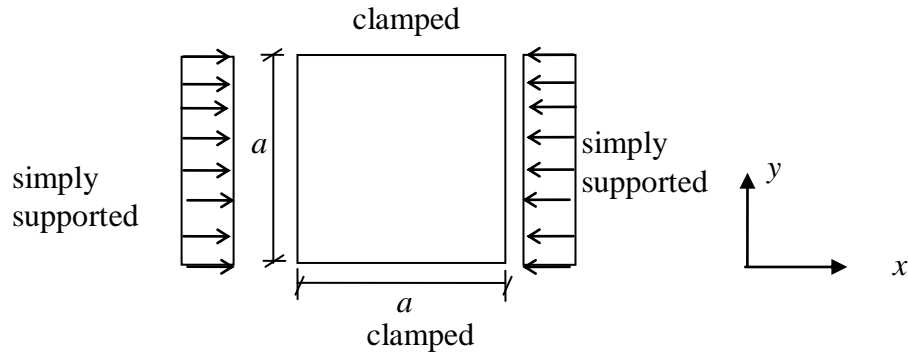


Figure 4.14 (S_h / C / S_h / C) plate under uniaxial load

Table 4.7 list the longitudinal displacement at the edge of the plate in the x direction, U , and central deflection, W , obtained using cubic strips. The FS result for linear buckling load for ten 4-noded cubic strips is obtained in the previous study [1] as 5.773 kN. The load is increased from 0.7732 kN to 10 kN.

Table 4.7 The longitudinal displacement at the edge of the plate, U , and central deflection, W , for postbuckling of a square (S_h / C / S_h / C) isotropic plate

Load (kN)	U (mm)		W (mm)	
	Present	ANSYS	Present	ANSYS
0.7732	0.00601	0.00632	0.0005	0.00052
1.7732	0.01371	0.01439	0.00142	0.0015
2.7732	0.0213	0.02236	0.00295	0.0031
3.7732	0.02882	0.03026	0.0059	0.00619
4.7732	0.03643	0.03826	0.01351	0.01419
5.7732	0.04557	0.04785	0.03728	0.03914
6.7732	0.05768	0.06056	0.06795	0.07135
7.7732	0.07097	0.07451	0.09235	0.09697
8.7732	0.08488	0.08912	0.11245	0.11807
9.7732	0.09932	0.10429	0.1298	0.13629
10.000	0.09376	0.10783	0.13347	0.14014

In Figure 4.15 and 4.16 the postbuckling behavior of isotropic square plates is given. The edge displacement in the x direction, U , is obtained as 0.04335 mm and the center deflection W is obtained as 0.03996 mm. The percentage differences between the computed postbuckling results and FE method results obtained by ANSYS program values, range from 0.43% to 5.0% which is quite reasonable.

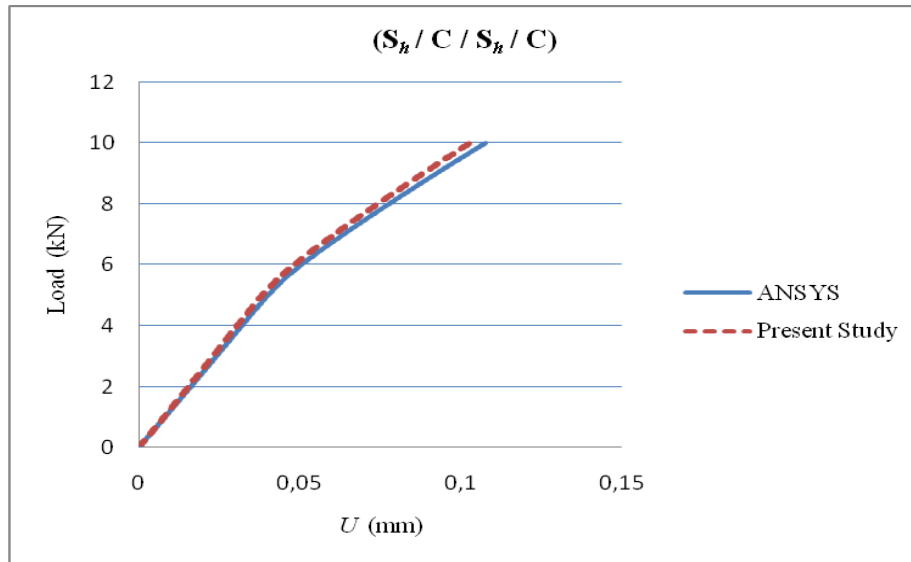


Figure 4.15 Variation of load versus the longitudinal displacement at the edge of the plate, U , for the postbuckling of a square ($S_h / C / S_h / C$) isotropic plate

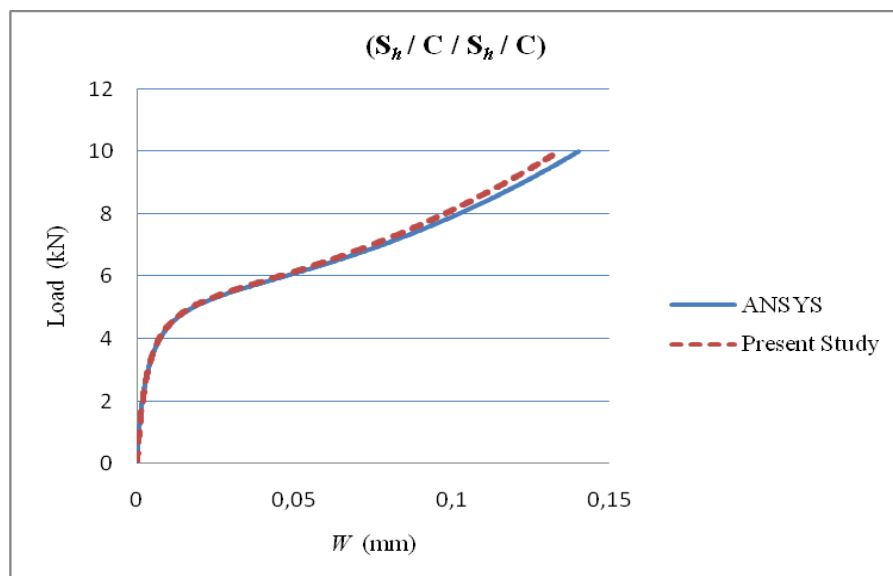


Figure 4.16 Variation of load versus the deflection at the center of the plate, W , for the postbuckling of a square ($S_h / C / S_h / C$) isotropic plate

4.6.2 Postbuckling of straight stiffened plate

Stiffened panels due to high strength to weight ratio have wide use in ships, airplanes and some land-based structures as the building block of the primary load-carrying structure. The design of large parts of ship and airplane structures is primarily driven by compressive strength where for civil transport aircraft the structural response of the upper wing and the lower fuselage shell. The structural stability of these thin-walled structures subjected to compressive loads is dependent on the buckling strength of the structure as a whole and of each structural member.

Ekmekyapar [115] investigated different types of stiffened panels which are illustrated in Figure 4.17. He studied the linear buckling and optimization of buckling loads for these types of plates by experimental studies using FS method.

In this example postbuckling analysis of straight stiffened plates with 3, 4, and 5 stiffeners which are subjected to linear buckling analysis by Ekmekyapar [115] is considered. The material used in stiffened plates is aluminum-alloy that has $E = 73000\text{MPa}$ modulus of elasticity and $\nu = 0.33$ Poisson's ratio. The height of the stiffeners is equal to 28.0 mm. The geometric properties for 3 stiffeners are given in Figure 4.17. Loading and boundary conditions are given in Figure 4.18.

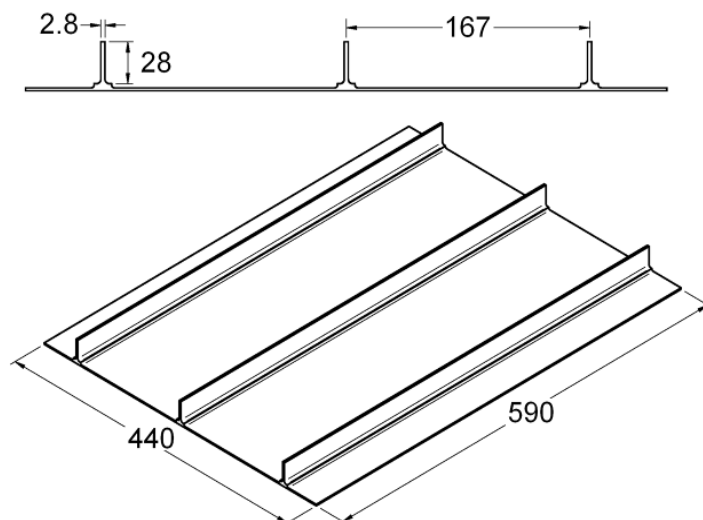


Figure 4.17 Dimensions of typical stiffened panel

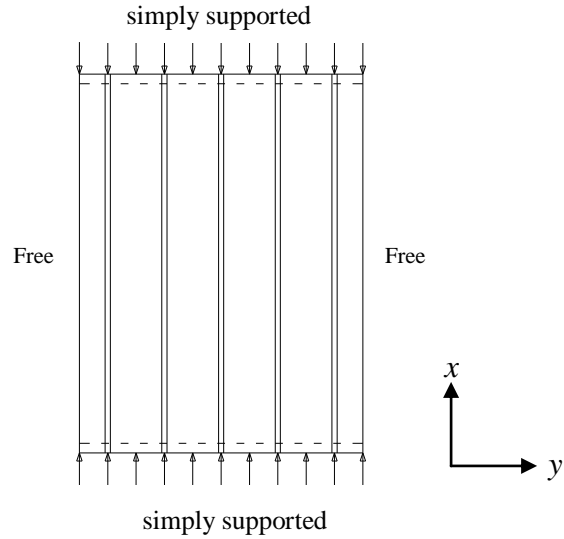


Figure 4.18 Loading and boundary conditions of stiffened plate

Linear buckling load for cubic strips is obtained using FS method [115] as 59731.7 kN for 3 stiffeners, 97565.0 kN for 4 stiffeners and 136548.5 kN for 5 stiffeners. The plate is subjected to load steps with small load increment and followed into the postbuckling region. Load steps versus longitudinal shortening of the stiffened plate in the x direction are given in Table 4.8.

Table 4.8 Longitudinal shortening of the straight stiffened plate

Load (kN)	Longitudinal shortening (mm)					
	3 stiffeners		4 stiffeners		5 stiffeners	
	Present	ANSYS	Present	ANSYS	Present	ANSYS
30	0.00019	0.0002	0.00019	0.0002	0.00019	0.0002
13554	0.0865	0.09169	0.08777	0.09177	0.08728	0.09184
28554	0.1822	0.19313	0.18487	0.19331	0.18384	0.19345
43554	0.27787	0.29454	0.28194	0.2948	0.28036	0.29503
58554	0.37497	0.39747	0.37897	0.39626	0.37685	0.39657
73554	0.50778	0.53824	0.47598	0.4977	0.47331	0.49807
88554	0.65195	0.69107	0.573	0.59914	0.56974	0.59954
103554	0.80244	0.85059	0.6816	0.7127	0.66613	0.70098
118554	0.95841	1.01591	0.81167	0.84871	0.76252	0.80241
133554	1.12093	1.18819	0.9521	0.99554	0.8595	0.90447
144108	1.2524	1.32754	1.06031	1.10868	0.94027	0.98946

Load steps and longitudinal shortening varies nearly linearly up to the bifurcation point. After that point shortening increases rapidly compared to load value. The results generated by the present approach are given in Figures 4.19-21. A good agreement is observed between FS method results and FE method results obtained by ANSYS program. The comparison of the postbuckling performance of 3, 4 and 5 stiffener plates shows that increasing the stiffener number improves the strength against initial imperfection (Figure 4.22).

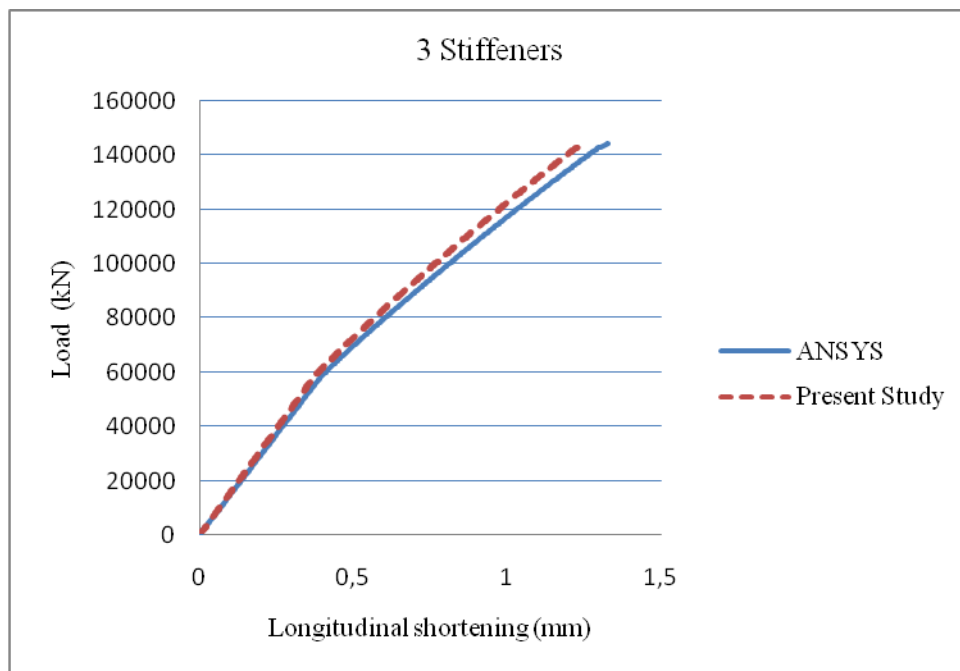


Figure 4.19 Variation of load versus the longitudinal shortening of the plate with 3 stiffeners

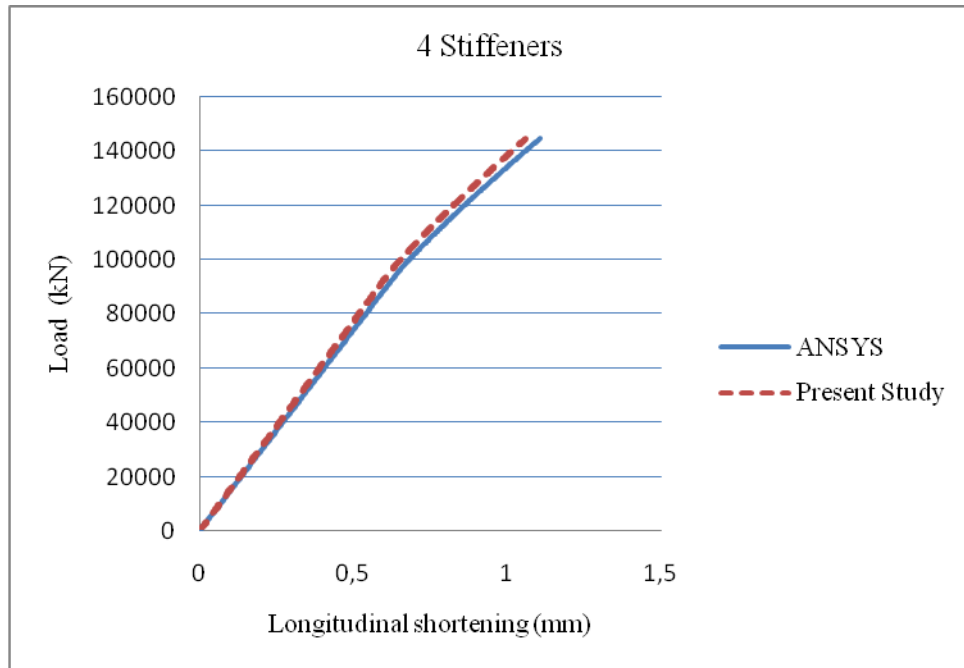


Figure 4.20 Variation of load versus the longitudinal shortening of the plate with 4 stiffeners

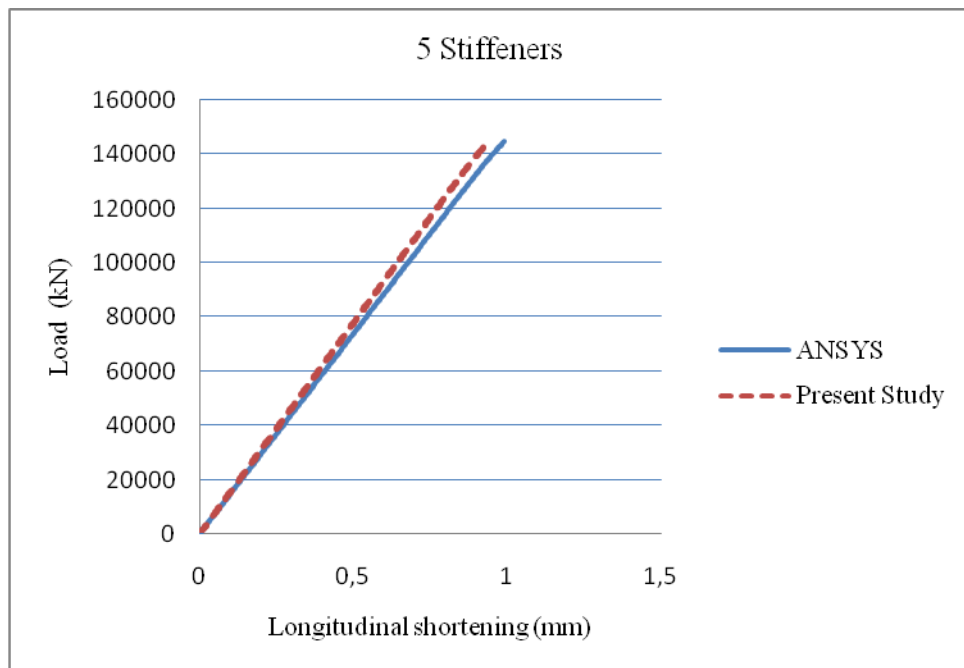


Figure 4.21 Variation of load versus the longitudinal shortening of the plate with 5 stiffeners

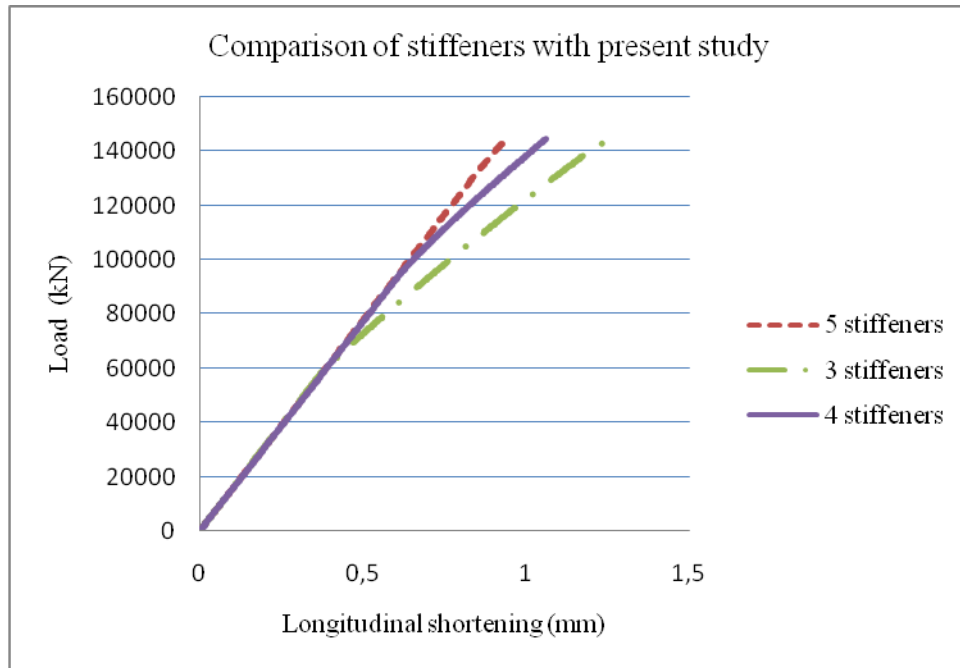


Figure 4.22 Comparison of postbuckling performance of straight stiffened plates

4.6.2 Comparison of postbuckling performance of optimized stiffened plate

Stiffened panels are easily designed through the use of a structural shape optimization procedure. The buckling load carrying capacities of stiffened panels are improved by decreasing weight of the structures. However, in many cases the stiffness of the panel as a whole is significantly reduced after buckling, where the ultimate strength of the panel has normally not yet been reached since the panel enters into a post-buckling regime causing panel failure or collapse. Thus, the optimum design of stiffened panels under compressive loads needs also post-buckling behavior analysis to carry the loads safely and economically.

There are five different stiffened plate types with straight stiffeners illustrated in Figure 4.18. The effect of the number of main stiffeners on critical buckling load from three to five is investigated. Note that Figure 4.23 shows only plate types with five stiffeners. During the baseline design before optimization, the initial values of plate base thickness and stiffener thickness are considered to have same values and sub-stiffener thickness is taken $\frac{1}{2}$ of them (BL). Accordingly, the initial values of design variables are listed in Table 4.9 [115]. Then, beginning with initial values optimization process is performed and critical buckling loads are maximized.

Improvements on linear buckling load are considerable serious. Structural elements which are used as design variables are thicknesses and heights of stiffeners and sub-stiffeners (C1) and widths of pads (C2).

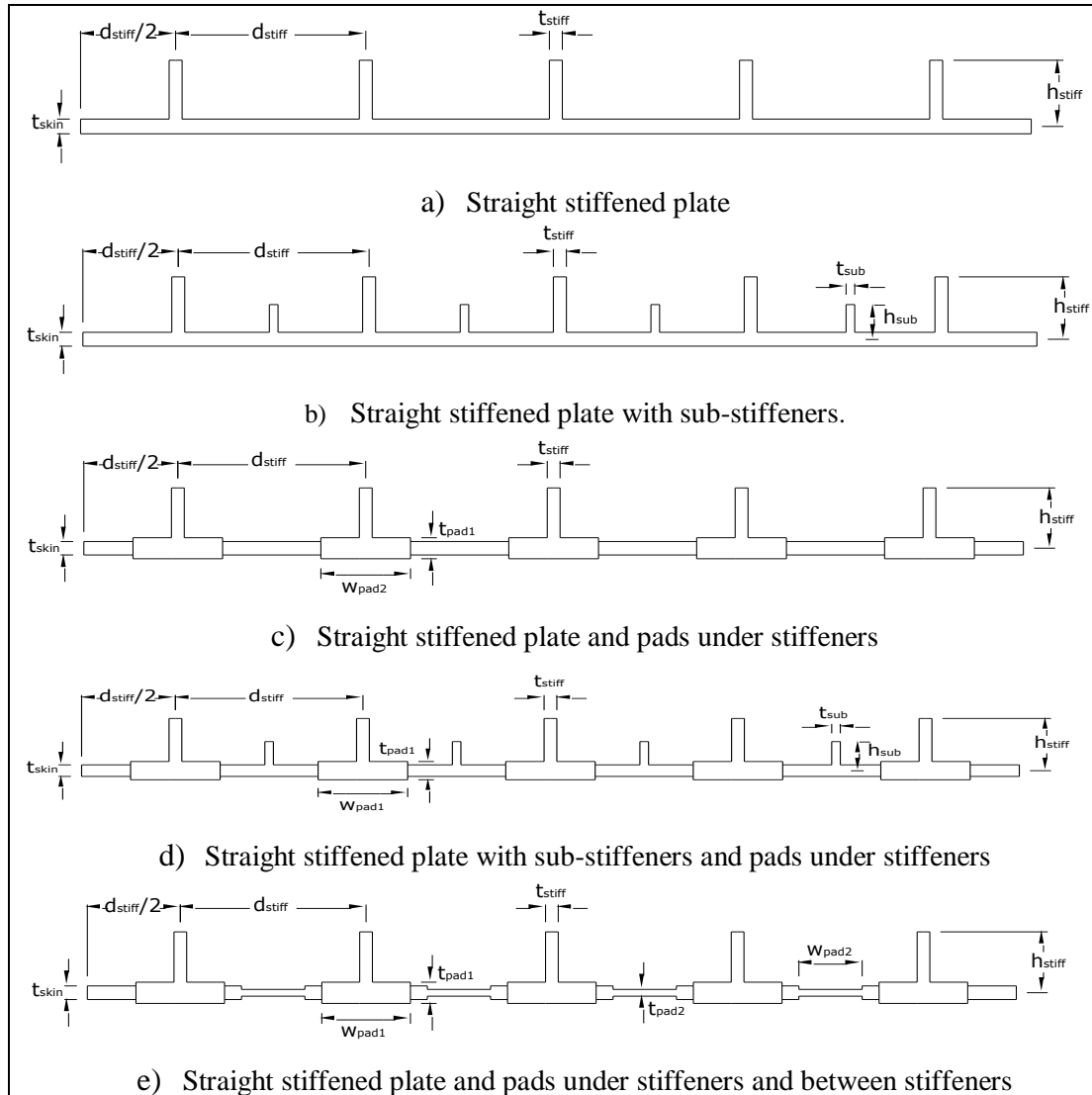


Figure 4.23 Examined stiffened plate types

After obtaining linear buckling results of optimized plates nonlinear analysis is carried out by the program developed. First, geometric nonlinearity is included in the analyses and collapse loads of stiffened plates are found. Newton-Raphson method is used in the solution of nonlinear problems.

Table 4.9 Stiffened plate types and their baseline design rules

Type	Optimized stiffened plate types	Baseline values
a	Straight stiffened plate (base profile)	$t_{skin} = t_{stiff}$
b	Straight stiffened plate with sub-stiffeners	$t_{skin} = t_{stiff}$ $t_{sub} = 0.75 \times t_{stiff}$
c	Straight stiffened plate and pads under stiffeners	$t_{skin} = t_{stiff}$ $t_{pad1} = 2 \times t_{stiff}$
d	Straight stiffened plate with sub-stiffeners and pads under stiffeners	$t_{skin} = t_{stiff}$ $t_{pad1} = 2 \times t_{stiff}$ $t_{sub} = 0.75 \times t_{stiff}$
e	Straight stiffened plate and pads under stiffeners and between stiffeners	$t_{skin} = t_{stiff} = t_{pad2}$ $t_{pad1} = 2 \times t_{stiff}$

As discussed above, to initiate a nonlinear buckling eigenmode initial imperfection is preferred. The eigenmode imperfection reflects the real structure behavior. The structure exhibits most of the nonlinear behavior after linear buckling. So, it should be taken into account to enforce the structure to go into real buckling mode in nonlinear analysis. Tables 4.10-11 illustrate the collapse loads of stiffened plate types when geometric nonlinearity is considered.

Observing Tables 4.10-14 and Figures 4.24-28 depicts the significance of the number of main stiffeners and optimization on the postbuckling behavior of stiffened panels. The increment of the number of stiffeners is the crucial parameter of improving the buckling and collapse loads. The postbuckling performance in Table 4.10 is 4.6%, in Table 4.11 is 53.7 %, in Table 4.12 is 16.97%, and in Table 4.13 is 38.93%. As seen from Figures 4.24-28, optimization process increased linear buckling loads but generally decreased the collapse loads and postbuckling performance for all types of stiffeners.

Table 4.10 Initial, optimum design variables, critical buckling loads and postbuckling collapse loads of ‘type a’

	3 stiffeners			4 stiffeners			5 stiffeners		
	BL	C 1	C 2	BL	C 1	C 2	BL	C 1	C 2
t _{skin}	2.237	2.434	2.443	2.123	2.324	2.311	2.020	2.200	2.161
t _{stiff}	2.237	1.200	1.229	2.123	1.342	1.954	2.020	1.456	2.209
h _{stiff}			26.405			20.00			20.00
P _{cr}	59.73	62.78	64.25	96.56	105.54	109.94	135.54	148.77	154.61
P _{collapse}	142.50	135.60	135.90	190.80	189.00	147.00	279.00	198.60	183.00

Table 4.11 Initial, optimum design variables, critical buckling loads and postbuckling collapse loads of ‘type b’

	3 stiffeners			4 stiffeners			5 stiffeners		
	BL	C 1	C 2	BL	C 1	C 2	BL	C 1	C 2
t _{skin}	2.150	2.347	2.365	2.008	2.217	2.241	1.884	2.083	2.093
t _{stiff}	2.150	1.326	1.200	2.008	1.322	1.957	1.884	1.348	1.169
t _{sub}	1.6133	1.000	1.926	1.506	1.154	1.175	1.413	1.196	1.070
h _{stiff}			28.121			20.00			20.000
h _{sub}			8.000			8.033			8.000
P _{cr}	63.70	70.34	72.62	98.63	110.72	113.92	134.62	151.21	159.53
P _{collapse}	237.60	154.40	110.00	303.00	191.200	92.00	310.40	218.40	104.00

Table 4.12 Initial, optimum design variables, critical buckling loads and postbuckling collapse loads of ‘type c’

	3 stiffeners			4 stiffeners			5 stiffeners		
	BL	C 1	C 2	BL	C 1	C 2	BL	C 1	C 2
t _{skin}	1.962	1.918	1.908	1.874	1.885	1.816	1.794	1.831	1.812
t _{stiff}	1.962	1.214	1.294	1.874	1.414	1.998	1.794	1.521	2.071
t _{pad1}	3.924	5.000	5.000	3.748	4.396	4.725	3.588	3.922	4.084
h _{stiff}			27.233			20.000			20.081
P _{cr}	69.4	76.5	78.1	112.7	122.0	125.1	158.8	166.4	173.1
P _{collapse}	212.10	175.80	176.10	302.40	238.20	148.80	312.60	271.80	185.40

Table 4.13 Initial, optimum design variables, critical buckling loads and postbuckling collapse loads of ‘type d’

	3 stiffeners			4 stiffeners			5 stiffeners		
	BL	C 1	C 2	BL	C 1	C 2	BL	C 1	C 2
t _{skin}	1.895	1.996	1.999	1.784	1.938	1.936	1.685	1.776	1.865
t _{stiff}	1.895	1.234	1.257	1.784	1.358	1.882	1.685	1.441	2.010
t _{sub}	1.421	1.000	1.000	1.338	1.037	1.000	1.264	1.029	1.109
t _{pad1}	3.791	4.208	4.246	3.569	3.624	3.921	3.371	3.566	3.187
h _{stiff}			27.163			20.000			21.246
h _{sub}			13.372			8.000			9.186
P _{cr}	71.78	79.55	80.99	110.61	124.38	128.07	154.52	165.45	173.19
P _{collapse}	258.90	159.00	158.10	152.40	200.40	149.40	303.60	141.00	228.00

Table 4.14 Initial, optimum design variables, critical buckling loads and postbuckling collapse loads of ‘type e’

	3 stiffeners			4 stiffeners			5 stiffeners		
	BL	C 1	C 2	BL	C 1	C 2	BL	C 1	C 2
t _{skin}	1.962	2.013	2.000	1.874	1.877	1.916	1.794	1.767	1.842
t _{stiff}	1.962	1.275	1.200	1.874	1.465	1.947	1.794	1.581	1.993
t _{pad1}	3.924	5.000	5.000	3.748	4.708	4.678	3.588	4.581	4.232
t _{pad2}	1.962	1.200	1.256	1.874	1.253	1.200	1.794	1.205	1.200
h _{stiff}			29.333			20.000			22.642
P _{cr}	69.41	80.09	82.56	112.76	127.78	131.54	158.85	173.19	179.63
P _{collapse}	219.60	221.40	124.20	307.20	277.20	165.00	300.60	338.40	201.60

Longitudinal shortenings of stiffened plates with load increase introduce the performance of structure during the nonlinear analyses. Figures 4.24-29 illustrate longitudinal shortenings of stiffened plates until collapse loads.

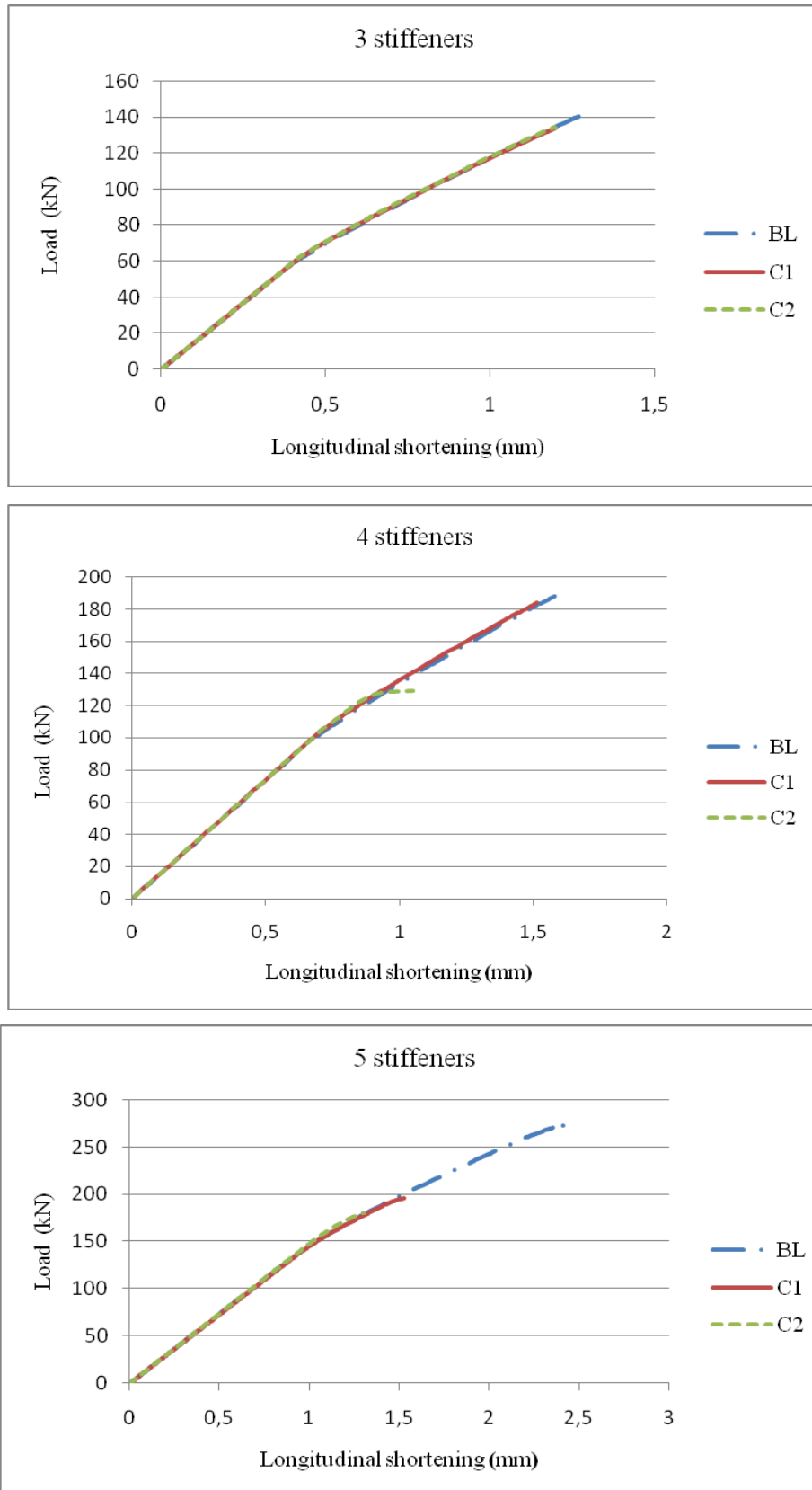


Figure 4.24 Comparison of postbuckling loads according to the number of stiffeners

‘type a’

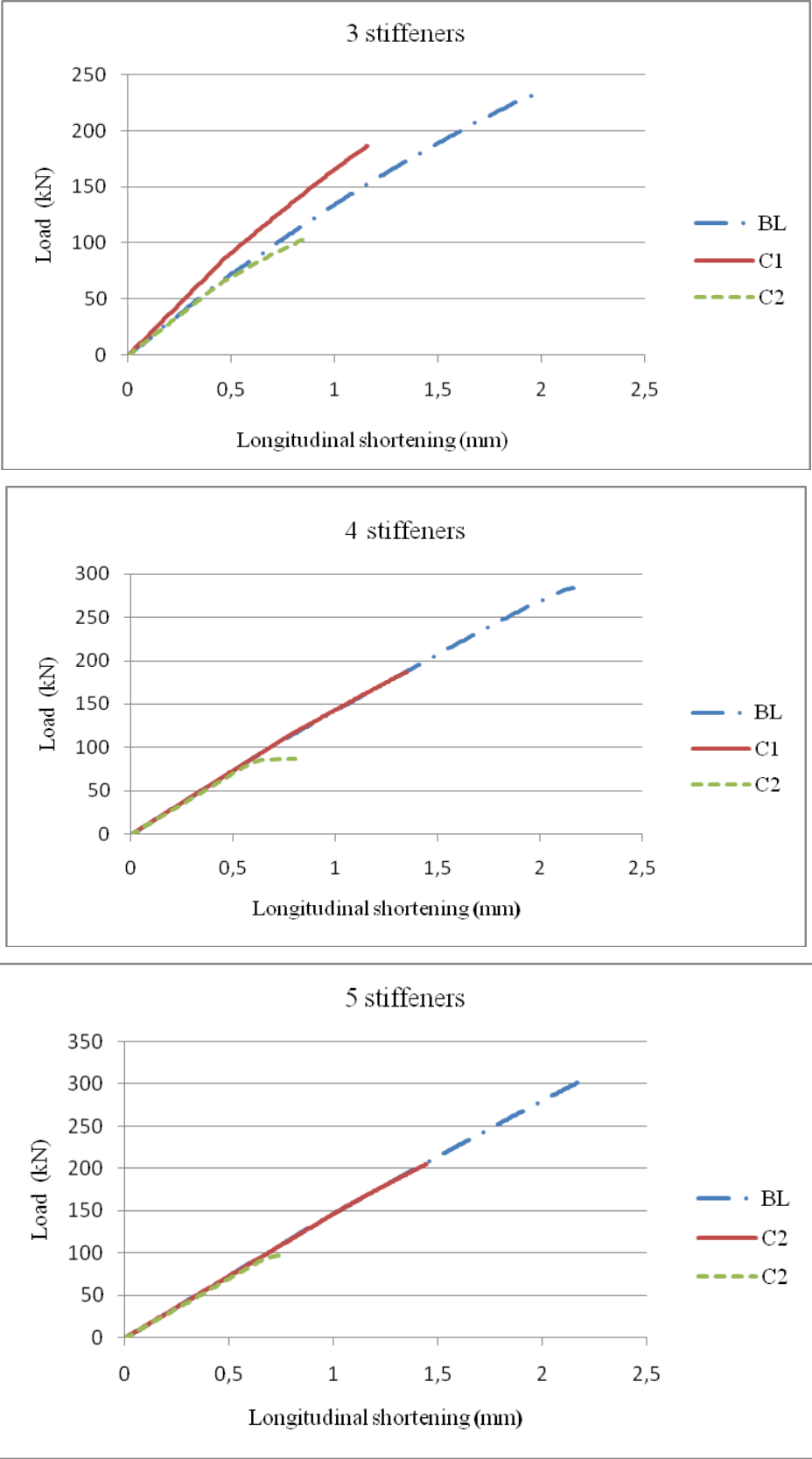


Figure 4.25 Comparison of postbuckling loads according to the number of stiffeners ‘type b’

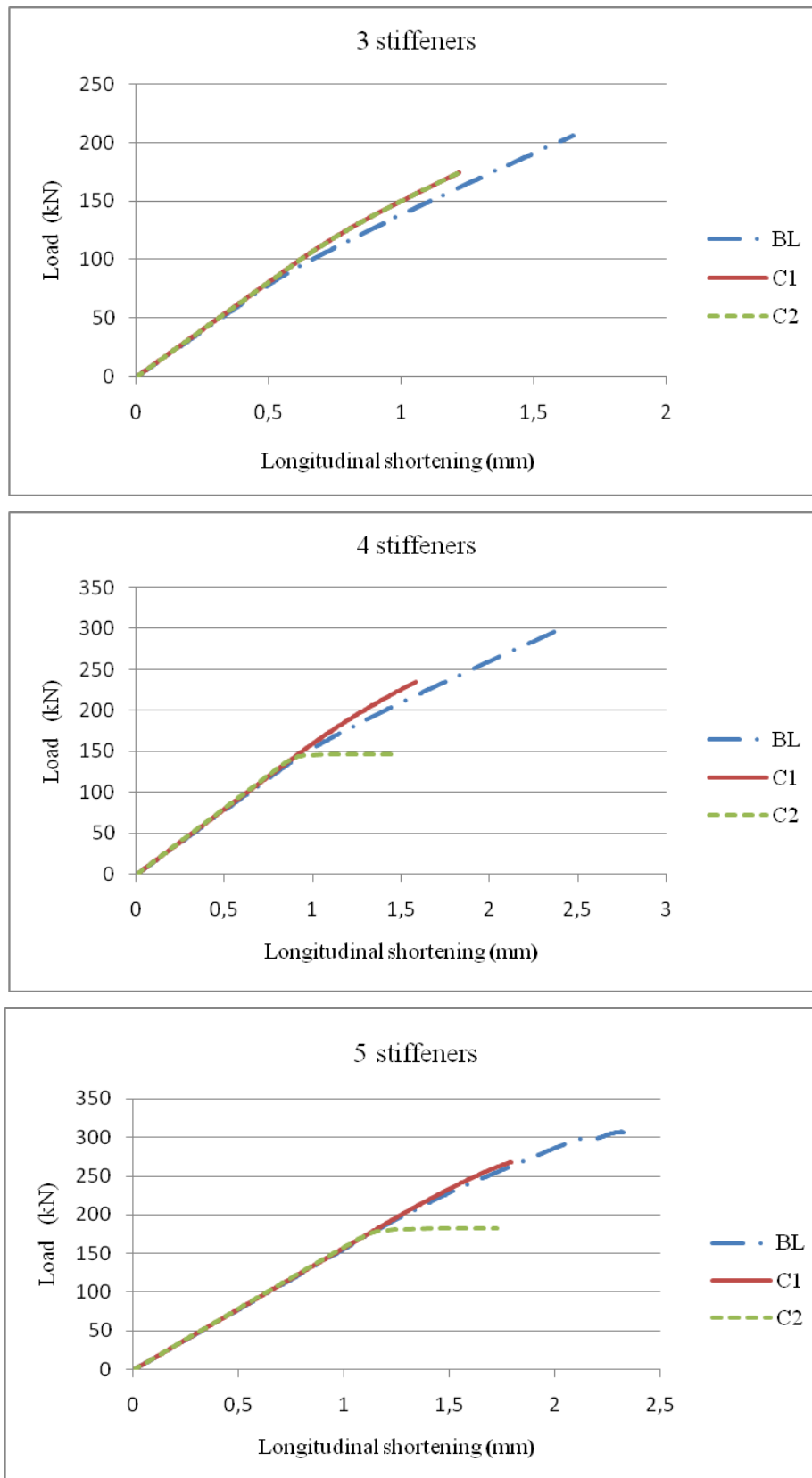


Figure 4.26 Comparison of postbuckling loads according to the number of stiffeners

‘type c’

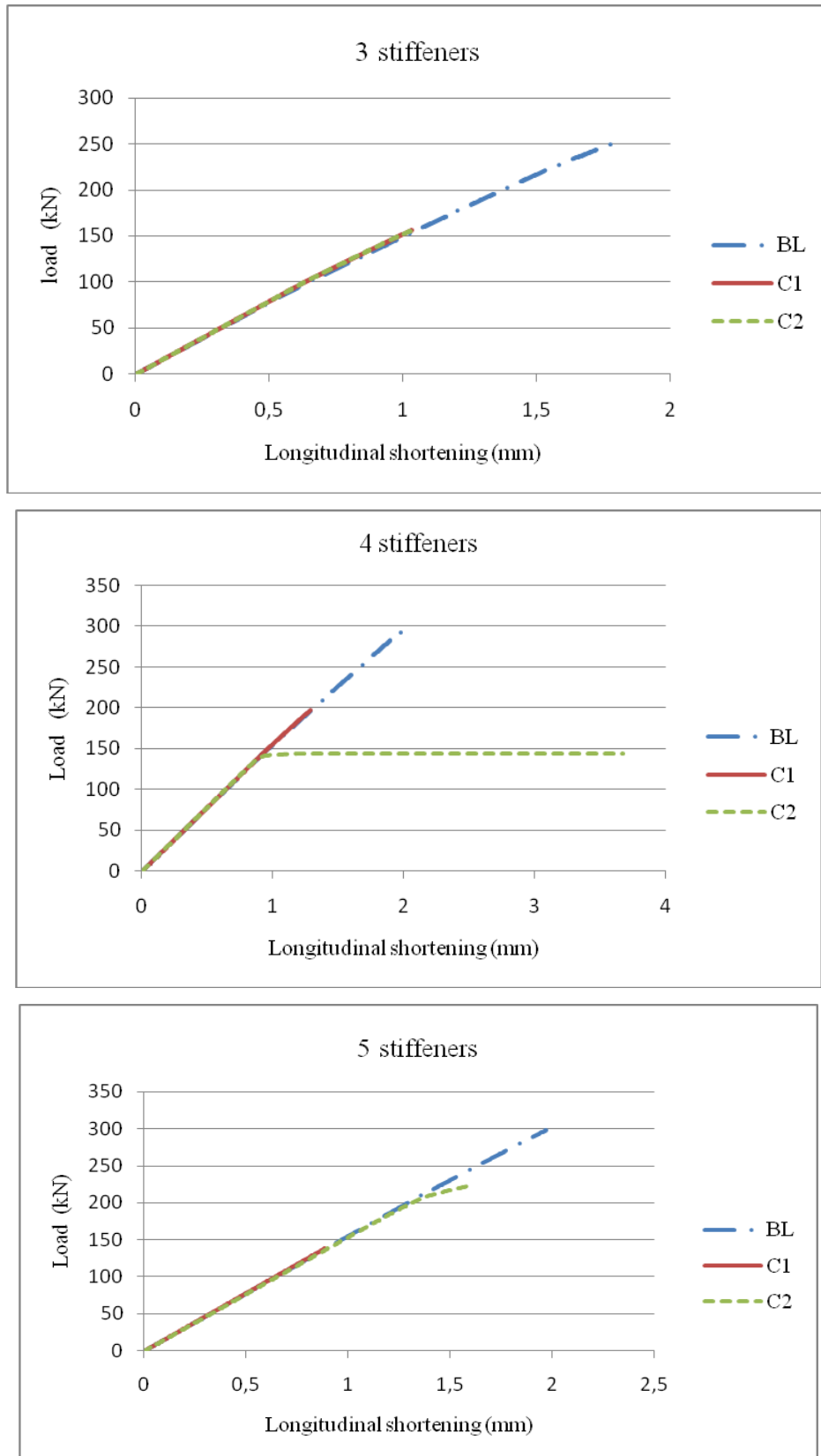


Figure 4.27 Comparison of postbuckling loads according to the number of stiffeners ‘type d’

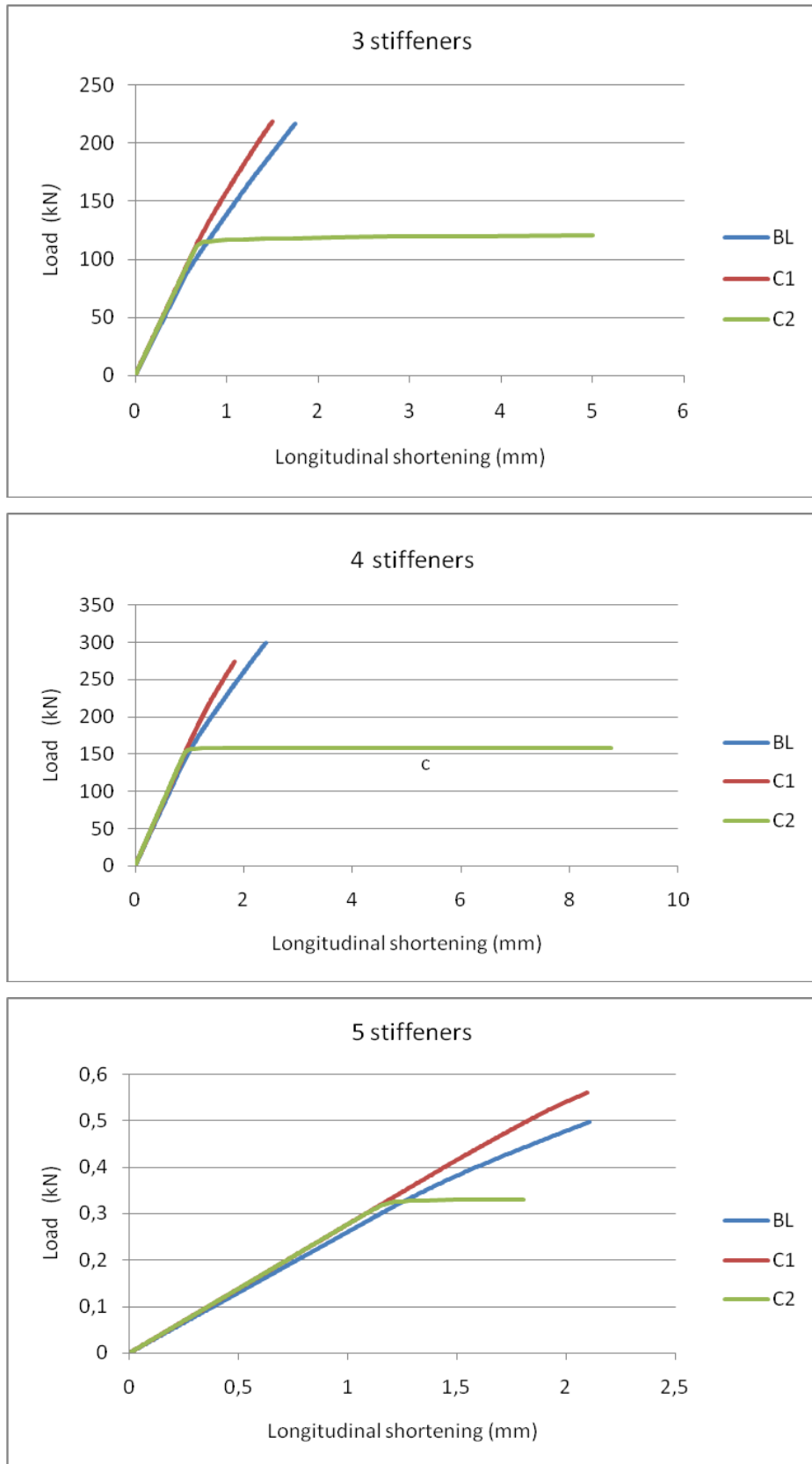


Figure 4.28 Comparison of postbuckling loads according to the number of stiffeners

'type

CHAPTER 5

OPTIMIZATION OF BUCKLING PERFORMANCE

5.1 Introduction

The general principle by Maupertuis proclaims “*If there occur some changes in nature, the amount of action necessary for this change must be as small as possible*”. In this view, the main purpose of optimization is obtaining the best outcome of a given problem while assuring some restrictions. The objective varies depending on problem types and desired functions of problem.

The importance of minimum weight design of structures was first recognized by the aerospace industry where aircraft structural designs are often controlled more by weight than by cost considerations. In other industries dealing with civil, mechanical and automotive engineering systems, cost may be the primary consideration although the weight of the system does affect its cost and performance. A growing realization of the scarcity of raw materials and a rapid depletion of our conventional energy sources is being translated into a demand for lightweight, efficient and low cost structures [116].

Critical buckling load capacity of plates and stiffened plates can be increased to very high values by using properly dimensioned stiffened plate elements. In this point it is necessary to mention about the essentiality of structural optimization procedure. This procedure involves iterative solutions and requires reanalyzing of the problem several times before obtaining the optimum solution. In this study objective function is maximization of the critical buckling load capacity of stiffened plates while satisfying constant volume constraint.

5.2 Structural Optimization Algorithm

The basic algorithm for structural shape optimization is given in Figure 5.1. Özakça et al [117] summarized the basic algorithm of structural optimization, using FS as an analysis method and sequential quadratic programming as an optimization method, in following steps.

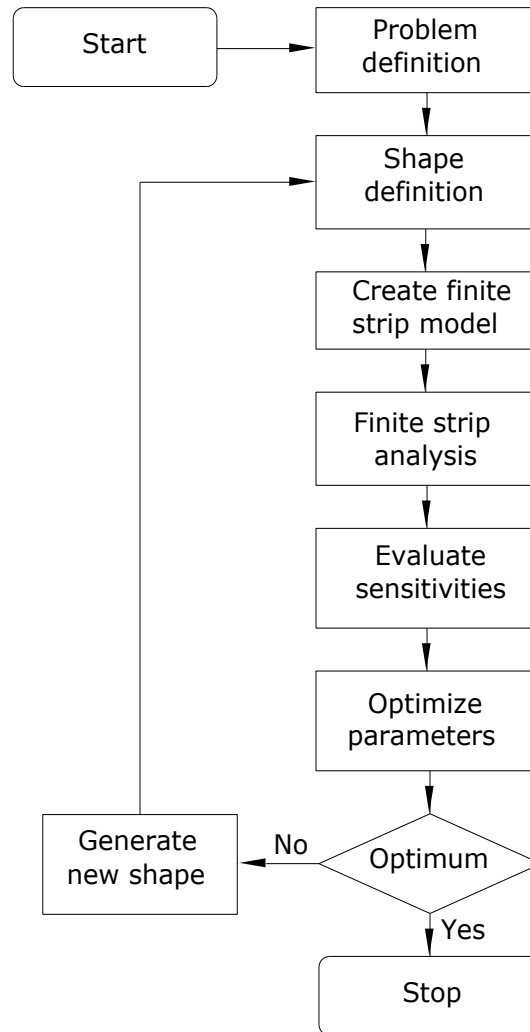


Figure 5.1 Structural optimization flowchart

1. *Problem definition*: Consider the case of the structural optimization of a panel structure in which we wish to maximize the critical buckling load subject to the constraints that the total volume of the panel should remain constant and first ten buckling loads should be greater than critical buckling load. Other types of constraints such as bounds on the design variables must also be introduced.

2. *Shape definition*: The shape of the panel cross section is defined in some convenient form that allows us to examine the sensitivities of the design to small changes in shape. Here, we describe the geometry of the plate cross section using parametric cubic spline segments with the coordinates specified at certain key points.

3. *Create finite strip model*: The next step is to generate a mesh of suitable FSs. Here, an unstructured mesh generator with mesh density specified at some key points and then interpolated through the segments appropriately is used. In order to ensure the accuracy of the FS model, it is necessary to make sure de-refinement does not occur during the analysis in each optimization iteration. This means that, the strip size distribution (mesh density) remains unchanged during redesign. As the structural shape changes during the optimization process, the re-meshing is based on predetermined mesh density at every iteration. As with normal FS analysis also the boundary conditions and material properties must be defined.

4. *Finite strip analysis*: Next we carry out a FS analysis and in the present work the structure is modeled using linear, variable thickness, Mindlin-Reissner, $C(0)$ FS.

5. *Sensitivity analysis*: The sensitivities of the buckling loads and the volume of the current design to small changes in the design variables are then evaluated. These design sensitivities are generally nonlinear implicit functions of the design variables and are therefore difficult and expensive to calculate. The numerical accuracy of sensitivity analysis affects the search directions that are used in optimization algorithms.

6. *Optimize parameters*: Using the objective and constraint functions and their derivatives, the sequential quadratic programming optimization algorithm is employed to optimize the parameters or design variables. The new set of values will result in a modified design. Furthermore, the constraints must be satisfied if the new design is to be deemed acceptable. If a convergence criterion for optimization algorithm is satisfied, then the optimum solution has been found and the solution process is terminated.

7. *Update optimization model*: After the optimization, it is necessary to update the geometric model, i.e. the coordinates and/or thicknesses of the primary design variables in structural optimization. This is the only part of the original input data which has to be updated for each optimization iteration. If no convergence has been achieved, the new geometry is sent to the mesh generator which automatically generates a new analysis model and the whole process is repeated from step 2.

5.2.1 Mathematical definition of optimization problem

Problems of structural optimization are characterized by various objectives and constraints, which are generally nonlinear functions of the design variables. These functions can be discontinuous and nonconvex. Each objective and constraint choice defines a different optimization problem, and the solution can be found using several mathematical programming methods.

In general the constraint functions are grouped into three classes: equality constraints h_j , inequality constraints g_i , and the geometric (regional) constraints defined by the upper and the lower bounds of the design variables.

However, all optimization problems can be expressed in standard mathematical terms as:

minimize (or maximize)

$$F(\mathbf{s}) \tag{5.1}$$

subject to:

$$\begin{aligned} g_i(s) &\leq 0 & i = 1, \dots, m \\ h_j(s) &= 0 & j = 1, \dots, l \\ s_k^l &\leq s_k \leq s_k^u & k = 1, \dots, n_{dv} \end{aligned} \tag{5.2}$$

The notion of improving or optimizing a structure implicitly presupposes some freedom to change the structure. The potential for change is typically expressed in terms of ranges of permissible changes of a group of parameters. Such parameters are usually called design variables in structural optimization terminology. Design variables can be cross-sectional dimensions or member sizes; they can be parameters

controlling the geometry of the structure and its material properties, etc., in which, \mathbf{s} is the design variables vector.

The notion of optimization also implies that there is a merit function $F(\mathbf{s})$ or some merit functions $\mathbf{F}(\mathbf{s})=[F1(\mathbf{s}),F2(\mathbf{s}),F3(\mathbf{s}),\dots]$ that can be improved and can be used as a measure of effectiveness of the design. The common terminology for such functions is objective functions. For structural optimization problems, weight, displacements, stresses, vibration frequencies, buckling loads, and cost or any combination of these can be used as objective functions.

In optimization process of structures, there are limits about design variables. Sometimes design constraints may be dimensions of structural elements, weight of structure, vibration frequency, and displacement of a point, $g_i(s)$ and $h_j(s)$ are the constraint functions. Finally, s_k^l and s_k^u represent the lower and the upper bounds of the design variables, m is the number of design variables used.

In this study, the objective function is maximization of critical buckling load of stiffened plates. When maximizing critical buckling load of stiffened plates first constraint is an equality for the constant material volume constraint. Optimized plate widths and lengths are constant. Also there are upper and lower limits inequality constraints of design variables. Buckling load constraint $g(s)$ can be expressed as

$$g(s) = 1 - \frac{(\sigma_{cr})_i}{(\sigma_{cr})_{max}} \quad (5.3)$$

where $(\sigma_{cr})_{max}$ defines the upper limit on buckling load and $(\sigma_{cr})_i$ describing the buckling load of the current design. Similarly

$$g(s) = \frac{V_i}{V_{max}} - 1 \quad (5.4)$$

defines the volume constraint. V_i and V_{max} are the current value and upper limit of the volume respectively.

5.2.2 Shape definition

Structural shape definition: The designation of geometric model and control the parameters of optimization procedure for an appropriate flow algorithm is complex and requires attention. The cross section of a typical stiffened plate structure is shown in Figure 5.2.

To form the cross section geometry of stiffened plates to introduce a computer code, the segments must be generated one by one. Generating a straight segment can be done by entering the geometrical coordinates of key points of it as input data.

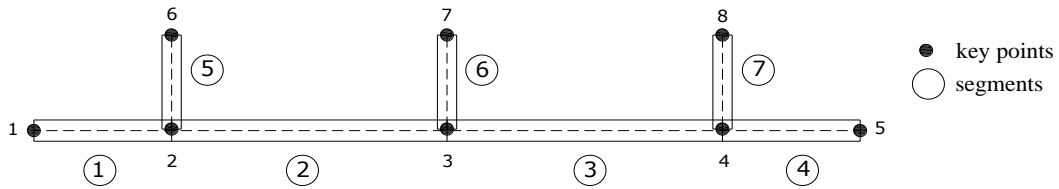


Figure 5.2 Geometric representation of a stiffened plate

Defining the number of key points to form the cross sectional shapes of stiffened plates are important for computational algorithm. More key points mean more design variables for the computer code. Hence, increasing the defined number of key points cause increasing computational time.

For the applicability to real life, increasing the efficiency of computational effort and symmetrical behavior of structural elements it is a necessary situation to link the design variables at two or more key points. By linking of design variables, the length of a considered segment can be assigned as a design variable and symmetry of shape in an axis can be easily achieved. In this regard, the number of design variables for optimization is considerably reduced.

Structural thickness definition: The thicknesses of the stiffened plate elements are specified at some or all of the key points for the desired initial element shape of the structure and then interpolated by the program.

5.2.3 Mesh generation for finite strip analysis

After defining the geometry, the next step is to generate a proper FE mesh for the cross section of stiffened plate. This meshing procedure can be carried out with an automatic mesh generator for desired mesh density. Automatic mesh generator has the capability of meshing the arbitrary complex geometry given no input other than the geometric representation of the domain to be meshed and an associated mesh density distribution. Mesh generation should be robust, versatile, and efficient to obtain more accurate results. Here, we use a mesh generator which allows refinement of FE meshes. It also allows for a significant variation in mesh spacing throughout the region of interest. The mesh generator can generate meshes of two, three and four noded elements and strips.

To mesh the cross section properly, it is a very significant factor for obtaining more accurate results. In this regard, mesh operation should be carried out considering the critical points in the cross section. Also meshes in segments should be compatible with each other. Figure 5.3 shows a mesh example of stiffened plates.

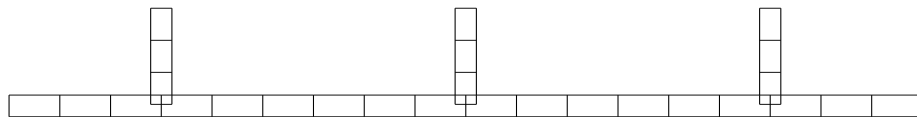


Figure 5.3 Mesh representation of plates

The mesh density is a piecewise linear function of the values of mesh size δ at some points along the mid-surface of the structure.

5.2.4 Structural finite strip analysis

It is the important factor for optimization methods to reach the optimum solution in minimum computational time. Hence, the efficiency of the optimization methods is based on the computational time required in the process. Most of the numerical optimization methods have iterative procedures. So the number of structural analyses required to reach at the optimum solution is large. In this regard, to reduce the cost of a problem, an efficient and inexpensive structural analysis method should be used.

In such a case, FS method is the best approach to the problem. As discussed in Chapter 3 the FS method has proven to be an inexpensive and useful tool in the analysis of structures having regular prismatic type geometries which simply supported diaphragms at two opposite edges with the remaining edges arbitrarily restrained. The theory and implementation of FS method for buckling analyses are given in Chapter 3.

5.2.5 Sensitivity analysis

Sensitivity analysis is a crucial part of an optimization procedure. After completing the FS analysis the sensitivities of the current design should be evaluated with small changes in the design variables. We calculate the sensitivities of items such as buckling load based on finite differences.

Sensitivity analysis is based on the systematic calculation of the derivatives of the response for the FS model with respect to parameters forming the model geometry *i.e.* the design variables which may be length, thickness or shape. The first partial derivatives of the structural response quantities with respect to the shape (or other) variables provide the essential information required to couple mathematical programming methods and structural analysis procedures. The sensitivities of responses provide the mathematical programming algorithm with search directions for optimum solutions [1].

In the present study, PLATEV_1 code uses the finite difference to calculate sensitivities. For the numerical approximation of derivatives, the finite difference method uses a difference formula. The finite difference scheme is accurate and computationally efficient.

5.2.6 Derivative of buckling load

The governing equation in the FS solution for buckling case may be defined as [1]

$$[\mathbf{K}^{pp} + \lambda^p \mathbf{K}_\sigma^{pp}] \bar{\mathbf{d}}^p = 0 \quad (5.5)$$

where \mathbf{K}^{pp} is the stiffness matrix for the p th harmonic, \mathbf{K}_σ^{pp} is the load matrix, λ^p is the buckling factor and $\bar{\mathbf{d}}_p$ is the buckling mode shape which is normalized so that

$$\bar{\mathbf{d}}_p^T \mathbf{K}_\sigma^{pp} \bar{\mathbf{d}}_p = 1 \quad (5.6)$$

When the eigenvalues are distinct, the expression for the buckling derivative with respect to design variable s_i can be derived from (5.5) and (5.6) so that

$$\frac{\partial \lambda^p}{\partial s_i} = \bar{\mathbf{d}}_p^T \left(\frac{\partial \mathbf{K}^{pp}}{\partial s_i} - \lambda^p \frac{\partial \mathbf{K}_\sigma^{pp}}{\partial s_i} \right) \bar{\mathbf{d}}_p \quad (5.7)$$

The derivatives are computed by re-calculating \mathbf{K}^{pp} and \mathbf{K}_σ^{pp} for a small perturbation Δs_i of the design variable (coordinates or thicknesses). The derivatives of the stiffness matrices with respect to the design variable s_i may then be written as

$$\frac{\partial \mathbf{K}^{pp}}{\partial s_i} \approx \frac{\mathbf{K}^{pp}(s_i + \Delta s_i) - \mathbf{K}^{pp}(s_i)}{\Delta s_i} \quad (5.8)$$

$$\frac{\partial \mathbf{K}_\sigma^{pp}}{\partial s_i} \approx \frac{\mathbf{K}_\sigma^{pp}(s_i + \Delta s_i) - \mathbf{K}_\sigma^{pp}(s_i)}{\Delta s_i} \quad (5.9)$$

5.2.4 Derivative of volume

A forward finite difference approximation is used to evaluate the volume derivative [1].

$$\frac{\partial V}{\partial s_i} \approx \frac{V(s_i + \Delta s_i) - V(s_i)}{\Delta s_i} \quad (5.10)$$

Where the volume V of the whole structure (or cross-sectional area of the structure may also be used) can be calculated by adding the volumes of numerically integrated FS.

5.3 Mathematical Programming

The sequential quadratic programming is used as a mathematical programming to generate shapes with improved objective function values using the information derived from the analysis and design sensitivities. No effort has been made to study

the mathematical programming methods used for structural optimization procedures and the sequential quadratic programming algorithm is used here essentially as a ‘black box’.

5.4 Examples

The main interest of this study is maximizing the buckling load carrying capacity of stiffened plates by optimizing the plate section dimensions under constant volume constraint.

5.4.1 Maximization of critical buckling load of square isotropic plates

In this example square simply supported plate which is analyzed in Chapter 3 is optimized. Plate is modeled using one segment and two, three, four, five key points. The location of the design variables for symmetric and nonsymmetrical are shown in Figure 5.4. Thickness design variables are the thicknesses of the key points of the plate. The initial dimensions of the plate are given in Table 3.1. The following material properties are assumed: Poisson's ratio $\nu = 0.3$, elasticity modulus $E = 110643$ and thickness $t = 0.1$.

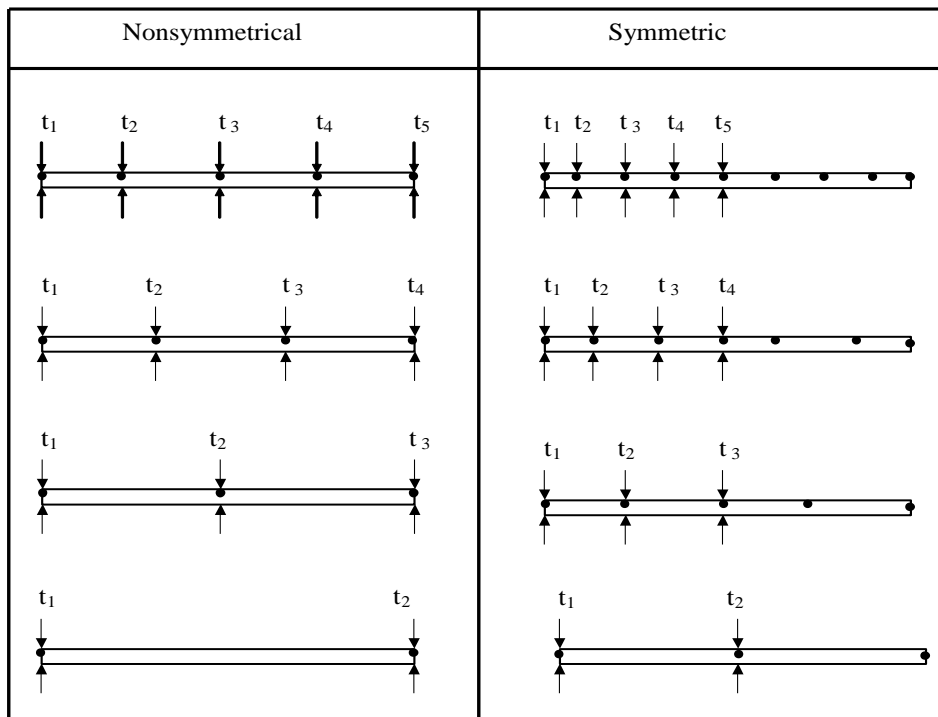


Figure 5.4 Position of design variables of plate

i-) Plates under uniaxial force: The objective is to minimize the volume of the plate subject to buckling loads $\lambda_1 \dots, \lambda_{10} \geq 3.731$ constraints. Initial value of total volume is 0.1. The optimum values of design variables and percent reduction of objective function are given in Table 5.1 for two, three, four and five design variable cases. The highest improvement is obtained with four design variables with 11.03 % decrease in volume.

Table 5.1 Square plate with ($S_h / S_h / S_h / S_h$) boundary condition under uniaxial force: values of the optimal design variables and volume

No of design variables	optimal values of design variables					% decrease in volume
	t_1	t_2	t_3	t_4	t_5	
2	0.03339	0.15228	-	-	-	7.17
3	0.03771	0.09029	0.15646	-	-	7.16
4	0.05798	0.025	0.14888	0.13113	-	11.03
5	0.06808	0.02938	0.09111	0.14875	0.1244	9.05
Constraints: $t_{\min} = 0.025$, $t_{\max} = 0.3$ and $\lambda_1, \lambda_2, \dots, \lambda_{10} \geq 3.731$						
Initial values: $V_i = 0.1$ and $t_i = 0.1$						

The initial critical buckling load of the plate is equal to 3.731. The optimization is carried out for maximization of the critical buckling load subject to volume and buckling load constraints. The optimal thickness variations obtained for the different thickness representations considered are presented in Table 5.2. The optimal critical buckling loads are equal to 4.074, 4.157, 4.174 and 4.181 for two, three, four and five design variables, respectively. The improvements in buckling loads are presented in buckling ratio ($R = K_{opt} / K_u$) form and compared with values in Table 3.1 given in Chapter 3. K_{opt} and K_u are the optimum plate and uniform thickness plate critical buckling loads, respectively. We obtain the highest buckling ratio with five design variables as 1.1206 than the solution given in Table 3.1 as 1.1127.

Table 5.2 Square plate with ($S_h / S_h / S_h / S_h$) boundary condition under uniaxial force: values of the optimal design variables and buckling ratio

No of design variables	optimal values of design variables					$R = K_{opt} / K_u$ buckling ratio
	t_1	t_2	t_3	t_4	t_5	
2	0.05541	0.14459	-	-	-	1.0919
3	0.03738	0.11332	0.11813	-	-	1.1142
4	0.03076	0.09913	0.11485	0.13086		1.1187
5	0.02714	0.08886	0.10755	0.12127	0.12511	1.1206
Constraints: $t_{min} = 0.025$, $t_{max} = 0.3$ and Initial values: $\lambda_1, \lambda_2, \dots, \lambda_{10} \geq 3.731$ and $t_i = 0.1$						

ii-) *Plates under uniaxial stress*: Table 5.3 represents volume minimization with constant stress. Initial value of volume is 0.1. Best solution is obtained with four design variables as 18.64 % reduction in volume.

Table 5.3 Square plate with ($S_h / S_h / S_h / S_h$) boundary condition under uniaxial stress: values of the optimal design variables and volume

No of design variables	optimal values of design variables					% decrease in volume
	t_1	t_2	t_3	t_4	t_5	
2	0.15875	0.025	-	-	-	8.12
3	0.1705	0.08167	0,02500	-	-	12.3
4	0.025	0.15826	0,03755	0.04679	-	18.64
5	0.14916	0.12114	0.08055	0.03015	0.05412	18.11
Constraints: $t_{min} = 0.025$, $t_{max} = 0.3$ and $\lambda_1, \lambda_2, \dots, \lambda_{10} \geq 3.731$ Initial values: $V_i = 0.1$ and $t_i = 0.1$						

Table 5.4 presents the maximization of the critical buckling load with constant stress. Initial value of total buckling load is 1.2998. Best solution 1.3876 is compared with initial buckling load.

Table 5.4 Square plate with ($S_h / S_h / S_h / S_h$) boundary condition under uniaxial stress: values of the optimal design variables and buckling ratio

No of design variables	optimal values of design variables					$R = K_{opt} / K_u$ buckling ratio
	t_1	t_2	t_3	t_4	t_5	
2	0.17507	0.025	-	-	-	1.19
3	0.19286	0.09464	0.025	-	-	1.2782
4	0.10762	0.16404	0.05544	0.03896		1.3876
5	0.1872	0.14732	0.06072	0.0602	0.08381	1.2436
Constraints: $t_{min} = 0.025$, $t_{max} = 0.3$ and Initial values: $\lambda_1, \lambda_2, \dots, \lambda_{10} \geq 3.731$ and $t_i = 0.1$						

5.4.2 Maximization of critical buckling load of straight stiffened plates

It is desired that two separate linear eigenvalue optimizations are run. The design is carried out for obtaining thickness of initial values by providing constant cross sectional area. In this example we consider only straight stiffened plates. Straight stiffened plate with substiffeners and pads are given in references [115].

The baseline panel is the foundation for the stiffened plate design. The plate cross section is constant along its length. The baseline plate cross section has a total area of 1172 mm² of skin material available for manipulation.

There are a number of design constraints based on either the general design strategy or the manufacturing process as outlined below. The plates have the common fixed constraints as shown in Table 5.5. The common constraints are shown on a three dimensional aspect of five straight stiffened plate in Figure 5.5.

Table 5.5 Common constraints

Plate width	440 mm
Plate length	590 mm
Total plate volume	691480 mm ³

The used material properties are:

Modulus of elasticity $E=73\times 10^9$ N/m²

Poisson's ratio $\nu=0.33$

The loading direction and boundary conditions are shown in Figure 5.6.

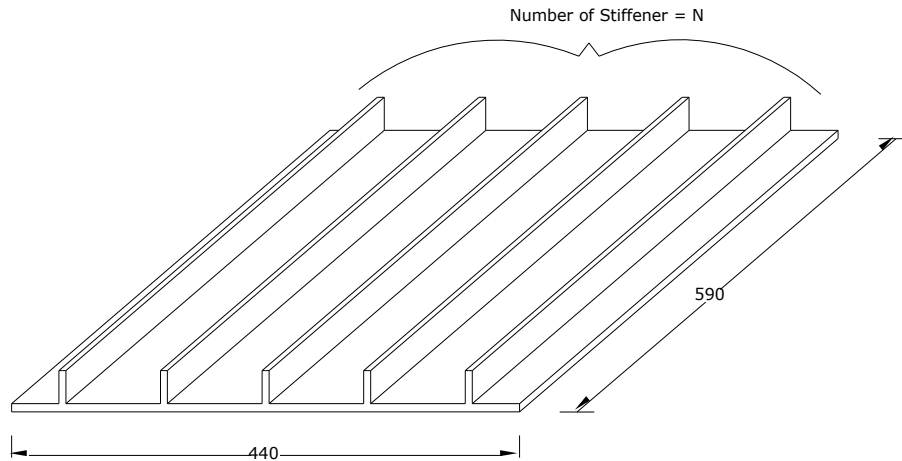


Figure 5.5 A sample three-dimensional aspect of stiffened plate (with five straight stiffeners)

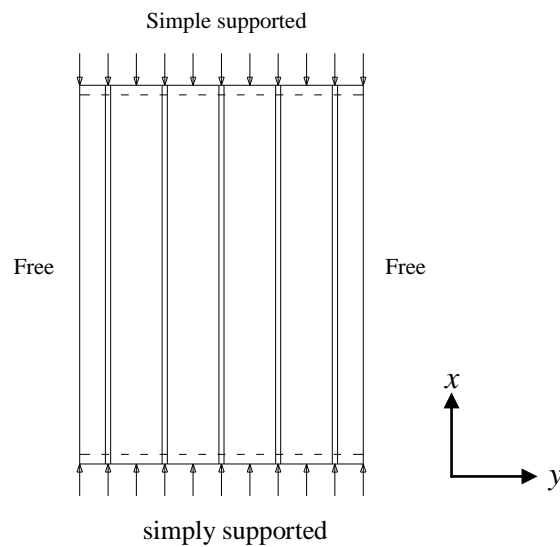


Figure 5.6 Loading and boundary conditions

The loaded sides of plate are simply supported and the other two sides are free. The plate is loaded in uniform compression in stiffeners direction. Figure 5.7 shows straight stiffened plate with five stiffeners.

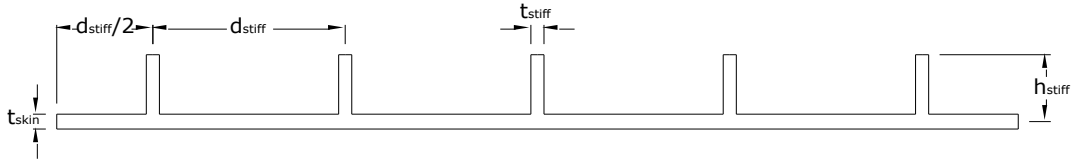


Figure 5.7 Straight stiffened plate

- i) *Size optimization:* Optimization is performed using thickness of plate skin (t_{skin}) and thickness of stiffeners (t_{stiff}). During this stage height of stiffeners (h_{stiff}) have constant value of 28.0 mm (see Figure 5.7).
- ii) *Shape optimization:* Height of stiffeners (h_{stiff}) included as design variable in this stage (see Figure 5.7).

Design constraints of two stages are specified in Table 5.6. Optimization process is repeated from two to eight stiffeners.

Table 5.6 Design constraints of straight stiffened plate

Design variables		Min (mm)	Max (mm)
Thickness of plate	t_{skin}	1.4	3
Thickness of stiffener	t_{stiff}	1.3	4
Height of stiffener	h_{stiff}	8	40

Two types of optimization are performed. These are size optimization with two design variables ($t_{skin} - t_{stiff}$) and shape optimization with three design variables ($t_{skin} - t_{stiff} - h_{stiff}$). Effect of number of stiffeners is also observed. Number of stiffeners from two to eight is optimized. Optimizations are carried out for maximization of critical buckling load subject to constant volume constraint.

- i) *Size optimization:* Thicknesses of plate and stiffeners are kept equal at the initial design. The height of stiffeners is constant and equal to 28.0 mm. The optimum values of design variables and critical buckling load are given in Table 5.7. The highest improvement is obtained for four stiffeners case and approximately equal to 10.25 %. The stiffened panel is analyzed using cubic strips. In order to obtain more accurate results the large number of degrees of freedom is taken in all analysis. The

highest critical buckling load is obtained in eight stiffeners case and equal to 219833 N. The improvement of critical buckling load for eight stiffeners is 664 % compared to two stiffeners case. Moreover, it is important to note that in optimum results skin thickness is thicker than stiffener thickness except eight stiffeners case and by the increasing the number of stiffeners skin thickness is going to be thinner and stiffener thickness is going to be thicker.

Table 5.7 Size optimization of straight stiffened plate

n_{stiff}	Optimum DVs values		Buckling loads		(%) Imp
	t_{skin}	t_{stiff}	P_i	P_{max}	
2	2.49	1.3	27392.7	28749.313	4.952
3	2.41	1.3	59731.7	64479.292	7.948
4	2.32	1.34	97565.0	107542.933	10.227
5	2.19	1.47	136548.5	148318.65	8.620
6	2.08	1.52	173160.7	183581.163	6.018
7	1.96	1.57	202204.3	206859.051	2.302
8	1.75	1.79	219819.9	219833.336	0.006

ii) *Shape optimization*: In addition to thickness of the plate and stiffeners, the height of the stiffeners is also considered as a design variable. (Note: During the optimization process, the height of stiffeners is all equal). The optimum values of design variables and critical buckling loads are presented in Table 5.8.

Table 5.8 Shape optimization of straight stiffened plate

n_{stiff}	Optimum DVs values			Buckling loads		(%) Imp
	t_{skin}	t_{stiff}	h_{stiff}	P_i	P_{max}	
2	2.52	3.99	8.00	27392.7	30266.2	10.490
3	2.19	4.00	17.29	59731.7	66979.9	12.135
4	2.15	4.00	14.01	97565.0	114501.6	17.359
5	2.13	4.00	11.78	136548.5	171359.7	25.494
6	2.06	4.00	11.05	173160.7	237776	37.315
7	2.15	4.00	8.00	202204.2	283451.4	40.181
8	2.07	4.00	8.11	219819.9	310826.7	41.401

The highest improvement, which is 41.40 %, is obtained from eight stiffeners. When the number of stiffeners is increased critical buckling load is also increased similar to size optimization. The largest critical buckling load is again obtained from eight stiffeners case. The improvement is 926 % compared with two stiffeners case. Plate skin is thinner than stiffeners in optimum results and stiffener thicknesses reach upper limits.

5.4.3 Maximization of critical buckling load of sub-stiffened plates

In this example panels with three sub-stiffening subjected to longitudinal compression which is analyzed in Chapter 3 is optimized for minimum weight and maximum performance. Using FS analysis, the initial buckling mode of profile 3 was successfully reproduced (Figure 5.8). Given the uncertainty on the skin buckling loads (large differences between experiment and FE analysis, plus the slight difference in boundary conditions between FS analysis on the one hand and FE analysis and experiment on the other), the reproduction of the skin buckling load was also considered sufficiently accurate.

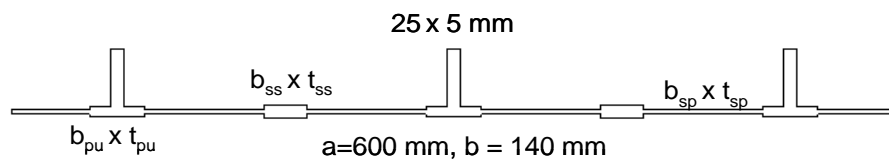


Figure 5.8 Design variables of sub-stiffened plate

For the sub-stiffened panels, the optimum as computed by FS analysis had both a high-inertia substiffener and pad-ups under stiffeners (Figure 5.9, Table 5.9), the former increasing the out-of-plane stiffness of the skin and the latter providing rotational restraint at the edges.

Results of FS optimisations with various numbers of free design variables (DV) (derived values in italics). The buckling mode was maximised subject to the constraint of constant cross-sectional area. Sub-scripts: sp = skin-pocket, pu = pad-up, ss= sub-stiffener.

Table 5.9 The optimised critical buckling load for sub-stiffened plates

	design variables (DV)			optimum					
	min.	initial	max.	3 DV ($t_{pu}=t_{ss}$)	4 DV	3 DV ($t_{pu}=t_{ss}$)	4 DV	4 DV ($t_{pu}=t_{ss}$)	5 DV
				I	II	III	IV	V	VI
t_{sp} (mm)	0.6	1.2	2.4	0.942	0.931	---	---	1.31	1.16
b_{sp} (mm)	20	40.5	60	20.0	20.0	31.8	37.8	36.0	41.0
t_{pu} (mm)	1.1	2.2	3.3	2.00	2.07	2.02	1.79	2.02	2.13
b_{pu} (mm)	20	41	50	61.5	61.5	40.4	45.5	32.1	48.9
t_{ss} (mm)	1.1	2.2	3.3	1.996	1.86	2.02	3.29	2.02	3.30
b_{ss} (mm)	9	18	36	38.5	38.5	36.0	18.8	36.0	9.00
critical buckling load (kN)				63.090	63.920	61.058	62.130	61.294	65.030
% improvement				7.7%	9.2%	4.3%	6.1%	4.7%	11.1%

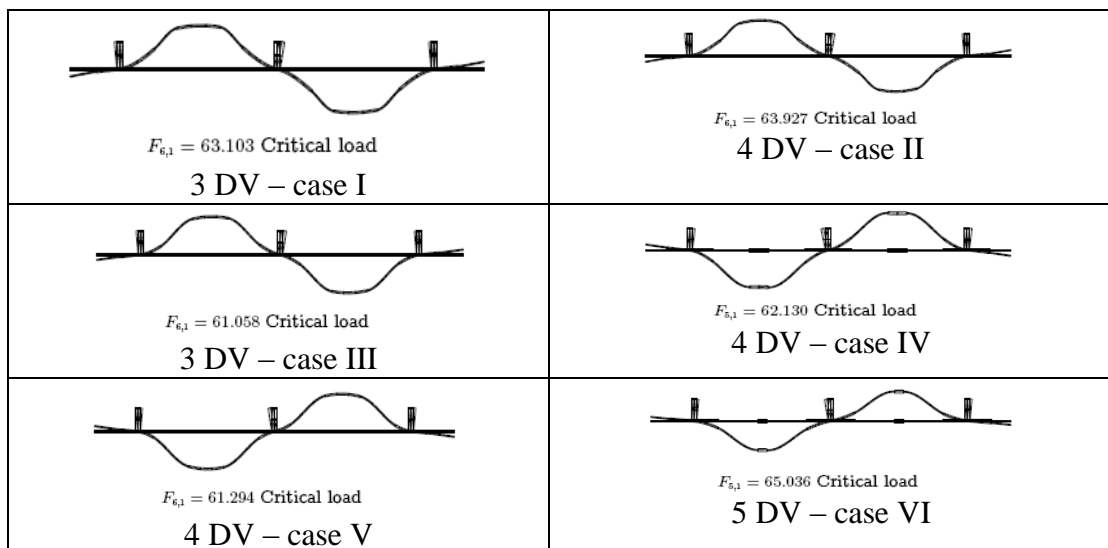


Figure 5.9 Buckling modes corresponding to each of the optimum designs of Table 5.9: from 3 DV – case I on top left to 5 DV – case VI on bottom right

5.4.4 Maximization of critical buckling load of sculpted skin panels

From these analyses, it was concluded that in order to increase not only skin buckling but also collapse performance, at least part of the sub-stiffening material should be used as pad-ups underneath stiffeners. This is in-line with generally accepted post-buckling design principles. Several numerical (FE analysis) experiments were carried out, showing that significant padding is indeed effective in post-buckling, but *too*

great a change in thickness between pad-up and skin can lead to buckling of skin between pad-ups. A new concept was therefore devised, “sculpted skin”, which consists in gradually changing the thickness (Figure 5.10 and 5.11).

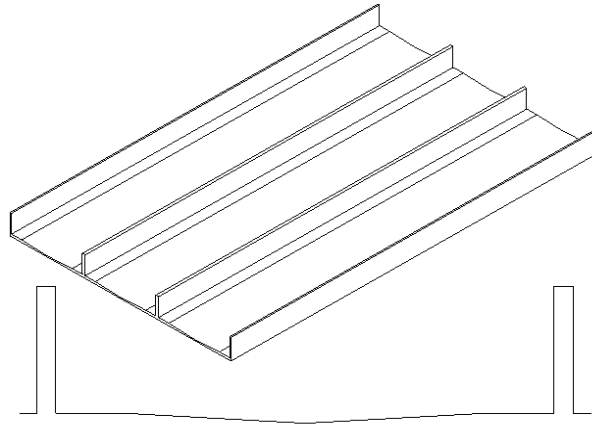


Figure 5.10 Sculpted skin panels

To gain insight in the design sensitivity of sculpted skins, the linear variable thickness FS optimisation was applied. Since no experiments had been run on this concept, it was decided to start by concentrating on a simply supported plate. Results are given in Table 5.10 and Figure 5.12.

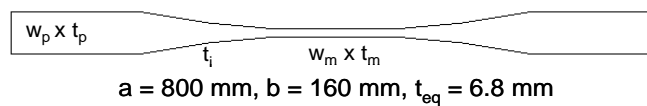


Figure 5.11 Design variables of sculpted skin panels

Table 5.10 The optimised critical buckling load for sculpted skin panels

	initial	case 1	case 2	case 3	case 4	case 5
w_p (mm)	32.5	---	---	---	---	---
t_p (mm)	9.00	---	---	10.5	10.4	10.4
t_i (mm)	6.25	---	7.80	4.68	5.01	---
w_m (mm)	33.0	53.0	---	---	29.8	54.1
t_m (mm)	3.50	4.24	2.00 (limit)	2.36	2.00 (limit)	2.67
Critical load (kN)	542.81	550.32	559.88	719.70	728.48	720.51
% improvement		1.4%	3.1%	33%	34%	33%

Results of FS optimisations of one bay of simply supported, sculpted skin. The buckling mode was maximised subject to the constraint of constant cross-sectional area. Subscripts denote: p=pad-up, i=intermediate, m=middle. Note that shell offsets

were not accounted for; in real-life aircraft applications, one of the sides of the plate would probably have to remain flush. “----” = unchanged from initial value.

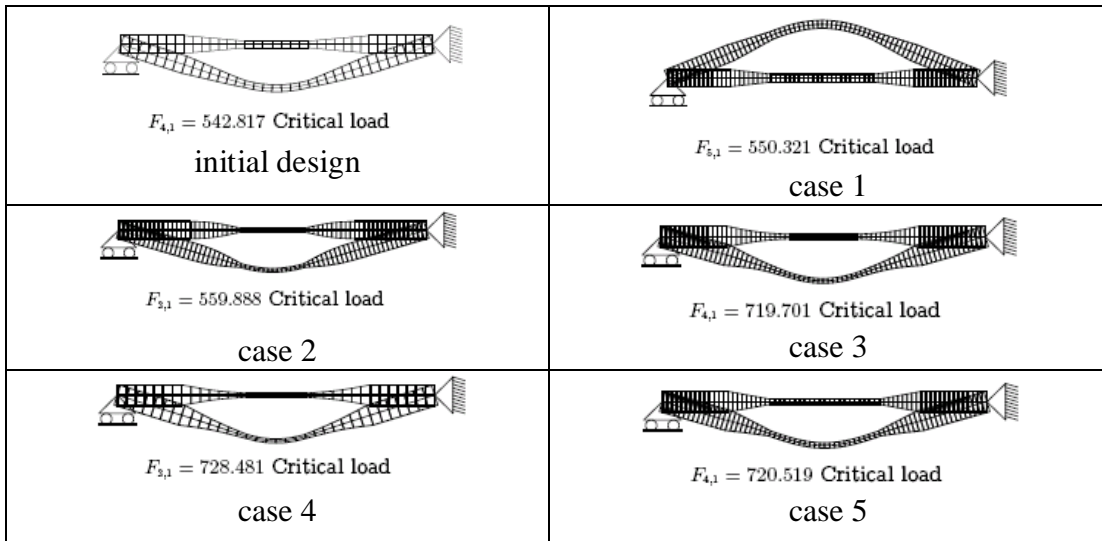


Figure 5.12 Buckling modes for the sculpted skin design, from the initial design on top left to optimised case 5 (Table 5.10) on bottom right

CHAPTER 6

CONCLUSION

6.1 Introduction

The FS method is used to obtain geometrically nonlinear analysis of plates and shells to get load increment curve under distributed loading and inplane loading for plates and biaxial load for plane stress-plane strain. For this purpose, Newton Raphson iteration methods are carried out for considered plate types. The results are obtained and detailed discussions are mentioned in Chapter 4. This chapter deals with a general look about results.

6.2 Conclusion

The geometrically nonlinear analysis of plane stress problem is successfully studied using the FE program. Excellent agreement has been found between the column results and the published literature. The Newton-Raphson technique is used for the nonlinear solution process and relaxation technique is employed to prevent possible divergence of iteration. The aim of programming is to reduce the residual force (unbalanced forces). For each load step residual force is decreased with iteration and displacements found.

FS Mindlin formulation has been given for geometrically nonlinear analysis of prismatic plates and shells. The performance of linear, quadratic and cubic strips under distributed loading has been given by comparing results with analytical and some other plate solutions. Then, the postbuckling performance of plates with different boundary conditions is successfully studied. After that, postbuckling performance of optimized panels with sub-stiffening was investigated.

The panels had been optimized for minimum weight or maximum performance. The linear elastic eigenvalue FS code which has a built-in optimizer provided a practical way of doing so, at least for the initial (skin) buckling. Optimization was also used to obtain insight into the importance of different design variables, and derive a method for sizing. Linear FS analysis allowed optimization of one of the sub-stiffened panels, revealing a potential for further improvement of the initial buckling load. Non-linear FS of an application of this concept to realistic, optimized aircraft panels loaded in slight bi-compression confirmed initial buckling gains of up to 10%. The potential improvement in buckling performance over unstiffened plates of equal weight was as high as 500%. More relevantly, the effect of variable stiffness sub-stiffening was estimated over two times higher than that of orthogonal sub-stiffening.

A result has been presented for the geometrically nonlinear analysis of compressively loaded initial and optimized sub-stiffened panels. The permitted structural loading is uniaxial compression, or biaxial compression. Geometric shape imperfections are permitted, and the longitudinal ends of the structure are assumed to be simply supported. Structures are modeled as assemblages of flat plate strips which are rigidly joined along mutual longitudinal edges. The optimization has been implemented on a digital computer in a FORTRAN computer program. Nonlinear analysis result was developed by FS code close to the ANSYS results.

6.3 Recommendation of future work

In present study linear buckling analysis, geometric nonlinear analysis and optimization of plates and stiffened plates is performed. However, structures may undergo nonlinear elasticity, plasticity. For this situation geometric and material nonlinearity can be investigated which requires more complex equations and more computational time.

Postbuckling analysis can be applied to straight, T shaped, L shaped, U shaped tube, Y shaped composite stiffened plates. It is necessary to examine these types of stiffened plates to possess general behaviors of buckling and design structures that include axially compressive loaded stiffened plates.

Another case that causes buckling of structures is torsional effects. In present study, only cross section axially compressive loading was considered. In practice, structures may be subjected to torsional forces and the buckling case in this situation is called as torsional buckling. Torsional effects can be investigated according to sustained structural loading types.

In FS method, two opposite edges are simply supported and other two sides can be defined in any boundary condition. Some modifications can be made to apply any boundary conditions.

REFERENCES

- [1] Kolcu, F. (2000). *Buckling Analysis and Shape Optimization of Variable Thickness Prismatic and Axisymmetric Plates and Shells*. Ms. Thesis, Department of Civil Engineering, University of Gaziantep.
- [2] Özakça, M. (1993). *Analysis and Optimal Design of Structures with Adaptivity*. Ph. D. thesis, Department of Civil Engineering University College of Swansea, U.K.
- [3] C. A. Ellis and D. M. Brown (1933). *Leonardo Euler's "Elastic curves" translated and annotated by W. A. Oldfather*.
- [4] Timoshenko, S. P. and Gere, J. M. (1961). *Theory of Elastic Stability 2/e*, McGraw-Hill.
- [5] Brush, Don O. and Almroth, Bo O. (1975). *Buckling Analysis of Shells and Plate*, McGraw-Hill.
- [6] Ley, R. P., Johnson, E. R. and Gürdal, Z. (1994). Buckling of imperfect, anisotropic, ring-stiffened cylinders under combined loads, *AIAA Journal*, **32**, 1302-1309.
- [7] Allman, D.J. (1975). Calculation of elastic buckling loads of thin flat plates using triangular finite element. *International Journal for Numerical Methods in Engineering*, **9**, 415-432.
- [8] Przemieniecki, J.S. (1973). Finite element structural analysis of local stability. *AIAA Journal*, **11**, 33-39.

- [9] Fafard, M., Beaulieu, D. and Dhatt, G. (1987). Buckling of thin walled members by finite element method. *Computers and Structures*, **25**, 183-19.
- [10] Anderson R.G., Irons B.M. and Zienkiewicz O.C. (1968). Vibration and stability of plates using finite elements. *International Journal of Solids and Structures*, **4**,1031-1055
- [11] Sheikh, I.A., Grodin, G.Y. and Elwi A.E. (2002). Stiffened steel plates under uniaxial compression. *Jornal of Constructional Steel research*, **58**, 1061-1080
- [12] Sridharan S. and Zeggane Matjid Z. (2001). Stiffened plates and cylindrical shells under interactive buckling. *Finite Element in Analysis and Design*, **38**, 155-178
- [13] Grondin, G.Y., Elwi, A.E. and Cheng, J.J.R. (1999). Buckling of stiffened steel plates-a parametric study. *Journal of Constructional Steel Research* , **50**, 151-175
- [14] Jiang, W., Bao, G. and Roberts, J.C. (1997). Finite Element Modelling of Stiffened and Unstiffened Orthotropic Plates. *Computers and Structures*, **63**, 105-117
- [15] Mukhopadhyay, M. and Mukherjee, A. (1990). Finite element buckling analysis of stiffened plates, *Computers and Structures*, **34**, 795-803.
- [16] Wang, C. M., Liew, K. M., Xiang, Y. and Kitipornchai, S. (1992). *Buckling of Rectangular Mindlin Plates with Internal Line Supports*, Department of Civil Engineering The University of Queensland ,Australia.
- [17] Wang, C. M., Member, ASCE, Xiang, Y. and Kitipornchai, S., Fellow, ASCE (1994). Buckling solutions of rectangular mindlin plates under uniform shear, *Journal of Engineering Mechanics*, **120**, 2462-2469.

- [18] Wang, C. M., Member, ASCE, Xiang, Y., S. Kitipornchai, Fellow, ASCE, and Liew, K. M. (1993). Axisymmetric buckling of circular mindlin plates with ring supports, *Journal of Structural Engineering*, **119**, 782-793.
- [19] Teng, J. and Rotter J. M. (1992). Buckling of pressurized axisymmetrically imperfect cylinders under axial loads, *Journal of Engineering Mechanics*, **118**, 229-247.
- [20] Rao, P. S. and Ramanjaneyulu, K. (1993). Stability of cooling tower shell with modified wind pressure coefficients, *Journal of Engineering Mechanics*, **119**, 2207-2225.
- [21] Sato, K. (1992). Elastic buckling of incomplete composite plates, *Journal of Engineering Mechanics*, **118**, 1-4.
- [22] Singh, J. P. and Dey, S. S. (1990). Variational finite difference approach to buckling of plates of variable stiffness, *Computers and Structures*, **36**, 39-45.
- [23] Cheung, Y. K. (1968). The finite strip method in the analysis of elastic plates with two opposite simply supported ends, *Proc. Inst. Civ. Eng.*
- [24] Dawe, D. J. (1977). Finite strip buckling analysis of curved plate assemblies under biaxial loading, *Solids Structures*, **13**, 1141-1155.
- [25] Dawe, D. J. and Roufaeil, O. L. (1982). Buckling of rectangular Mindlin plates, *Computers and Structures*, **15**, 1249-1266.
- [26] Dawe, D. J. and Craig, T. J. (1988). Buckling and vibration of shear deformable prismatic plate structures by complex finite strip methods, *International Journal of Mechanical. Science*, **30**, 77-99.
- [27] Peshkam, V. and Dawe, D. J. (1989). Buckling and vibration of finite-length composite prismatic plate structures with diaphragm ends, Part I: Finite strip

formulation, *Computer Methods for Applied Mechanics and Engineering*, **77**, 1-30.

- [28] Peshkam, V. and Dawe, D. J. (1989). Buckling and vibration of finite-length composite prismatic plate structures with diaphragm ends, Part II: Computer programs and buckling applications, *Computer Methods for Applied Mechanics and Engineering*, **77**, 227-252.
- [29] Dawe, D. J. and Peshkam, V. (1990). Buckling and vibration of long plate structures by complex finite strip methods, *International Journal of Mechanical Science*, **32**, 743-766.
- [30] Dawe, D. J., Lam S. S. E. and Azizian, Z. G. (1993). Finite strip post-local buckling analysis of composite prismatic plate structures, *Computers and Structures*, **48**, 1011-1023.
- [31] Wang, S. and Dawe, D. J. (1996). Finite strip large deflection and post-overall-buckling analysis of diaphragm-supported plate structures, *Computers and Structures*, **61**, 155-170.
- [32] Benson, P. and Hinton, E. (1976). A thick finite strip solution for static, free vibration and stability problems, *Journal of Numerical Methods in Engineering*, **10**, 665-678.
- [33] Hinton, E., Özakça, M. and Rao, N. V. R. (1995). Free vibration analysis and shape optimization of variable thickness prismatic folded plates and curved shells-Part I: Finite strip formulation, *Journal of Sound and Vibration*, **181**, 553-566.
- [34] Özakça, M., Hinton, E. and Rao, N. V. R. (1994). Free vibration analysis and shape optimization of variable thickness prismatic folded plates and shells with curved planform, *Journal of Numerical Methods in Engineering*, **37**, 1713-1739.

- [35] Hinton, E. and Rao, N. V. R. (1994). Structural shape optimization of shells and folded plates using two noded finite strips, *Computers and Structures*, **46**, 1055-1071.
- [36] Hinton, E. and Rao, N. V. R. (1993). Analysis and shape optimization of variable thickness prismatic folded plates and curved shells. Part II: Shape optimization, *Thin Walled Structures*, **17**, 161-183.
- [37] Hinton, E., Petrinic, N. and Özakça, M. (1993). Buckling analysis and shape optimization of variable thickness prismatic folded plates. Part I: Finite strip formulation, *Engineering Computations*, **10**, 483-498.
- [38] Wang, X. (1994). *Finite strip formulations for strength, buckling and post-buckling analysis of stiffened plates*, Ph. D thesis, Institute of Lightweight Structures and Aerospace Engineering Vienna University of Technology.
- [39] Kwon, Y. B. and Hancock, G. J. (1991). A non-linear elastic spline finite strip analysis for thin walled sections, *Thin Walled Structures*, **12**, 295-319.
- [40] Takahasni, K. and Nakazawa, S. (1999). Vibration and buckling of plate girders by finite strip method. *Theory and Applied Mechanics*, **48**, 127-133
- [41] Hinton, E. (1978). Buckling of initially Stressed Mindlin plates using Finite strip method. *Computers and Structures*, **8**, 99-105.
- [42] Hinton, E., Petrinic, N. and Özakça, M. (1993). Buckling analysis and shape optimization of variable thickness prismatic folded plates Part 1: Finite strip formulation. *Engineering Computations*, **10**, 483-498
- [43] Navazi H. M, Haddadpour H. and Rasekh M. (2006). An analytical solution for nonlinear cylindrical bending of functionally graded plates, *Thin Walled Structures*, **44**, 1129-1137.

- [44] Bisagni C. and Vesconi R. (2009). Analytical formulation for local buckling and postbuckling analysis of stiffened laminated panels, *Thin Walled Structures*, **47**, 318-334.
- [45] Turner, M.J., Dill, E.H., Martin, H.C. and Melosh, R.J. (1960). Large Deflections of Structures Subjected to Heating and External Loads, *Journal of Aerospace Sciences*, **17**.
- [46] Gallagher, R.J. and Padlog, J. (1963). Discrete Element Approach to Structural Stability Analysis, *AIAA Journal*, **1**, 1437-1439.
- [47] Archer, R.R. (1962). On the Numerical Solution of The nonlinear Equations for Shells of Revolution, *Journal of Mathematics and Physics*, Cambridge, Mass. **40**.
- [48] Archer, J.S. (1965). Consistent Matrix Formulation for Structural Analysis Using Finite Elements Techniques, *AIAA Journal*, **3**, 1910-1918.
- [49] Gallagher, R.J. and Padlog, J. (1963). Discrete Element Approach to Structural Stability Analysis, *AIAA Journal*, **1**, 1437-1439.
- [50] Famili, J. and Archer, R.R. (1965). Finite Asymmetric Deformation of Shallow Spherical Shells, *AIAA Journal*, **3**, 506-510.
- [51] Stricklin, J.A., Haisler, W.E., MacDougall, H.R., and Stebbins, F.J. (1968). Nonlinear Analysis of Shells of Revolution by the Matrix Displacement Method, *AIAA Journal*, **6**, 2306-2312.
- [52] Ball, R.E. (1968). A Geometrically Nonlinear Analysis of Arbitrarily Loaded Shells of Revolution, CR-909, NASA.
- [53] Perrone, N. and Kao, R. (1970). Large Deflection Response and Buckling of Partially and Fully Loaded Spherical Cap, *AIAA Journal*, **8**, 2130- 2136.

- [54] Kawai, T., and Yoshimura, N. (1969). Analysis of Large Deflection of Plates by the Finite Element Method, *International Journal for Numerical Methods in Engineering*, **1**, 123-133.
- [55] Felippa, C.A. (1966). *Refined Finite Element Analysis of Linear and Nonlinear Two- Dimensional Structures*, Ph.D. dissertation, University of California, Berkeley, California.
- [56] Oden, J.T. (1969). Finite Element Applications in Nonlinear Structural Analysis, *Proceedings of the Conference on the Finite Element Methods*, Vanderbilt Univ., Tenn.
- [57] Greenbaum, G.A. and Conroy, D.C. (1970). Post-wrinkling Behavior of a Conical Shell of Revolution Subjected to Bending Loads, *AIAA Journal*, **8**, 700-707.
- [58] Murray, D.W. and Wilson, E.L. (1969). Finite Element Large Deflection Analysis of Plates, *Journal of the Engineering Mechanics Division*, ASCE, **95**, 143-165.
- [59] Hofmeister, L.D. Greenbaum, G.A., and Evenson, D.A. (1970) Large Strain, Elasto- Plastic Finite Element Analysis, *Proceedings of the AIAA/ASME 11th Structures*, 250-259.
- [60] Wood R.D. and Zienkiewicz O.C. (1977). Geometrically nonlinear finite element analysis of beams, frames, arches and axisymmetric shells, *Computers and Structures*, **7**, 725-735.
- [61] Sabir, A.B. and Djoudi M.S. (1995). Shallow Shell Finite Element for the Large Deflection Geometrically Nonlinear Analysis of Shells and Plates, *International Journal Thin-Walled Structures* **21**, 253-267.
- [62] Sabir, A.B. (1995). Elastic buckling, stability and vibration of linear and geometrically non-linear behaviour of structures, Proc International

- Conferences on Structural Dynamics and Vibrations PD, *American Society of Mechanical Engineers*, **70**, 175-181.
- [63] Sabir, A.B. (1995). Elastic buckling, stability and vibration of linear and geometrically non-linear behaviour of structures, Proc International Conferences on Structural Dynamics and Vibrations PD, *American Society of Mechanical Engineers*, **70**, 175-181.
- [64] Plank, R.J. (1973). *The initial buckling of thin walled structures under combined loading*, PhD thesis, University of Birmingham.
- [65] Cho C., Park H.C. and Lee S.W. (1998). Stability analysis using a geometrically nonlinear assumed strain solid shell element model, *Finite Elements in Analysis and Design*, **29**, 121-135.
- [66] Kumar, P., Nukala, V.V. and White, D.W. (2004). A mixed finite element for three-dimensional nonlinear analysis of steel frames, *Computer Methods in Applied Mechanics and Engineering*, **193**, 2507-2545.
- [67] Levy, R. and Spillers W.R. (1995). *Analysis of geometrically nonlinear structures*, second edition, Kluwer Academic Publishers.
- [68] Tvergaard, Viggo (1973). Influence of Post-Buckling Behavior on Optimum Design of Stiffened Panels, *International Journal of Solids and Structures*, **9**, 1519-1534.
- [69] Thurston, G.A., Brogan, F.A., and Stehlin, P. (1986). Postbuckling Analysis Using a General-Purpose Code, *AIAA Journal*, **24**, 6,1013-1020.
- [70] Sheikh, I.A., Grodin, G.Y. and Elwi A.E. (2002). Stiffened steel plates under uniaxial compression. *Journal of Constructional Steel research*, **58**, 1061-1080.

- [71] Nian-Zhong Chen, C. Guedes Soares (2007). Reliability assessment of post-buckling compressive strength of laminated composite plates and stiffened panels under axial compression, *International Journal of Solids and Structures*, **44**, 7167–7182.
- [72] Sridharan, S., and Graves-Smith, T.R. (1981). Postbuckling Analysis with Finite Strips, *Journal of the Engineering Mechanics Division, ASCE*, **107**, 5, 869-888.
- [73] Frederick Stoll, Zafer Gürdal, James H. Starnes, Jr. (1991). Center for Composite Materials and Structures, Virginia Tech.
- [74] Sheikh, A.H. and Mukhopadhyay, M. (2000). Geometric nonlinear analysis of stiffened plates by the spline finite strip method, *Computers and Structures*. **76**, 765-785.
- [75] Özakça, M., Tayşi, N., Kolcu, F. (2003). Buckling analysis and shape optimization of elastic variable thickness circular and annular plates—II. Shape optimization, *Engineering Structures*, **25**, 193-199.
- [76] Delcourt, C.R. (1978). *Linear and geometrically nonlinear analysis of flatted-walled structures by the finite strip method*, PhD thesis, University of Adelaide, Australia.
- [77] Bushnell, D. and Almroth, B. O. (1970). *Finite-Difference Energy Method for Nonlinear Shell Analysis*, Computer Oriented Analysis of Shell Structures, Lockheed Co., Palo Alto, California, Aug. 10-14.
- [78] Cheung, M.S. and Li, W. (1989). A modified finite strip method for geometrically nonlinear analysis of plates, *Computers and Structures*, **33**, 1031-1035.
- [79] Gierlinski, J.T. and Graves-Smith, T.R. (1984). The geometric nonlinear analysis of thin-walled structures by finite strips, *Thin-walled Struct*, **2**, 27-50.

- [80] Langel, P. and Cusens, A.R. (1983). Finite strip method for the geometrically nonlinear analysis of plate structures, *International Journal for Numerical Methods in Engineering*, **19**, 331-340.
- [81] Abayakoon, S.B.S., Olson, M.D. and Anderson, D.L. (1989). Large deflection elastic-plastic analysis of plate structures by the finite strip method, *International Journal for Numerical Methods in Engineering*, **28**, 331-358.
- [82] Kumar, P., Olson, M.D. and Anderson, D.L. (1991). Large deflection elastic-plastic analysis of plate cylindrical shells using the finite strip method, *International Journal for Numerical Methods in Engineering*, **31**, 837-857.
- [83] Khalil, M.R., Olson, M.D., and Anderson, D.L. (1988). Nonlinear dynamic analysis of stiffened plates, *Computers and Structures*, **29**, 929-941.
- [84] Azizian Z.G. and Dawe D.J. (1985). Geometrically nonlinear analysis of rectangular Mindlin plates using the finite strip method, *Computers and Structures*, **21**, 423-436.
- [85] Dawe, D.J. and Azizian, Z.G. (1986). The performance of Mindlin plate finite strips in geometrically nonlinear analysis, *Computers and Structures*, **23**, 1-14.
- [86] Azizian Z.G. and Dawe D.J. (1985). Analysis of the large deflection behaviour of laminated composite plates using the finite strip method, *Composite Structures*, **3**, 677-691.
- [87] Wang S. and Dawe D.J. (1996). Finite strip large deflection and post-overall-buckling analysis of diaphragm-supported plate structures, *Computers and Structures*, **61**, 155-170.
- [88] Dawe, D.J., Lam, S.S.E. and Azizian, Z.G. (1992). Nonlinear finite strip analysis of rectangular laminates under end shortening, using classical plate theory, *International Journal for Numerical Methods in Engineering*, **35**, 1087-1110.

- [89] Lam, S.S.E., Dawe, D.J., and Azizian, Z.G. (1993). Nonlinear finite strip analysis of rectangular laminates under end shortening, using shear deformation plate theory, *International Journal for Numerical Methods in Engineering*, **36**, 1045-1064.
- [90] Dawe, D.J., Lam, S.S.E. and Azizian, Z.G. (1993). Finite strip post-buckling analysis of composite prismatic plate structures, *Computers and Structures*, **48**, 1011-1023.
- [91] Sekulovic, M. and Milasinovic, D. (1987). Nonlinear analysis of plate and folded structures by the finite strip method, *Engineering Computations*, **4**, 41-47.
- [92] Cheung, M. and Milansinovic, D. (1988). Nonlinear analysis of plate and folded structures by the finite strip method, *Computers and Structures*, **29**, 687-692.
- [93] Cheung M.S. and Wenchang Li (1989). A Modified Finite Strip Method for Geometrically Nonlinear Analysis of Plates, *Journal of Computers and Structures*, **33**, 1031- 1035.
- [94] Cheung Y.K. and Tham L.G. (1998). *Finite strip method*, CRC Press.
- [95] Kwon, Y.B. (1992). *Post-buckling behaviour of thin-walled channel sections*, PhD thesis, School of Civil and Mining Engineering, University of Sydney.
- [96] Kwon, Y.B. and Hancock, G.J. (1991). A nonlinear elastic spline finite strip analysis for thin-walled section, *Thin-walled Structures*, **12**, 295-319.
- [97] Zhu, D.S. and Cheung, Y.K. (1988). Large deflection analysis of arbitrary shaped thin plates, *Computers and Structures*, **29**, 687-692.
- [98] Zhu, D.S. and Cheung, Y.K. (1989). Postbuckling analysis of shells by spline finite strip method, *Computers and Structures*, **31**, 357-364.

- [99] Akhras G., Cheung M.S. and Li W. (1998). Geometrically Nonlinear Finite Strip Analysis of Laminated composite plates, *Composites Part 29B*, 489-495.
- [100] Zienkiewicz, O.C. and Campbell, J.S. (1973). Shape optimization and sequential linear programming. *Optimum Structural Design*. John Wiley, Chichester.
- [101] Levy, R. and Ganz, A. (1991). Analysis of optimized plates for buckling. *Computers and Structures*, **41**, 1379-1385.
- [102] Hojjat, A. and Kok, Y.M. (1988). Architecture of coupled expert system for optimum design of plate girder bridges *Engineering Applications of Artificial Intelligence*, **1**, 277-285.
- [103] Jarmai, K., Snyman, J.A. and Farkas, J. (2006). Minimum cost design of welded orthogonally stiffened cylindrical shell *Computers and Structures*, **84**, 787-797.
- [104] Osama, K.B. (1998). A contribution to the stability of stiffened plates under uniform compression. *Computers and Structures*, **66**, 535-570.
- [105] Bisagni, C., Lanzi, L. (2002). Post-buckling optimisation of composite stiffened panels using neural networks. *Composite Structures*, **58**, 237-247.
- [106] Kang., J.H. and Kim, C.G. (2005). Minimum weight design of compressively loaded composite plates and stiffened panels for postbuckling strength by Genetic Algorithm *Composite Structures*, **69**, 239-246.
- [107] Hinton, E. (1987). *Numerical Methods and Software for Dynamic Analysis of Plates and Shells*, Pineridge Press, Swansea, UK.

- [108] Özakça, M., Murphy, A., Vanderveen, S. (2005). T Buckling and Post-Buckling of Sub-stiffened or Locally Tailored Aluminium Panels, 25th *International Congress of the Aeronautical Sciences*.
- [109] Booth, A.D. (1966). *Numerical Methods*, Butterworth, London.
- [110] Zienkiewicz O.C., Taylor R.L. (2000). *The finite element method*, **1**.
- [111] Fung, Y. C. (1965). *Foundations of Solid Mechanics*, Prentice Hall.
- [112] Wood, R. D., Zienkiewicz, O. C. (1977). Geometrically nonlinear finite element analysis of beams, frames, arches and axisymmetric shells, *Computers and Structures*, **7**, 725-35.
- [113] Rushton, K: R. (1970). Large deflection of plates with initial curvature, *International Journal of Mechanical Sciences*, **23**, 21-26.
- [114] Levy S. (1942). Square plate with clamped edges under normal pressure producing large deflections, NACA, Tech. Note 847.
- [115] Ekmekyapar, T. (2008). *Structural Buckling Optimization of Stiffened Plates*, Ms. Thesis, Department of Civil Engineering, University of Gaziantep.
- [116] Haftka, R.T, and Gürdal, Z. (1992). *Elements of Structural Optimization*, Kluwer Academic Publishers.
- [117] Özakça, M., Tayşi, N. and Kolcu, F. (2003). Buckling optimization of variable thickness prismatic folded plates, *Thin Walled Structures*, **41**, 711-730.

APPENDIX A: Strain components, strain-displacement matrices, elemental volumes, membrane rigidity matrix, flexural rigidity matrix, and shear rigidity matrix

$\boldsymbol{\varepsilon}_m$	$\left[\frac{\partial u}{\partial \ell} \cos\alpha + \frac{\partial w}{\partial \ell} \sin\alpha, \frac{\partial v}{\partial y}, \frac{\partial u}{\partial y} \cos\alpha + \frac{\partial w}{\partial y} \sin\alpha + \frac{\partial v}{\partial \ell} \right]^T$
$\boldsymbol{\varepsilon}_b$	$\left[\frac{\partial \phi}{\partial \ell}, \frac{\partial \psi}{\partial y}, \left(\frac{\partial \phi}{\partial y} + \frac{\partial \psi}{\partial \ell} \right) + \left(\frac{\partial u}{\partial y} \cos\alpha + \frac{\partial w}{\partial y} \sin\alpha \right) \right] \frac{d\alpha^T}{d\ell}$
$\boldsymbol{\varepsilon}_s$	$\left[-\frac{\partial u}{\partial \ell} \sin\alpha + \frac{\partial w}{\partial \ell} \cos\alpha - \phi, -\frac{\partial u}{\partial y} \sin\alpha + \frac{\partial w}{\partial y} \cos\alpha - \psi \right]^T$
\mathbf{B}_{mi}^p	$\begin{bmatrix} (dN_i/d\ell)S_p \cos\alpha & 0 & (dN_i/d\ell)S_p \sin\alpha & 0 & 0 \\ 0 & -\bar{p}N_i S_p & 0 & 0 & 0 \\ \bar{p}N_i C_p \cos\alpha & (dN_i/d\ell)C_p & \bar{p}N_i C_p \sin\alpha & 0 & 0 \end{bmatrix}$
\mathbf{B}_{bi}^p	$\begin{bmatrix} 0 & 0 & 0 & -(dN_i/d\ell)S_p & 0 \\ 0 & 0 & 0 & 0 & \bar{p}N_i S_p \\ (\bar{p}N_i C_p \cos\alpha)/R & 0 & (\bar{p}N_i C_p \sin\alpha)/R & -\bar{p}N_i C_p & (-dN_i/d\ell)C_p \end{bmatrix}$
\mathbf{B}_{si}^p	$\begin{bmatrix} -(dN_i/d\ell)S_p \sin\alpha & 0 & (dN_i/d\ell)S_p \cos\alpha & -N_i S_p & 0 \\ -\bar{p}N_i C_p \sin\alpha & 0 & \bar{p}N_i C_p \cos\alpha & 0 & -N_i C_p \end{bmatrix}$
V	$\int_0^b \int_{\ell^e} d\ell dy$
Ω	$\int_{-1}^{b+1} \int J d\xi dy$
\mathbf{D}_m	$\frac{Et}{(1-\nu^2)} \begin{bmatrix} 1 & \nu & 0 \\ \nu & 1 & 0 \\ 0 & 0 & (1-\nu)/2 \end{bmatrix}$
\mathbf{D}_b	$\frac{Et^3}{12(1-\nu^2)} \begin{bmatrix} 1 & \nu & 0 \\ \nu & 1 & 0 \\ 0 & 0 & (1-\nu)/2 \end{bmatrix}$
\mathbf{D}_s	$\frac{\kappa^2 Et}{2(1+\nu)} \begin{bmatrix} 1 & 0 \\ 0 & 1 \end{bmatrix}$

APPENDIX B. Geometric stiffness matrices and inplane matrices

\mathbf{S}_{ui}^p	$\begin{bmatrix} (dN_i/d\ell)S_p & 0 & 0 & 0 & 0 \\ N_i(p\pi/b)C_p & 0 & 0 & 0 & 0 \end{bmatrix}$
\mathbf{S}_{vi}^p	$\begin{bmatrix} 0 & (dN_i/d\ell)C_p & 0 & 0 & 0 \\ 0 & -N_i(p\pi/b)S_p & 0 & 0 & 0 \end{bmatrix}$
\mathbf{S}_{wi}^p	$\begin{bmatrix} 0 & 0 & (dN_i/d\ell)S_p & 0 & 0 \\ 0 & 0 & N_i(p\pi/b)C_p & 0 & 0 \end{bmatrix}$
\mathbf{Q}_i^p	$\begin{bmatrix} 0 & 0 & 0 & (dN_i/d\ell)S_p & 0 \\ 0 & 0 & 0 & 0 & -N_i(p\pi/b)S_p \end{bmatrix}$
\mathbf{R}_i^p	$\begin{bmatrix} 0 & 0 & 0 & 0 & (dN_i/d\ell)C_p \\ 0 & 0 & 0 & N_i(p\pi/b)C_p & 0 \end{bmatrix}$
\mathbf{H}	$\begin{bmatrix} \sigma_\ell^0 & 0 \\ 0 & \sigma_y^0 \end{bmatrix}$

CURRICULUM VITAE

PERSONAL INFORMATION

Surname, Name: KOLCU, Filiz

Nationality: Turkish (T.C.)

Date of Birth: 13 April 1974

Place of Birth: Stuttgart

Marital status: Married

Phone: 90 342 3171778

Fax: 90 342 360 11 70

e-mail: kolcu@gantep.edu.tr

EDUCATION

Degree	Institution	Year of Graduation
MS	Gaziantep Univ.-Civil. Engineering	2000
BS	Gaziantep Univ.-Civil. Engineering	1996
High school	Gaziantep High school	1991

WORK EXPERIENCE

Year	Place	Enrollment
1996-2001	Gaziantep Univ.-Civil. Engineering	Assistant
2001-Present	GAZÜ- Gaziantep Vocational high school	Instructor

FOREIGN LANGUAGE :English

PUBLICATION

1. Özakça, M., Tayşi N. and Kolcu F. (2003). Buckling optimization of variable thickness prismatic folded plates , *Thin Walled Structures*, **41**(8), 711-730.

2. Özakça, M., Tayşi N. and Kolcu F. (2003). Buckling analysis and shape optimization of elastic variable thickness circular and annular plates—I. Finite element formulation, *Engineering Structures*, **25**(2), 181-192.
3. Özakça, M., Tayşi N. and Kolcu F. (2003). Buckling analysis and shape optimization of elastic variable thickness circular and annular plates—II. Shape optimization, *Engineering Structures*, **25**(2), 193-199.
4. Kolcu, F., Ekmekyapar, T. and Özakça, M. (2010). Linear buckling optimization and post-buckling behavior of optimized cold formed steel members, *Scientific Research and Essays*, **5**(14), 1916-1924.